Design and Fabrication of Bio-inspired Transparent Materials

by

Zhen Yin

Department of Mechanical Engineering

McGill University

Montreal, Quebec, Canada

Feb 18th, 2020

A thesis submitted to McGill University in partial fulfillment of the requirements for a doctoral degree

Dedication

To my lovely grandparents ***Yishan*** *and* ***Tiying****, my parents* ***Jiansu*** *and* ***Le****, and my beloved girlfriend* ***Xuanteng*** *for their love and support*

Table of Contents

List of Figures

Abstract

Many hard biological materials, such as seashells and bones, are tough bio-ceramics with unique and attractive combination of stiffness, strength and toughness. These biological materials are made of brittle constituents and weak organic interfaces but achieve toughness magnitudes of times higher. The exceptional performances of hard biological materials come from its intricate microarchitectures, which are organized over several length scales. The size, shape and arrangement of the rigid building blocks in these materials trigger many toughening mechanisms such as crack bridging, tablet sliding and crack deflection. The organic interfaces that join the building blocks also play vital roles in governing the deformation and toughness of the biological materials. These organic interfaces dissipate energy through viscoplastic deformation and deflect cracks into configurations where further crack propagation is more difficult. These inorganic/organic biological materials provide ideal models and inspiration to implement new toughening mechanisms in brittle materials. Prime candidates are glasses, which have outstanding optical properties, hardness and durability. Glasses are in sustained demand in many applications but are limited by its inherent brittleness and low impact resistance. Lamination and tempering are two common approaches to improve the impact response of glass but neither of them suppress the brittleness and the improvement on toughness is limited. In this thesis, inspired from the microarchitectures of nacre, fish scales and arthropod cuticles, tough and deformable transparent glass-based materials were developed. laser engraving technique was used to carve weak interfaces into glass and obtained well-controlled microarchitectures with high geometric fidelity. The engraved glass sheets were then laminated with ductile polymer films to form multilayer structures. Our bioinspired multilayer glass materials successfully replicate many toughening mechanisms observed in biological materials. They have well distributed and progressive deformation, and toughness amplification up to 50 times compared to plain laminated glasses. In the out-of-plane puncture and impact performance, our materials surpassed plain laminated glasses and tempered glass by increasing the energy absorption about 2-3 times while maintaining little loss on strength compared to plain laminated glasses.

Résumé

De nombreux matériaux biologiques durs, tels que les coquillages et les os, sont des biocéramiques résistantes qui ont des combinaisons uniques et attrayantes de rigidité, de résistance et de ténacité. Ces matériaux biologiques sont constitués de constituants fragiles et d'interfaces organiques faibles mais atteignent des amplitudes de ténacité bien plus élevées que leur consituants. Les performances exceptionnelles des matériaux biologiques durs proviennent de leur microarchitecture complexe, organisée sur plusieurs échelles de longueur. La taille, la forme et la disposition des blocs de construction rigides dans ces matériaux déclenchent de nombreux mécanismes de durcissement tels que le glissement aux interfaces et la déviation des fissures. Les interfaces organiques qui joignent les blocs de construction jouent également un rôle vital dans le contrôle de la déformation et de la ténacité des matériaux biologiques. Ces interfaces organiques dissipent de l'énergie mécanique par leur déformation viscoplastique, et peuvent dévier les fissures vers des configurations où leur propagation est plus difficile. Ces architectures inorganiques / organiques nous fournissent des modèles idéaux pour ameliorer nos matériaux d'ingenierie. Notamment, Le verre à des propriétés optiques, une dureté et une durabilité exceptionnelles. Il est en demande soutenue dans de nombreuses applications, mais elle sont limitées par leur fragilité et leur faible résistance aux chocs. La stratification et la trempe sont deux moyens conventionnels d'améliorer la réponse aux chocs du verre, mais aucun d'eux ne supprime la fragilité et l'amélioration de la ténacité est limitée. Dans cette thèse, nous présentons des matériaux en verre transparent, résistants et déformables inspirés des microarchitectures de la nacre, des écailles de poisson et des cuticules d'arthropodes. Nous avons utilisé la technique de gravure au laser pour sculpter des interfaces faibles dans le verre et avons obtenu des microarchitectures bien contrôlées avec une fidélité géométrique élevée. Les feuilles de verre gravées ont ensuite été stratifiées avec

des films de polymère ductile pour former des structures multicouches. Ces matériaux bio-inspirés reproduisent de nombreux mécanismes de deformartion observés dans les matériaux biologiques. Ils ont une déformation bien répartie et progressive. Ces materiaux atteignent une amplification de la ténacité jusqu'à 50 fois sur des verres feuilletés simples. Pour les performances de perforation et d'impact, nos matériaux ont dépassé les verres feuilletés unis et le verre trempé en augmentant l'absorption d'énergie par un factor de 2 à 3 fois.

Acknowledgement

The completion of this thesis would never happen without the help, support and encouragement of a group of people including the professors at McGill, my family and my friends. First of all, I would like to express my sincere gratitude to my PhD advisor Prof. Francois Barthelat for his help, guidance and supervision during my study. Prof. Barthelat is a great mentor. His high standards on the research and his passion for science and technology will be a great model for my future professional career. This journey with Prof. Barthelat helped me build confidence in my career and maintain my passion for research and innovation. I would like to thank Prof. Markus J. Buehler at Massachusetts Institute of Technology for his advice and contribution on my first paper and his support for my academic career. I would also like to extend this gratitude to my PhD advisory committee: Prof. Pascal Hubert and Prof Srikar Thattai Vengallatore for their useful insights and suggestions, and Prof. Luc Mongeau, for providing the image correlation software

I appreciate the Faculty of Engineering at McGill University, the Natural Sciences and Engineering Research Council of Canada, the Canada Foundation for Innovation and the Fonds Québécois de la Recherche sur la Nature et les Technologies for their collaborative financial support for this project.

I would like to express my appreciation to the alumni and current members of the laboratory of advanced materials and bioinspiration at McGill University: Dr. Mohammad Mirkhalaf Valashani, Dr. Roberto Martini, Dr. Will Pro, Dr. Florent Hannard, Dr. Idris Malik, Dr. Najmul Abid, Aram Bahmani, Siyu Liu, Ahmed Dalaq, Sacha Cavelier, Ali Shafiei, Alireza Mirmohammadi and Laura Reiger. Thanks for their inspiration and help during the past years. I would also like to thank my other colleagues and friends: Binbin Ying, Xiao Li, Jiaming Zhou, Hao Fu, Pengfei Song, Kevin Hu and Xiaocheng Mi for their generous help and support.

Last but not least, I would like to say my deepest thanks to my grandparents, my parents, my aunt Yuenian and uncle Yitao for their love, support and encouragement throughout my ongoing journey in education. I would also like to express my deepest love and thanks to my beloved girlfriend Xuanteng, who have supported me with her love and encouragement in my PhD study. My deepest gratitude and yearning are again for my lovely grandparents, Yishan and Tiying, who were my role models, brought me to the hall of science and cared so much about me. They had faith in me when no one else did. I could never achieve what I had achieved without them.

Contributions of Authors

This is a manuscript-based thesis consisting of four journal articles. The title of the articles, name of the authors, and their contributions are listed below:

1) Structure and mechanics of interfaces in biological materials

Francois Barthelat[1], Zhen Yin[1] and Markus J. Buehler[2]

[1]Department of Mechanical Engineering, McGill University, 817 Sherbrooke Street West, Montreal, Quebec, Canada H3A 2K6

[2]Department of Civil and Environmental Engineering, 77 Massachusetts Avenue, Massachusetts Institute of Technology, Cambridge, Massachusetts 02139, USA.

Nature Reviews Materials, volume 1, Article number: 16007, March 2016

doi:10.1038/natrevmats.2016.7

Author contributions:

FB: Performed the literature review, prepared the figures and texts, and supervised the work

ZY: Performed the literature review, prepared the figures and texts of some sections.

MB: Helped editing the text, gave technical and scientific advice

2) Tough and deformable glasses with bioinspired cross-ply architectures

Zhen Yin[1], Ahmad Dastjerdi[1], Francois Barthelat[1]

[1]Department of Mechanical Engineering, McGill University, 817 Sherbrooke Street West, Montreal, Quebec, Canada H3A 2K6

Acta Biomaterialia, volume 75, July 2018

Doi: 10.1016/j.actbio.2018.05.012

Author contributions:

ZY: Developed the fabrication protocol of two-layer cross-ply architectured glasses, prepared samples, designed and performed experiments, analyzed and discussed results, developed finite element model, analyzed the simulation and discussed the mechanisms, prepared figures and wrote manuscripts.

AD: Performed some preliminary tests.

FB: Supervised the research, gave technical and scientific advice, edited the figures and manuscript.

3) Impact resistant nacre-like transparent materials

Zhen Yin[1], Florent Hannard[1] and Francois Barthelat[1]*

[1]Department of Mechanical Engineering, McGill University, 817 Sherbrooke Street West, Montreal, Quebec, Canada H3A 2K6

Science, volume 364, June 2019

Doi: 10.1126/science.aaw8988

Author contributions:

ZY: Designed the fabrication protocol of the nacre-like glass panels, the experimental setup and the testing protocol, fabricated and tested the samples, analyzed and discussed results, prepared the figures and wrote the manuscript.

FH: Developed the analysis protocol for the micro-CT scans and developed the codes for numerical processing, analyzed and discussed results, prepared the figures and wrote the manuscript.

FB: Supervised the research, gave technical and scientific advice, prepared the figures and wrote the manuscript.

4) Stiff, strong and tough laminated glasses with bio-inspired designs

Zhen Yin[1] and Francois Barthelat[1, 2]*

[1]Department of Mechanical Engineering, McGill University, 817 Sherbrooke Street West, Montreal, Quebec, Canada H3A 2K6

[2] Department of Mechanical Engineering, University of Colorado, 427 UCB, 1111 Engineering Dr, Boulder, CO 80309, United States

Submitted

Author contributions:

ZY: Designed the fabrication protocol, experimental setup and the testing protocol, fabricated and tested the samples, analyzed and discussed results, prepared the figures and wrote the manuscript.

FB: Supervised the research, gave technical and scientific advice, prepared the figures and wrote the manuscript.

Chapter 1:

Introduction

Chapter 1: Introduction

Glass is a fully recyclable material that receives increasing demands in civil constructions, biomedical applications and electronics for its high transparency, high hardness, high durability and chemical stability. However, glass is a brittle material with low toughness and low impact resistance, which limits its applications in a broader range. Conventionally, there are two ways to enhance the mechanical performances of glass: tempering and laminating. Tempering creates residual compressive stresses on the surface of glass through heat or chemical treatment to offset the tensile stresses arising from external loads. Tempering can increase the strength of glass by two to five times, but glass remains brittle and gets destroyed in a catastrophic and "explosive" way because of the release of elastic energy. Laminating glass is another way by intercalating glass layers with soft polymeric interlayers to form laminated glass. The polymeric layer can hold the glass fragments together in case of glass fracture, but the impact resistance is not improved significantly. Overcoming the brittleness of glass remains a challenge.

Interestingly nature "solved" the problem of material brittleness millions of years ago. Many biological materials such as mollusk shells [1-4] and teeth [5, 6] are mostly made of hard but brittle minerals, but their toughness can be thousands of times higher than their weak constituents. These biological materials achieve the unique combination of stiffness, strength and toughness due to their hierarchical material microarchitectures made of well-organized stiff mineral building blocks and ductile organic interfaces [7, 8]. For example, the microarchitectures of conch shells consist of hierarchical cross-ply structures, where the mineral (aragonite) lamellae were separated and adhered by thin organic interfaces [4, 9, 10]. Propagating cracks are deflected and guided by the weak organic interfaces, triggering toughening mechanisms such as crack bridging [11]. Cross-ply structures can also be found in other biological materials such as fish scales [12, 13] and teeth [6].

In many arthropod species, mineralized chitin fibers form into twisted-ply structures (Bouligand structures) that improve the fracture toughness by twisting the paths of crack propagation [14-17]. Highly organized brick-and-mortar structures can be found in nacre of mollusk shells [18]. The staggered arrangement of polygon aragonite tablets enables toughening mechanisms such as large-scale tablet sliding, crack deflection and crack bridging [3]. The wavy shape of the tablets also triggers a hardening mechanism that delocalize the deformation and tablet sliding. These tough biological materials provide excellent templates for researchers to design tough bioinspired materials from brittle constituents.

The development of bioinspired materials has been actively studied in the past two decades, but it remains a major challenge to fabricate large volumes of well-controlled microscopic material architectures and to duplicate the mechanical performances of biological materials [7, 19-23]. In this study, high-precision three-dimensional laser engraving was used to carving weak interfaces into glass sheets to form contours of bioinspired features with highly controlled size and geometry [24-26]. The engraved glass sheets were then laminated with ductile polymeric adhesive, forming multilayer materials with well-aligned three-dimensional material architectures inspired from mollusk shells and fish scales. The mechanical properties, the fundamental deformation and fracture mechanisms of the bioinspired architectured materials were also studied through both simulation and experimental approaches, under different loading conditions such as tension, bending, puncture and weight-dropping impact. Key elements contributing to the mechanical performances of the bioinspired multilayer materials were identified, and general design strategies towards simultaneously improved stiffness, strength and toughness were proposed. Finally, multilayer bioinspired glass was developed that is transparent, highly deformable, stiff, strong and ultra-tough.

1.1 Thesis objectives

The overall objective of this thesis was to develop bioinspired multilayer glass with high transparency, high deformability, high toughness, decent stiffness and strength. The project was divided into the following specific objectives:

(1) Design and optimize the fabrication protocol of bioinspired multilayer glass so that high transparency of the material, and highly periodic material architectures with precisely controlled size and geometry of the building blocks can be realized.

(2) Develop bioinspired glass with cross-ply architectures. Evaluate the mechanical performances under tension and fracture. Understand the deformation and fracture mechanics of cross-ply glass.

(3) Develop multilayer glass panels with nacre-inspired architectures. Evaluate the stiffness, puncture strength, and energy absorption of the glass panels under puncture and impact. Verify the deformation mechanisms

(4) Evaluate the mechanical performances of glass panels with different bioinspired architectures under puncture. Understand the mechanics behind the mechanical behaviors. Propose the design strategies for simultaneously stiff, strong and tough multilayer architectured glass panels.

1.2 Thesis organization

This is a manuscript-based thesis composed of six chapters. In this chapter, a brief introduction is presented on the background of tough biological materials and current challenges in developing bioinspired materials that can duplicate the mechanisms of biological materials. Chapter 2 presents a more detailed review of structure and mechanics of biological materials, focusing on the organic interfaces in nacre, bone and wood. State of the art development of bioinspired materials and general challenges of the fields are also concluded and discussed.

In Chapter 3, a tough and highly deformable bilayer architectured glass inspired by the cross-ply structure in conch shells is presented. The deformation modes and the mechanical properties including stiffness, strength, deformability and energy absorption, affected by the ply width and ply orientation angles, were identified under uniaxial tensile tests. The deformability and energy absorption of cross-ply glass were up to two orders higher than the plain laminated glass. The toughening and hardening mechanisms under tension were analyzed using finite element models. The damage tolerance of cross-ply glass was also evaluated under single-notch compact tension fracture tests. The failure modes under single-notch fracture were identified. Chapter 4 presents a type of transparent impact resistant nacre-like glass. The mechanical behaviors of nacre-like glass beams were investigated under four-point bending tests. The mechanical performances (stiffness, strength and energy absorption) of nacre-like glass panels were evaluated under both quasi-static puncture tests and weight-drop impact tests. The impact resistance of nacre-like glass panels outperformed all other engineering transparent materials including laminated glass and tempered glass. The loss on stiffness and strength of nacre-like glass panels were able to be compensated by the plain layer put on the front surface. The magnitude of table sliding in nacre-like glass was quantified and verified using micro-CT scanning. In Chapter 5, glass panels with different bioinspired architectures (cross-ply, Bouligand, segmented Bouligand, nacre-like and hybrid designs) were studied under quasi-static puncture tests. The mechanical performances (stiffness, strength and energy absorption), the deformation and failure mechanisms of each configuration were evaluated and identified. The design principles towards simultaneously stiff, strong and tough architecture materials were proposed. Finally, Chapter 6 discussed the accomplishments and the main contributions of this research. Some recommendations for future work are also recommended.

1.3 References

1. Jackson, A.P., J.F.V. Vincent, and R.M. Turner, *The mechanical design of nacre.* Proceedings of the Royal Society of London B, 1988. **234**(1277): p. 415-440.
2. Wang, R.Z., et al., *Deformation mechanisms in nacre.* Journal of Materials Research, 2001. **16**(9): p. 2485-2493.
3. Barthelat, F., et al., *On the mechanics of mother-of-pearl: A key feature in the material hierarchical structure.* Journal of the Mechanics and Physics of Solids, 2007. **55**(2): p. 306-337.
4. Kamat, S., et al., *Structural basis for the fracture toughness of the shell of the conch Strombus gigas.* Nature, 2000. **405**(6790): p. 1036-1040.
5. Yahyazadehfar, M., et al., *On the Mechanics of Fatigue and Fracture in Teeth.* Applied mechanics reviews, 2014. **66**(3): p. 0308031-3080319.
6. Bajaj, D. and D. Arola, *Role of prism decussation on fatigue crack growth and fracture of human enamel.* Acta Biomaterialia, 2009. **5**(8): p. 3045-3056.
7. Barthelat, F., Z. Yin, and M.J. Buehler, *Structure and mechanics of interfaces in biological materials.* Nature Reviews Materials, 2016. **1**(4): p. 16007.
8. Meyers, M.A., et al., *Biological materials: Structure and mechanical properties.* Progress in Materials Science, 2008. **53**(1): p. 1-206.
9. Kuhn-Spearing, L.T., et al., *Fracture mechanisms of the Strombus gigas conch shell: implications for the design of brittle laminates.* Journal of Materials Science, 1996. **31**(24): p. 6583-6594.
10. Menig, R., et al., *Quasi-static and dynamic mechanical response of Strombus gigas (conch) shells.* Materials Science and Engineering: A, 2001. **297**(1): p. 203-211.
11. Kamat, S., et al., *Fracture mechanisms of the Strombus gigas conch shell: II-micromechanics analyses of multiple cracking and large-scale crack bridging.* Acta Materialia, 2004. **52**(8): p. 2395-2406.
12. Zhu, D., et al., *Structure and Mechanical Performance of a "Modern" Fish Scale.* Advanced Engineering Materials, 2012. **14**(4): p. B185-B194.
13. Yang, W., et al., *Structure and fracture resistance of alligator gar (Atractosteus spatula) armored fish scales.* Acta Biomaterialia, 2013. **9**(4): p. 5876-5889.
14. Bouligand, Y., *Twisted fibrous arrangements in biological materials and cholesteric mesophases.* Tissue and Cell, 1972. **4**(2): p. 189-217.
15. Weaver, J.C., et al., *The Stomatopod Dactyl Club: A Formidable Damage-Tolerant Biological Hammer.* Science, 2012. **336**(6086): p. 1275.
16. Chen, P.-Y., et al., *Structure and mechanical properties of crab exoskeletons.* Acta Biomaterialia, 2008. **4**(3): p. 587-596.
17. Suksangpanya, N., et al., *Twisting cracks in Bouligand structures.* Journal of the Mechanical Behavior of Biomedical Materials, 2017. **76**: p. 38-57.
18. Jackson, A.P., et al., *The mechanical design of nacre.* Proceedings of the Royal Society of London. Series B. Biological Sciences, 1988. **234**(1277): p. 415-440.
19. Behr, S., et al., *Large-scale parallel alignment of platelet-shaped particles through gravitational sedimentation.* Scientific Reports, 2015. **5**(1): p. 9984.
20. Das, P., et al., *Nacre-mimetics with synthetic nanoclays up to ultrahigh aspect ratios.* Nature Communications, 2015. **6**(1): p. 5967.

21. Bonderer, L.J., A.R. Studart, and L.J. Gauckler, *Bioinspired Design and Assembly of Platelet Reinforced Polymer Films.* Science, 2008. **319**(5866): p. 1069.
22. Munch, E., et al., *Tough, Bio-Inspired Hybrid Materials.* Science, 2008. **322**(5907): p. 1516.
23. Barthelat, F., *Architectured materials in engineering and biology: fabrication, structure, mechanics and performance.* International Materials Reviews, 2015. **60**(8): p. 413-430.
24. Mirkhalaf, M., A.K. Dastjerdi, and F. Barthelat, *Overcoming the brittleness of glass through bio-inspiration and micro-architecture.* Nature Communications, 2014. **5**(1): p. 3166.
25. Yin, Z., A. Dastjerdi, and F. Barthelat, *Tough and deformable glasses with bioinspired cross-ply architectures.* Acta Biomaterialia, 2018. **75**: p. 439-450.
26. Yin, Z., F. Hannard, and F. Barthelat, *Impact-resistant nacre-like transparent materials.* Science, 2019. **364**(6447): p. 1260.

Chapter 2: Structure and mechanics of interfaces in biological materials

Francois Barthelat[1]*, Zhen Yin[1] and Markus J. Buehler[2]

[1] *Department of Mechanical Engineering, McGill University, 817 Sherbrooke Street West, Montreal, QC H3A 2K6, Canada*

[2] *Department of Civil and Environmental Engineering, Massachusetts Institute of Technology, 77 Massachusetts Avenue, Cambridge, MA 02139, USA*

*corresponding author: (francois.barthelat@mcgill.ca)

2.1 Abstract

Hard biological materials such as bone, seashells or wood fulfill critical structural functions and display unique and attractive combinations of stiffness, strength and toughness, thanks to their intricate micro-architectures organized over several length scales. The size, shape and arrangement of the "building blocks" of which these materials are made is critical in defining their properties and their exceptional performance, but there is also growing evidence that their deformation and toughness is also largely governed by the interfaces they contain. These interfaces join building blocks, channel nonlinear deformations and deflect cracks into configurations where propagation is more difficult. Here the composition, structure and mechanics of a set of representative biological interfaces within nacre, bone and wood are reviewed. Through a comparative review of these materials, it shows that biological interfaces possess unusual mechanical characteristics, which can inspire new strategies for advanced bio-inspired composites. The discussion is concluded with a review of recent studies in which such strategies are employed in the design and manufacturing of new composite materials.

2.2 Introduction

Biological materials display highly controlled structural features over several length scales, including down to the nano- and molecular scales. These materials show advanced properties despite being composed of modest ingredients and boast performances that are in some ways superior to those of engineering materials [1-7]. In addition, biological materials can adapt their composition and structure to their environment, and can self-repair and remodel. In terms of absolute structural performance, hard biological materials, such as bone or mollusc shells, are in general inferior to engineering materials, for example, steels or fibre-reinforced composites. However, the mechanical performance of hard biological materials is much higher than that of their components — brittle minerals and weak proteins — and it is this ‘property amplification’ achieved by these natural composites that is remarkable. In particular, biological materials are strong and tough — two properties that are typically mutually exclusive in engineering materials [8]. The structure and mechanics of biological materials have traditionally been characterized in terms of building blocks of finite size that are ordered into well-controlled arrangements, much like individual bricks in a wall. Nature tightly controls the size, shape and arrangement of these blocks and, as a result, the term ‘architecture’ is increasingly used instead of the term ‘microstructure’, which is traditionally used in materials science [9, 10]. This concept has been introduced as the universality–diversity paradigm [11]; according to this, a vast diversity of properties is achieved by arranging a limited set of ‘universal’ structural motifs at distinct length scales, often concurrently at multiple scales. In proteinaceous materials, these structural motifs include helices, crystals or disordered regions. At larger length scales, structural motifs have recently been classified into fibrous, helical, gradient, layered, tubular, cellular, suture and overlapping [9] building blocks. Owing to the combination of these structural motifs over multiple scales, natural materials achieve high performance at the macroscale [9, 12, 13].

In addition to these sophisticated architectures, it has now become evident that the deformation and fracture of these materials are largely governed by the interfaces contained within them [10, 14-16]. These interfaces may occupy a very small volume fraction in the material, but their importance is such that in recent work interfaces are themselves described as their own building block [17]. For example, proteins in enamel comprise just 1% of total enamel weight, and proteins taken from the interface between crystallite and rods have been shown to be critical for the overall toughness of the enamel, as removing these proteins results in a 40% decrease in fracture toughness [18]. Nacre from mollusc shells is another example of a hard but extremely tough material [19, 20]. It is mostly made of microscopic tablets of calcium carbonate, and organic materials — which constitute only 5% of the total volume — serve as 'mortar' between the tablets [21]. The deformability of the thin organic mortar is crucial for overall performance, and dehydrating the organic interfaces turns nacre from a quasi-ductile composite into a very brittle material similar to pure calcium carbonate [22]. Hard biological materials are packed with organic-rich interfaces that can glide and slide. These interfaces operate in synergy with specific architectures in the materials, providing nonlinear deformation mechanisms and turning inherently brittle materials into materials that can deform inelastically, redistribute stresses around defects and dissipate energy. Interfaces can also deflect cracks and channel them into configurations in which their propagation is hindered or arrested, generating tougher materials. In a material such as bone, these principles can be observed simultaneously over several hierarchical length scales [15, 23, 24]. Recent material models seek to incorporate the mechanical behaviour of biological interfaces explicitly [17, 25], and the development of bioinspired materials is increasingly focused on duplicating the features, mechanisms and properties of natural interfaces [26-30]. However, the composition, structure, properties and mechanics of biological interfaces are often complex and difficult to investigate, mainly because of their small thicknesses. There are still gaps in our quantitative understanding of the role of these interfaces, and there are associated controversies in our understanding of how they are constructed and how they operate.

Here, the composition, structure, mechanics and properties of three representative examples of biological interfaces are reviewed: nacre, bone and wood. Then the discussion extends to some general characteristics of these interfaces, which can serve as guidelines for the design of bioinspired composites.

2.3 The interfaces in nacre

Mollusc shells are mostly made of minerals (at least 95% by volume) and contain only a small fraction of organic materials (at most 5% by volume) [31]. Among the materials found in mollusc shells, nacre is the strongest and toughest [31] (Fig. 2-1). Nacre displays complex micromechanisms of deformation and fracture that generate high stiffness (70–80 GPa), high tensile strength (70–100 MPa) and high fracture toughness (4–10 MPa m1/2) [19, 21, 32]. However, nacre has a relatively simple brick-wall-like architecture composed of mineral polygonal tablets (0.2–1 μm in thickness and 5–10 μm in diameter; see Fig. 2-1a, b). The tablets are not perfectly flat and display a considerable waviness that can reach 200 nm in amplitude [22]. For many years, these tablets were thought to be made of large crystals of aragonite [1]; however, the tablets are actually ‘mesocrystals’ composed of nanograins with the same crystallographic orientation, thereby featuring another level of hierarchical structuring (Fig. 2-1e). The nanograins are delimited by organic materials [33, 34] that constitute the intracrystalline fraction of the total organic content in the material [35]. Forming the bulk of the tablets, the nanograins emerge at the surface of the tablets as nanoasperities [19]. Under tension, the tablets can slide on one another, which generates relatively large deformations (up to almost 1% strain) accompanied by energy dissipation [19, 22, 32]. Other deformation mechanisms associated with the nanostructure of the tablets have been proposed [36]; however, if these were to occur under tension, their contribution to the overall tensile deformation would be much smaller than that of tablet sliding.

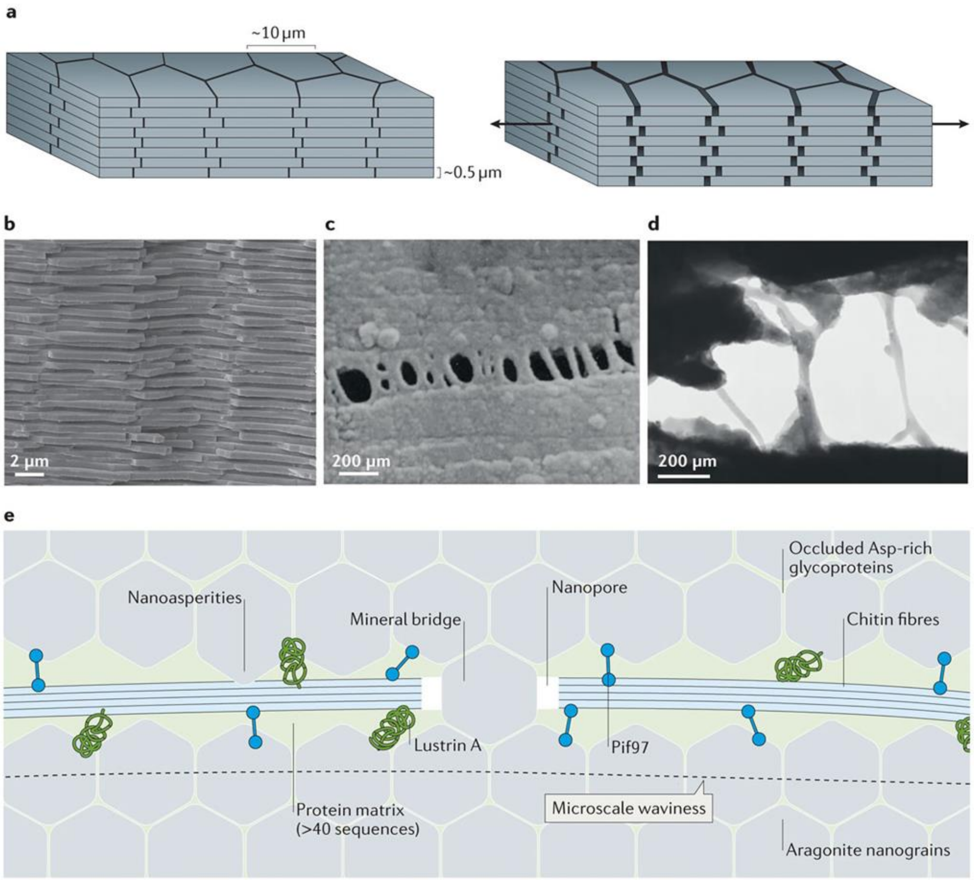

Fig. 2-1: The structure, deformation and interfaces of nacre. (a) A schematic of the brick-and-mortar structure of nacre. The deformation of nacre under tension is dominated by the sliding of the mineral tablets on one another. (b) A scanning electron microscopy (SEM) image of the fracture surface of red abalone nacre [22]. (c) Separating the tablets in the out-of-plane direction reveals a highly deformable matrix. The SEM image shows the formation of cavities and ligaments [32]. (d) The ligaments can elongate to great lengths. In this transmission electron microscopy image, the ligaments are up to 500 nm long, which is more than 10 times the initial thickness of the interface [37]. (e) A schematic of the interfaces in nacre. Panel b is reproduced with permission from REF. [22], Elsevier. Panel c is from REF. [32], Jackson, A. P., Vincent, J. F. V. & Turner, R. M., The mechanical design of nacre, Proc. R. Soc. Lond. B, 1988, 234, by permission of the Royal Society. Panel d is from REF. [37], Nature Publishing Group.

The relatively simple mechanism of tablet sliding leads to crack bridging and process-zone toughening [38], two powerful toughening mechanisms that make nacre several orders of magnitude tougher than aragonite [19, 20, 39]. The sliding and pullout of the tablets are mediated by the thin (20–40nm) interfaces between the tablets, which are rich in organic materials [40]. These organic materials are highly deformable and strongly adhere to the tablets, as shown by the formation of long ligaments when the interface is opened (mode I fracture) (Fig. 2-1c,d). Complete cleavage of the interface exposes organic materials on both fractured surfaces [16, 41], which also confirms that these materials strongly adhere to the surface of the tablets. The toughness of the interfaces [2, 16, 21] in mode I fracture is about 10 Jm^{-1}, which is roughly two orders of magnitude less than the toughness of nacre [39]. Weak interfaces are a requirement for the ability to deflect and guide incoming cracks. Under shear, the interfaces deform elastically up to a yield point of about 10–20MPa, followed by a region of large strains accompanied by strain hardening up to a maximum shear stress of 30–50MPa (REFS [19, 22, 42]). Mechanical tests on demineralized nacre confirm that the organic materials have low strength but high deformability [16, 43]. However, in demineralized nacre, the organic material is not confined, and its mechanical response may not fully reflect the mechanical response of the same material under nanoconfinement from the tablets [44]. The low strength of the interfaces is crucial to ensure that deformation and cracking occur at the interface [45], and high extensibility is essential to develop inelastic mechanisms over large volumes and to generate toughness at the macroscale [22]. Among other properties of the interfaces in nacre, it has been suggested that extensibility is the most important for the overall toughness of nacre [46]. The properties of the interfaces seem to be fine-tuned to achieve a high performance material [46], much like the interfaces between fibres and the matrix in engineering composites must be optimized. Disrupting this balance by desiccating the organic layers results in a stronger but more brittle material [22]. By contrast, removal of the organic materials — for example, by thermal treatment — leads to a sharp drop in strength and modulus [47].

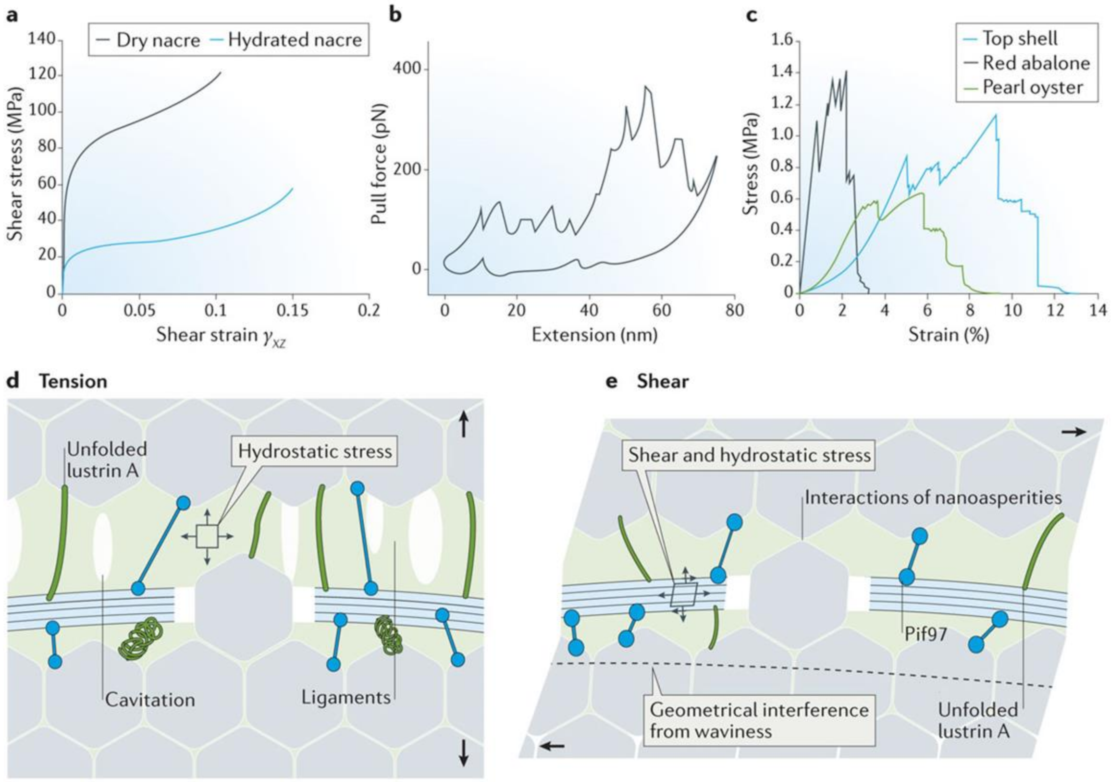

Fig. 2-2: Mechanical tests on the interfaces in nacre. (a) Deforming nacre under shear along the interfaces reveals large strains and strain hardening [22]. (b) A microcantilever in an atomic force microscope is used to pull individual molecules from cleaved nacre surfaces. The force–extension curves reveal a saw-tooth pattern characteristic of the breakage of sacrificial bonds [37]. (c) Tensile tests on demineralized nacre showing low strength but large extensions [16]. (d) Possible deformation mechanism for the interfaces in nacre when subjected to tension. (e) Possible deformation mechanism for the interfaces in nacre when subjected to shear. Panel a is adapted with permission from REF. [22], Elsevier. Panel b is from REF. [37], Nature Publishing Group. Panel c is adapted with permission from REF. [16], Elsevier.

The accepted model for the organic interfaces between layers of tablets consists of a layer of β-chitin fibrils sandwiched between two proteinaceous layers (Fig. 2-1e). The proteinaceous layers are bonded to the tablets, forming a continuous connection with the intracrystalline network [1, 34, 35, 40]. About 40 protein sequences have been identified so far, and further sequences remain to be identified [48]. The mechanical response of the interface can be assessed by shear tests on samples of nacre [22] (Fig. 2-2a). The response is strongly dependent on hydration, which suggests that the organic layer carries a significant portion of the shear stress. Under shear, the interfaces display a yield point (of about 20 MPa under hydrated conditions and 60 MPa under dry conditions), followed by hardening and failure at relatively large strains (10%). The two organic components that are most cited in relation to the mechanical properties of the interfaces in nacre are chitin [40] and lustrin A [37, 49]. Chitin is a polysaccharide that is very stiff and strong under tension and is the main component in arthropod cuticles [50]. In nacre, chitin is in the form of a dense mat of nanofibres interspersed with nanopores [51]. Chitin is believed to serve as reinforcement for the organic template before biomineralization [52], but its function in fully grown nacre is less clear. Molecular pull tests on the interfacial organic molecules, which are exposed by cleaving nacre, have revealed large extensibility and ‘sawtooth’ patterns in the force–extension curve, which are characteristics of molecules with sacrificial bonds and ‘hidden length’, such as lustrin A [37] (Fig. 2-2b). The unfolding of lustrin A is only initiated at a critical tensile force, which translates into a macroscale yield point for the proteinaceous mixture [53]. The large deformation generated by the sequential unfolding of lustrin A is believed to underlie the formation of ligaments in the organic materials [37] and may explain its high extensibility under tension (Fig. 2-2c), although the large strains observed under tension may also be a result of substantial deformations of the nanopores [54]. Proteins, polysaccharides and the mineral are tightly bonded at the interfaces. The adhesion of the proteinaceous layers to the mineral is strong, partly because they form a continuous network with the intracrystalline proteins. The proteinaceous layers are also tightly bonded to the chitin layer, possibly through covalent bonds [55]. In addition, another key protein called Pif97, which has both chitin-binding sites [56] and aragonite-binding sites [57], may function as a crosslinker between chitin and aragonite [28, 58]. Under tension, cavities rapidly grow in size [54] and turn into ligaments, providing cohesion over large deformations (Fig. 2-2d). This behaviour is consistent with an elastomeric adhesive confined between two adherents and stretched under tension, with strong adhesion to the surface of the tablets. Chitin is relatively stiff and brittle, and thus the formation of ligaments probably takes place within the proteinaceous layers.

Interestingly, although synthetic elastomers produce a linear response under shear even at large deformations, the shear response of biological elastomers containing sacrificial bonds exhibits a yield point and extremely large shear deformations [53]. A possible function of chitin could be to delay the shear fractures that can occur from the tensile stress that builds up as the interface is sheared [59, 60]. At the microscale, the resistance to sliding is generated, in part, by the waviness of the tablets, which produces progressive interlocking [22]. At other regions and mostly at the centre of the tablets, nanobridges of aragonite connect adjacent tablets [51, 61]. The interfaces in nacre are complex nanoscale subsystems composed of a network of proteins and polysaccharides with functions in both the growth and the mechanical strength of the material.

2.4 The interfaces in bone

Bone is a high-performance material that has various functions, the primary of which is mechanical support [62]. To fulfil this supporting role, bone is stiff and hard because of its mineral content, but it is also surprisingly tough [63] considering its content of brittle minerals and soft proteins. By weight, approximately 60% of bone is composed of mineral (calcium and phosphate), 10–20% of water and 20–30% of proteins. About 90% of the protein content is type I collagen, and the remaining 10% is non-collagenous proteins, including fibronectin, osteonectin, sialoprotein, osteocalcin and osteopontin [64]. Bone density and mineral content have long been used as the only predictors of bone strength; however, these measures have limitations (not discussed here) [65]. More recent research has considered bone as a composite material in which minerals, collagen and extracollagenous proteins contribute to its mechanical performance [15, 66]. Bone has a complex hierarchical structure [23, 24] (Fig. 2-3) with 3D features that are yet to be fully elucidated [67]. At the molecular scale, individual collagen molecules (known as tropocollagen) interact through coordinated hydrogen bonds [68] and self-assemble into fibrils (Fig. 2-3). Specific covalent crosslinks at the ends of the collagen molecules (telopeptide regions) provide cohesion and mechanical stability to the fibrils, and govern complex unravelling nanomechanisms as the fibrils are stretched [69]. Collagen fibrils are relatively stiff and strong [70], and they are further reinforced by nanocrystals of hydroxyapatite [23, 71, 72] following mineralization processes that are controlled by the arrangement of the collagen molecules as well as their crosslinking [73]. The fibrils bundle into fibres, which form the building blocks of bone at the next hierarchical level. In turn, the fibres arrange into cross plies and lamellae at the microscopic scale (Fig. 2-3). Lamellae wrap around the Haversian canals concentrically to form the osteons, which are the microscopic building blocks of mature cortical bone. Small-scale and in situ experiments, micromechanics and fracture mechanics have successfully captured the structural features governing the deformation and fracture of bone over these multiple length scales [15, 74-76]. Notably, the results of these experiments highlight the importance of the interfaces between these building blocks, which may be at least as crucial as the building blocks themselves for overall mechanical performance [14, 72, 77-81]. Here, the discussions focus on the composition, structure and mechanics of two of the critical interfaces within bone: the interfibrillar interfaces and the cement lines.

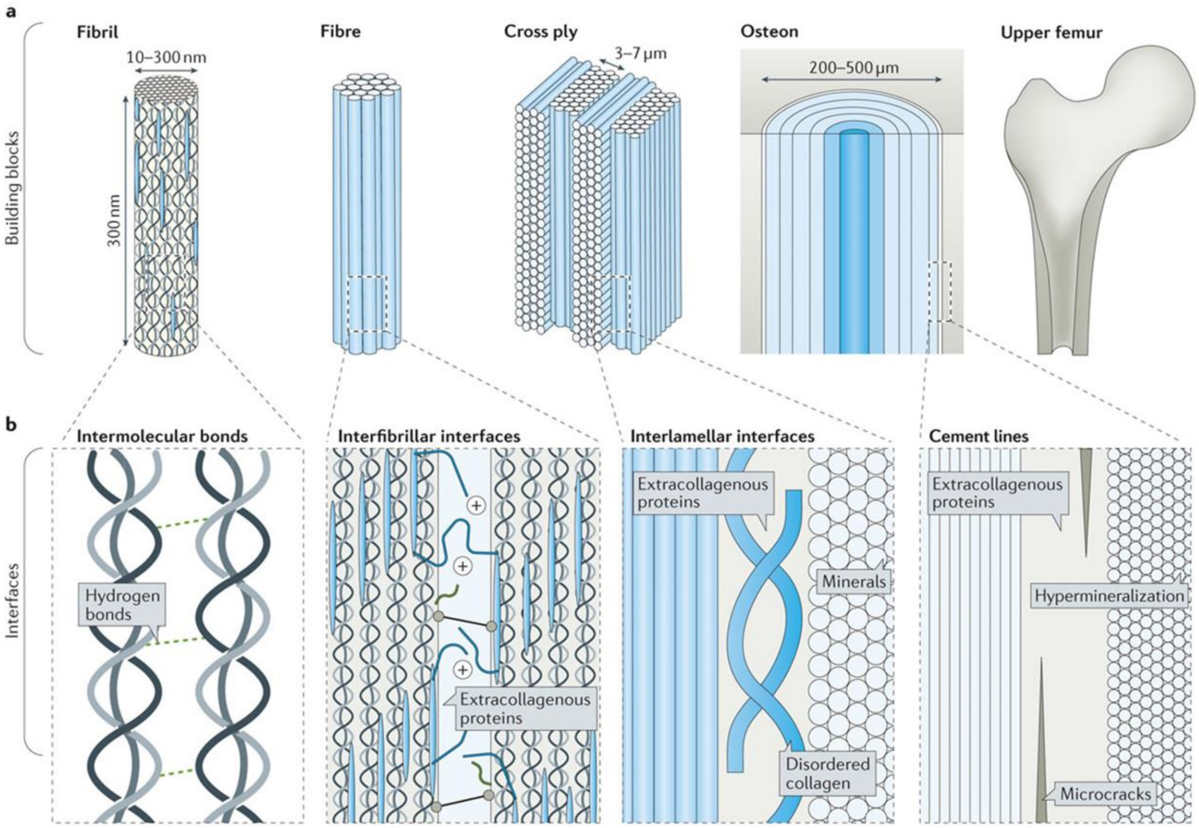

Fig. 2-3: The building blocks and interfaces of bone. (a) Bone has a hierarchical structure with building blocks that range from nanometres to hundreds of micrometres in size: fibril, fibre, cross ply and osteon. (b) The interfaces within each of these hierarchical structures, at different length scales, are shown. These interfaces differ in composition and size, but their function is the same: to transfer mechanical stresses between building blocks and across length scales. Panel b is adapted with permission from REF. [24], Elsevier.

Interfibrillar interfaces. Collagen fibres comprise bundles of fibrils that are held together by a 1–2 nm thick layer of non-collagenous interfibrillar matrix (Fig. 2-3). This proteinaceous adhesive is amorphous and contains various proteins, including osteocalcin and osteopontin [75]. This mixture of proteins is more compliant and weaker than the stiff, mineralized and aligned collagen fibrils, as demonstrated by the cleavage and fracture surfaces of lamellar bone at the microscale [81]. The proteins at the interfaces are, however, highly deformable, and separating the collagen fibrils in bone forms ligaments in the interfaces [81] (Fig. 2-4a); these observations are similar to those for nacre (Fig. 2-1c,d). In situ X-ray tensile testing on femoral bovine bone demonstrated that the shearing of the interfibrillar interfaces accounts for up to 60% of the overall tensile deformation of bone [82], a ‘nanoscale ductility’ that is key to energy dissipation and to the formation of dilation bands at the nanoscale [83, 84]. Propagating a crack in bone involves the pullout of individual fibres and fibrils from the crack faces [85, 86] as well as bridging, which increase the overall toughness of bone.

The pullout process is similar to the fracture processes in fibre-reinforced composites, which require the presence of weak interfaces between fibres and the matrix. It is difficult to obtain direct measurements of the mechanical properties of the interfibrillar interfaces. Pullout tests on individual collagen fibrils from antler bone reveal a shear strength of about 0.65MPa [87], which is much less than the macroscopic strength of antler bone (200–300MPa) [63]. The composition and the structure of the interfibrillar interfaces remain to be fully elucidated, but osteocalcin and osteopontin seem to be key to the mechanics of these interfaces. Osteocalcin and osteopontin can form a complex that promotes the adhesion of the mineral to collagen [88]. Osteopontin strongly adheres to hydroxyapatite, and it is decorated with negative charges that can form sacrificial bonds with positively charged calcium ions [89]. If the interface is opened or shear is applied, these electrostatic sacrificial bonds can break and release hidden lengths along the molecule, generating the saw-tooth pattern observed experimentally [81] (Fig. 2-4b). Tensile experiments on bovine cortical bone using stepwise changes in strain rates confirmed that the activation enthalpy associated with nonlinear deformation in bone corresponds to the disruption of electrostatic bonds [90]. Interestingly, these bonds can re-form rapidly [81], effectively healing bone at the nanoscale without the need for remodeling [91, 92]. Experiments have shown that suppressing the actions of these proteins has a considerable impact on the overall performance of bone, with a significant decrease in deformability and energy dissipation capabilities at the molecular scale [81, 93], a decrease in diffuse damage at the sub-micrometre scale [83] and a decrease in toughness at the macroscale [94].

Other mechanisms may also contribute to the mechanics at the interfibrillar interfaces. More specifically, the collagen fibrils are largely covered by hydroxyapatite nanocrystals [71], and, as a result, it is conceivable that the sliding of the fibrils on one another involves direct contact between nanocrystals of adjacent fibrils, which would generate frictional resistance to sliding [95] in a similar way to nacre [19]. Finally, additional contributions to bonding slowly develop over time. Ageing collagen is subject to slow non-enzymatic glycation, which generates advanced glycation end products (AGEs), such as pentosidine. AGEs increase the degree of crosslinking between collagen molecules and between collagen fibrils [96]. This makes the interfibrillar interface stiffer and stronger but also hinders nanoscale deformations [78] and reduces diffuse microdamage [97]. As a result, ageing bone tends to be stiffer and stronger but more brittle [78, 97]. The interfibrillar interfaces in bone are therefore complex systems in which several mechanisms concurrently contribute to tensile and shear responses (Fig. 2-4c).

Interfibrillar interfaces also govern the deformation and fracture of collagenous materials other than bone. For example, tendons are made of unidirectional collagen fibrils, and the interfaces between these fibrils are crucial for the deflection and blunting of incoming cracks, and to channel deformations [98, 99]. In fish scales, the collagen fibrils form cross plies, and the interfaces between the fibrils govern defibrillation, pullout, delamination and rotation of adjacent laminates [100, 101]. Tendons and fish scales are among the toughest biological materials known [98, 100], and this toughness results from powerful toughening mechanisms that are principally governed by the interfaces between collagen fibrils.

Cement lines. Bone accumulates fatigue microcracks from the repeated mechanical loads associated with normal activities [79]. The negative effects of this damage on the performance of bone are compensated by remodelling, a process by which old bone material is replaced by new bone. Remodelling is performed by the bone remodelling units that consist of osteoclast cells and osteoblast cells. Osteoclast cells dissolve and digest ‘old’ bone, and osteoblast cells generate ‘new’ bone by depositing collagen fibrils, which mineralize after deposition. These bone remodelling units migrate along the direction of long bones, leaving cylindrical wakes of newly remodelled bone, the osteons. Osteons are lined with a 1–5 μm thick boundary called the cement line, which functions as an interface between the osteons and the surrounding interstitial bone [102, 103]. Mature cortical bone can therefore be interpreted as a unidirectional fibre-reinforced composite, in which the osteons are the fibres and the interstitial bone is the matrix [104]. Similarly to the way that an interface composed of carbon or glass fibres in synthetic composites can deflect cracks and generate toughness by pullout, cracks can be deflected or twisted along the weaker cement lines [74, 105] (Fig. 2-4d). These powerful mechanisms make cortical bone five times tougher in the transverse direction than in the longitudinal ‘splitting’ direction [76].

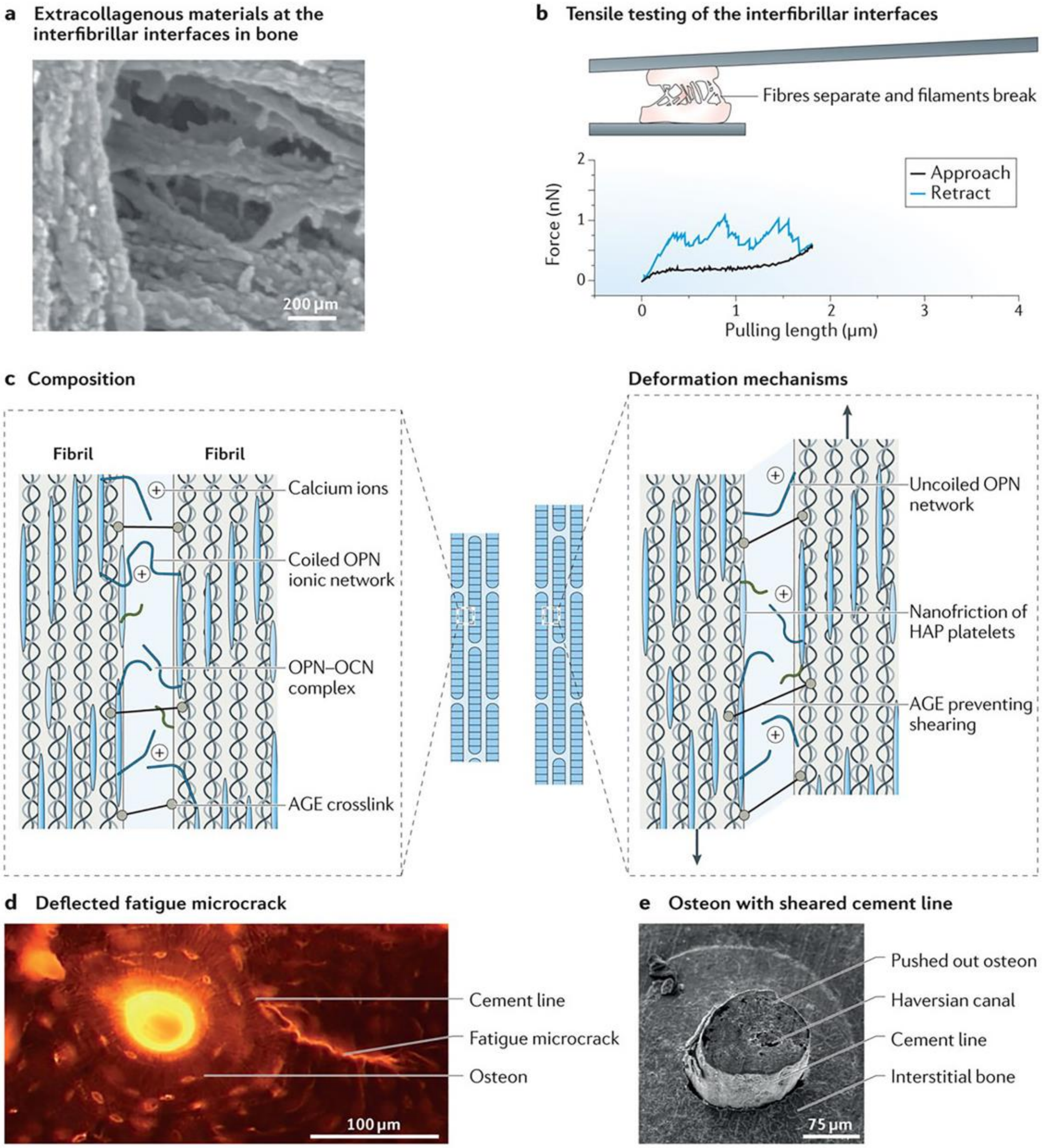

Fig. 2-4: The mechanics of the interfaces within bone. (a) Separating the collagen fibrils exposes highly deformable materials at the interfibrillar interfaces81. (b) Tensile testing on this interface reveals large extensions and the saw-tooth pattern characteristic of the breaking of sacrificial bonds, which can re-form upon unloading [81]. (c) A schematic of the interfibrillar interface showing some of its main structural components (left panel). The main deformation mechanisms at the interfibrillar interface under shear are shown in the right panel. (d) A fatigue microcrack is deflected into a cement line [106]. Cement lines are preferred sites for microcracks. (e) An out-of-position individual osteon after a push-out test in which the cement line is sheared [107]. AGE, advanced glycation end product; HAP, hydroxyapatite; OCN, osteocalcin; OPN, osteopontin. Panels a and b are from REF. [81], Nature Publishing Group. Panel d is reproduced with permission from REF. [106], Elsevier. Panel e is reproduced with permission from REF. [107], Elsevier.

To deflect incoming cracks properly, the cement line must be considerably weaker than both the osteons and the interstitial bone. The shearing behaviour of the cement line can be evaluated by pushing the osteon along its axis and out of its interstitial bone surrounding using thin cross sections of cortical bone [107, 108] (Fig. 2-4e). This test revealed that the shear strength of the cement lines (8MPa) is an order of magnitude lower than that of the surrounding interlamellar interfaces within the osteon (73MPa) [109]. Once the cement line has broken, frictional pullout ensues [107], a mechanism that is also observed and exploited in synthetic fibres used in engineering composites. The fracture toughness of cement lines can be estimated from the toughness of cortical bone in the splitting direction because, in that orientation, the crack mostly propagates along the cement lines. By this measure, the toughness of the cement line is 1–2 MPa $m^{1/2}$, which is an order of magnitude lower than the toughness of bone in the transverse direction [105]. These experiments confirm the strong contrast between the strength of cement lines and that of the surrounding bone material, which can be explained by differences in composition and structure. Cement lines are more mineralized than the surrounding bone [103], which makes them more brittle. Short microcracks are typically deflected by the cement line [106], where they accumulate preferentially [110, 111]. They also have lower collagen content than their surroundings and a high level of non-collagenous proteins, including osteocalcin, osteopontin and bone sialoprotein [103]. The combination of lower collagen content, higher mineralization and the accumulation of damage explains why cement lines are so much weaker than the surrounding bone. The main toughening mechanisms associated with the cement line are crack deflection and twisting [15, 105, 112], although debonding followed by frictional pullout has also been suggested as an important toughening mechanism associated with osteons [113, 114].

Bone has been historically interpreted as a ceramic, then as a composite of mineral and collagen, and then as a hierarchical structure with building blocks at distinct length scales. This hierarchy of structures and mechanisms gives rise to unusual combinations of high stiffness, high strength and high toughness [3, 115, 116]. Recent studies on the mechanics of bone [15, 105] suggest a picture in which the interfaces between the building blocks operate synergistically to produce a high-performance material. The ductile deformation of bone is governed by nonlinear mechanisms at the nanoscale, with the interfibrillar interfaces as the main contributor [84]. By contrast, fracture appears to be governed by the brittle and fragile cement lines around the osteons, which deflect and twist incoming cracks [15, 105, 112]. Other mechanisms, such as crack deflection on the collagen lamellae within osteons [117], confined microcracking [118], pullout of collagen fibrils [85] and pullout of osteons [113, 114], have also been suggested. However, experiments and fracture-mechanics models suggest that crack deflection and twisting are the primary toughening mechanisms for cortical bone [15, 105, 112].

Disrupting the finely tuned structures and mechanisms of these interfaces in bone can have a profound impact on overall performance. For example, suppressing key interface proteins, such as osteopontin, has immediate and dramatic consequences on overall toughness [83, 94], and recent studies have shown that the decline in the mechanical properties of bone with age can be explained by the increase in covalent crosslinks at the nanointerfaces, which results in stiffness and brittleness [78]. These results clarify that bone must be understood as an integration of structural building blocks connected by interfaces.

2.5 The interfaces in wood

Wood is widely used in the construction industry because it is a relatively stiff and strong material; spruce wood has a modulus of 30 GPa and a strength of 300 MPa along the grain [119]. The work of fracture of wood is in the range of 15–30 kJ m^{-2}, which is comparable to that of metals such as aluminium and mild steel [120-122]. Wood has a cellular structure composed of parallel hollow tubes (known as cells or tracheids) that are about 20 inches in diameter [3, 123] (Fig. 2-5a). Each tracheid is composed of several concentric secondary layers, the thickest being the S2 layer (Fig. 2-5b), which accounts for approximately 80–90% of the wood tracheid by weight and is its principal load-bearing element [5, 124]. The S2 layer is composed of laminates of cellulose microfibrils (about 45% by volume) that helically wind around the long axis of the tracheid and are embedded in a matrix of hemicelluloses (35% by volume; usually xylan and glucomannan) and lignin (20% by volume) [5, 119] (Fig. 2-5b). The orientation of the microfibrils is characterized by the microfibril angle (MFA), which is defined as the angle between the fibrils and the axis of the tracheid. In the S2 layer, the MFA can vary between 0° and 45° to the longitudinal axis [3, 125]. Cellulose microfibrils are semicrystalline assemblies of cellulose molecules, with a diameter of approximately 10–25 nm. Cellulose is a high-molecular-weight polysaccharide with a covalent backbone, and, when part of the microfibril, cellulose molecules interact through the formation of covalent bonds and hydrogen bonds [126, 127]. In the crystalline regions, the backbone of the molecules is aligned with the axis of the microfibrils, which makes microfibrils both very stiff (with an elastic modulus of 120–140 GPa) and very strong (with a tensile strength of 750–1,080 MPa) [119].

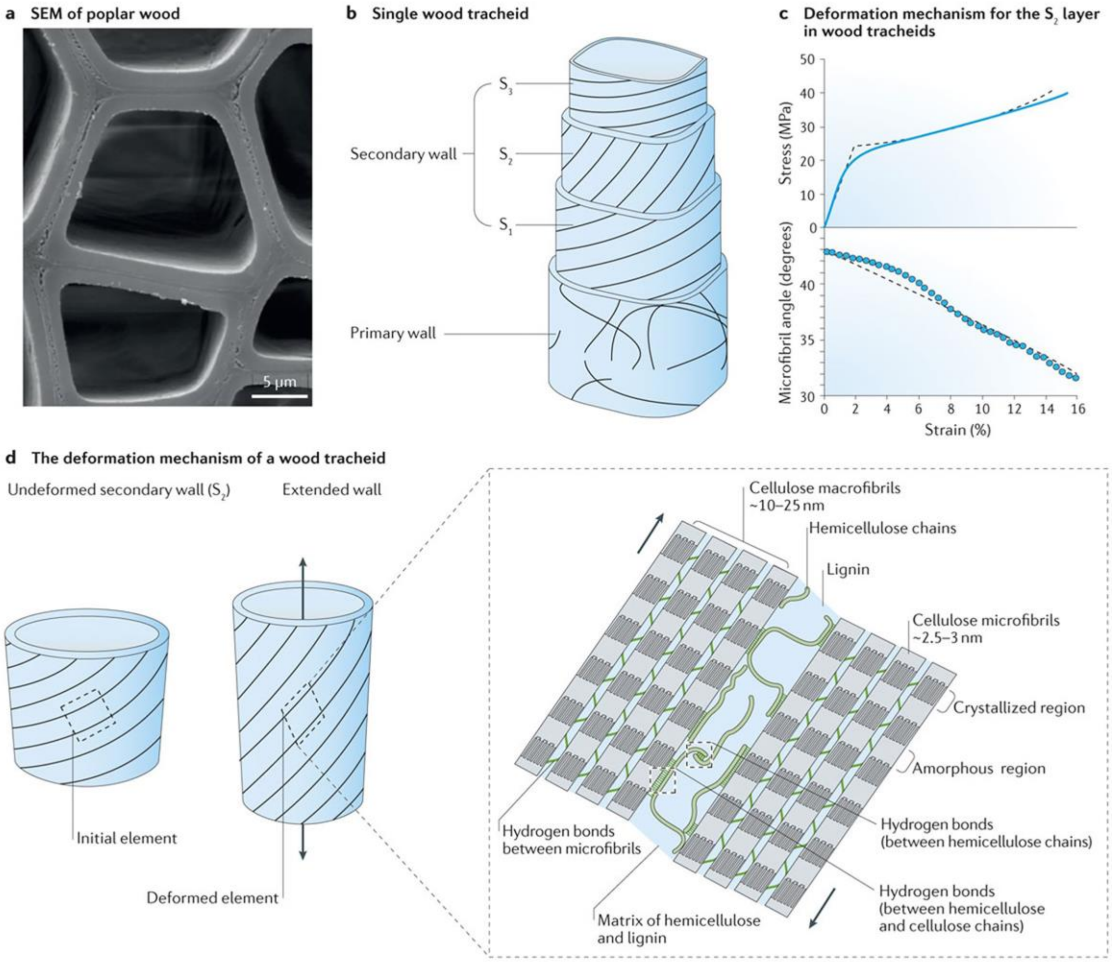

Fig. 2-5: The structure and mechanics of wood. (a) A scanning electron micrograph (SEM) of poplar wood depicting tracheids [124]. (b) The hierarchical structure of an individual wood tracheid. (c) An experimental stress–strain curve for spruce wood, showing large nonlinear strains and a progressive change in microfibril angle with deformation [128, 129]. (d) The deformation mechanism of a wood tracheid under axial tension, resembling that of a spring. The change in conformation of the spring-like tracheid involves shear deformations at the interface. The zoomed-out schematic shows the key components of the interfibrillar interface and its Velcro-like behaviour. Panel a is reproduced with permission from REF. [124], Elsevier. Panel c is adapted with permission from REF. [129], © Carl Hanser Verlag, Muenchen.

Hemicelluloses are very similar to cellulose, but they are more compliant because they lack the two hydrogen bonds flanking the glycosidic linkages in cellulose [130]. As a result, the elastic modulus of hydrated hemicellulose (about 20 MPa [131]) is three orders of magnitude lower than that of cellulose. Hemicelluloses can form hydrogen bonds with cellulose microfibrils, possibly by matching the patterns of hydrogen-bond-forming sites with those of cellulose and forming strong periodic patterns of hydrogen bonds [132]. Lignin is stiffer than hemicellulose under hydrated conditions but softer than cellulose. It has an elastic modulus of approximately 2 GPa under both dry and wet conditions [119, 131, 133]. In the S2 layer, the hydrated mixture of hemicellulose and lignin has an elastic modulus of only about 0.75 GPa (evaluated using the rule of mixtures), which is about 170 times softer than the cellulose microfibrils. The S2 layer is therefore composed of stiff and strong fibres that are bonded by much softer, nanometre-thick interfaces. Although it does not allow for dislocations, wood has a stress–strain behaviour similar to that of ductile metals (Fig. 2-5c). When loaded under tension along the direction of the tracheids, wood initially displays a linear elastic response, with a modulus strongly dependent on the MFA [121, 134]. Wood then displays a yield point (at 10–20 MPa for compressive woods [128]) followed by large and irreversible deformation in excess of 20% strain and with pronounced strain hardening (Fig. 2-5c). The accumulation of damage in the hemicellulose, which was compensated by a reduction in the MFA and in stiffness, was proposed as a mechanism for large deformation [135]. However, these inelastic deformations are not accompanied by a decrease in stiffness, which implies that there is little or no accumulation of damage beyond the elastic limit [136].

In situ small-scale experiments and theoretical models have captured the deformation mechanisms of wood [128, 130, 137]. Recent studies include sophisticated computational models that incorporate interfaces and structures from the molecular scale to the mesoscale [138-141]. In situ X-ray tensile tests on wood and on isolated wood cells have revealed that the inelastic deformations can be attributed to micromechanisms within the wood cell walls [128, 137]. More specifically, the helically wound cellulose microfibrils extend like springs and produce large strains, whereas the stiff microfibrils undergo little or no extension (Fig. 2-5d). In this process, the microfibrils align towards the direction of pulling, the MFA decreases (Fig. 2-5c) and the microfibrils slide on one another, which is resisted by the shearing of the interfaces. A Velcro-like recovery mechanism at the interface between cellulose fibrils has been proposed to explain the stiffness and strength recovery of wood after the release of stress [128]. When a critical shear stress at the interface is exceeded, the bonding — more specifically, the hydrogen bonds between hemicellulose chains and cellulose fibrils — breaks and re-forms to provide cohesive behaviour over a large sliding distance. When the stress is released, the bonds re-form so that the fibrils are locked into their deformed position, without the accumulation of damage or loss of stiffness [128]. It is possible that this Velcrolike behaviour is mediated by the hemicellulose and the lignin, which may entangle and disentangle in the shearing process [128, 142] (Fig. 2-5d). However, this entanglement-based interaction may not be the only potential configuration at the interfaces between cellulose fibrils [129]. Other studies indicate that the entanglement cohesion of hemicellulose (specifically, xylans) is relatively weak and that a minimum length of approximately ten monomer residues of the hemicellulose segment is required for entanglement to produce substantial adhesion [142, 143].

In a modified model for the Velcro-like mechanism, it has been proposed that the interfibrillar cohesion is mediated by hemicellulose chains that bridge adjacent cellulose macrofibrils [130] (Fig. 2-6a). The lateral binding between hemicellulose chains and cellulose fibrils requires that some of the hemicellulose chains form hydrogen bonds and align with the cellulose fibrils over some distance, forming discontinuous hemicellulose bridges across the interface [130, 144]. When the interface is under stress, the hemicellulose loop may detach from one of the fibrils, which provides free length to the hemicellulose chain, releases some of the bridging strength and allows shear deformations between fibrils (Fig. 2-6b). When the stress is released, the hemicellulose loop can re-approach and re-attach to the cellulose fibrils through hydrogen bonding to maintain the overall stiffness. In this model for the hemicellulose chain segments between cellulose microfibrils, both entanglement and bridging cohesion could coexist [130] (Fig. 2-6a). These combined mechanisms were captured by mesoscale coarse-grain computational modelling [139]. The model demonstrated how entanglement and bridging govern the shearing of the interfaces, which occurs by the reconfiguration of the hemicellulose interface and by the 'stick–slip' of the hemicellulose, a phenomenon governed by the dynamic breaking and re-forming of hydrogen bonds at the interfaces between hemicellulose and cellulose, onto the cellulose microfibrils (Fig. 2-6c). This model also captured how large shear strains at the interfaces translate into large tensile strains at the macroscale through the cellulose MFAs. More recently, molecular models with atomistic resolution, and including the cellulose fibril, the hemicellulose and the lignin, revealed more details of these interfacial mechanisms [138] (Fig. 2-6d). These models uncovered an initial elastic response, followed by the yielding of the matrix. Finally, the matrix sled along the cellulose fibrils in a stick–slip manner. These molecular mechanisms provide cohesive stress during shear deformation over long sliding distances and without the loss of stiffness or strength, much like a dislocation motion in metals. Although the molecular mechanisms occurring at the interfibrillar interfaces have yet to be observed experimentally, the models reviewed here are based on the fundamental knowledge of the molecular interactions among hemicellulose, lignin and cellulose and therefore provide strong support for the Velcro-like mechanism.

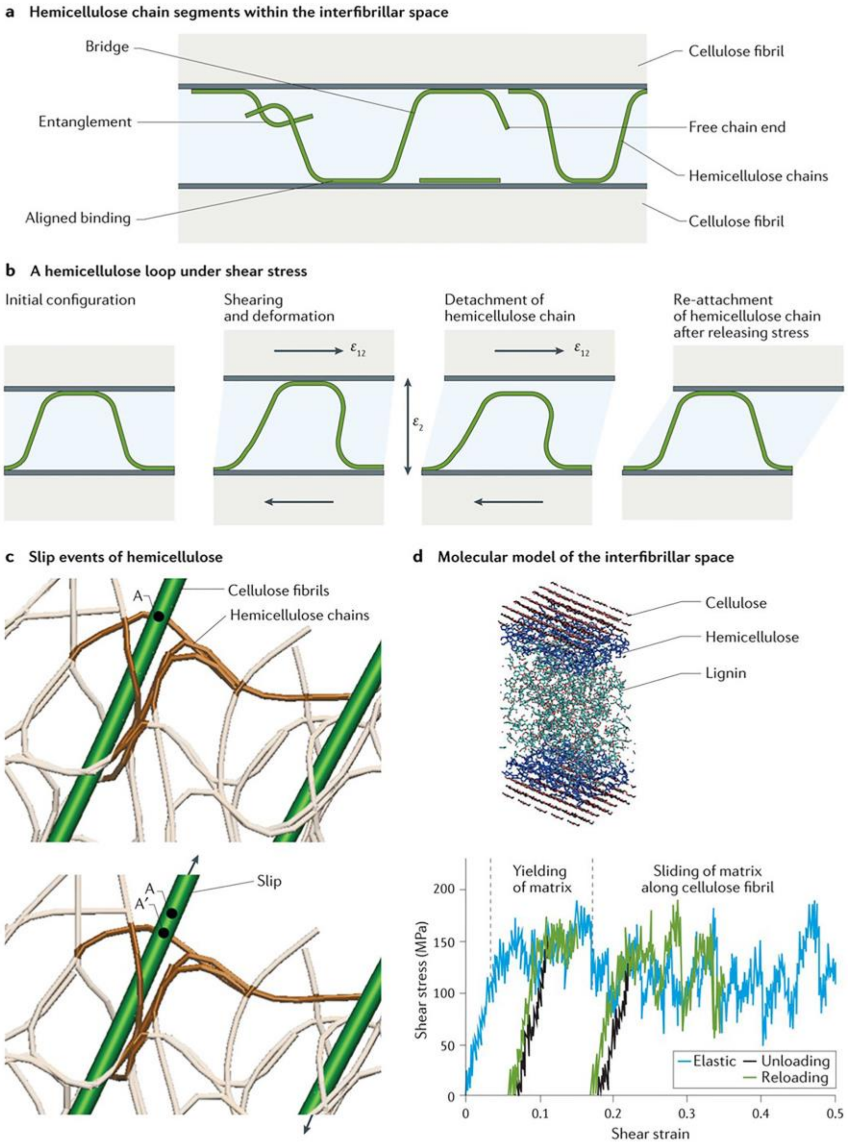

Fig. 2-6: The structure and mechanics of the interfaces between cellulose fibrils. (a) Possible configurations of the hemicellulose chain segments within the interfibrillar space. (b) A sequence showing the debonding of a hemicellulose loop from cellulose macrofibrils, and the re-approach and re-attachment after the releasing of shear stress as described in Altaner and Jarvis' model [130]. (c) Slip events of hemicellulose captured in a coarse-grain model [139]. (d) A more detailed atomistic model including cellulose crystals, hemicellulose and lignin. When this model is deformed under shear, an initial linear elastic region is followed by matrix yielding and then sliding of the matrix on the cellulose. Through these inelastic processes, the stiffness of the interface is preserved [138]. A, attachment point between hemicellulose and cellulose before slip; A′, attachment point between hemicellulose and cellulose after slip; ε_{12}, shear strain; ε_{2}, extensional across the interface. Panels a and b are adapted with permission from REF. [130], Elsevier. Panel c is adapted with permission from REF. [139], Royal Society of Chemistry. Panel d is adapted with permission from REF. [138], Elsevier.

Another important set of interfaces in wood consists of the middle lamellae, which bond the tracheids together [145] (Fig. 2-5a). This thin interface is composed of lignin (~50% by weight) and other compounds, such as pectic acids, arabinose and galactose [145-147], and it is weaker than the tracheid walls. The fracture of wood is a competition between the fracture of the tracheids and the fracture of the middle lamellae. In the splitting fracture direction, along the direction of the tracheids, wood is stressed in a tangential direction and the crack propagates in the longitudinal direction. In this configuration, cracks propagate along the middle lamellae, leaving the tracheids largely intact [148]. The splitting mode, in which wood is the weakest, provides estimates for the toughness [63, 149] of the middle lamellae (0.1–0.3 kJ m^{-2}) and the tensile strength [63, 150] in the order of 1–10 MPa, which is one to two orders of magnitude weaker than the toughness and strength of wood when it is fractured across the grains [63]. Experimental data and observations show that cracks propagating in wood strongly interact with the weak lamella interfaces [148, 149]. From this point of view, wood can be described as a fibre-reinforced composite [149], in which the fibres are the individual tracheids, and the weaker middle lamellae govern toughening mechanisms, such as crack deflection and fibre pullout [149], in a similar way to osteons in cortical bone.

2.6 Summary and outlook

The examples discussed in this Review highlight the critical role of interfaces in the deformation and fracture of biological materials. A material properties chart (Fig. 2-7) of the strength and toughness of bone, nacre and wood, and their interfaces, illustrates that the strength and toughness of the interfaces are two to three orders of magnitude lower than the strength and toughness of the materials themselves. As a general rule, the interfaces must be sufficiently strong to maintain cohesion between the building blocks and to ensure the structural integrity of the material. However, the interface must be considerably weaker than the rest of the material to channel deformations and cracks, and for the intricate architectures to generate attractive mechanisms and properties. Models developed for synthetic layered ceramics can be useful as guidelines: for example, if an interface was designed to deflect cracks then its toughness should be less than one-quarter of the toughness of the surrounding material [151]. The case of ductile interfaces is more complex, but models now exist to guide the design of the interfacial strength [45, 152].

Natural materials, such as mollusc shells, bone or wood, contain interfaces whose strength has been finely tuned through evolution to fulfil these conflicting requirements. The exact strength required is not a universal value, but it depends on the strength of the building blocks, the architecture of the building blocks, the loading mode of the material and, ultimately, its function within the larger organism. Another universal characteristic of interfaces in natural materials is their ability to maintain cohesion during openings or over sliding distances, which can be several times their thickness. These large deformations at the interface are critical for energy absorption and for producing large deformations at the macroscale, as well as powerful toughening mechanisms [38, 153]. The interfaces of nacre, bone and wood illustrate three strategies to achieve this behaviour: first, organic materials show large deformations generated by molecular sacrificial bonds (as seen in nacre and in nanoscale bone); second, frictional forces provide resistance to interfacial sliding over unlimited sliding distances, as seen in nacre [19], at interfibrillar interfaces [95] and at the cement line [107] in bone; third, hydrogen bonds, which are inherently weak, can still provide appreciable cohesion in large coordinated numbers [154]. Hydrogen bonds can break and re-form dynamically, providing cohesion over long sliding distances (as seen in wood). The composition and mechanics of the interfaces are finely tuned to interact with the architecture to produce desirable properties.

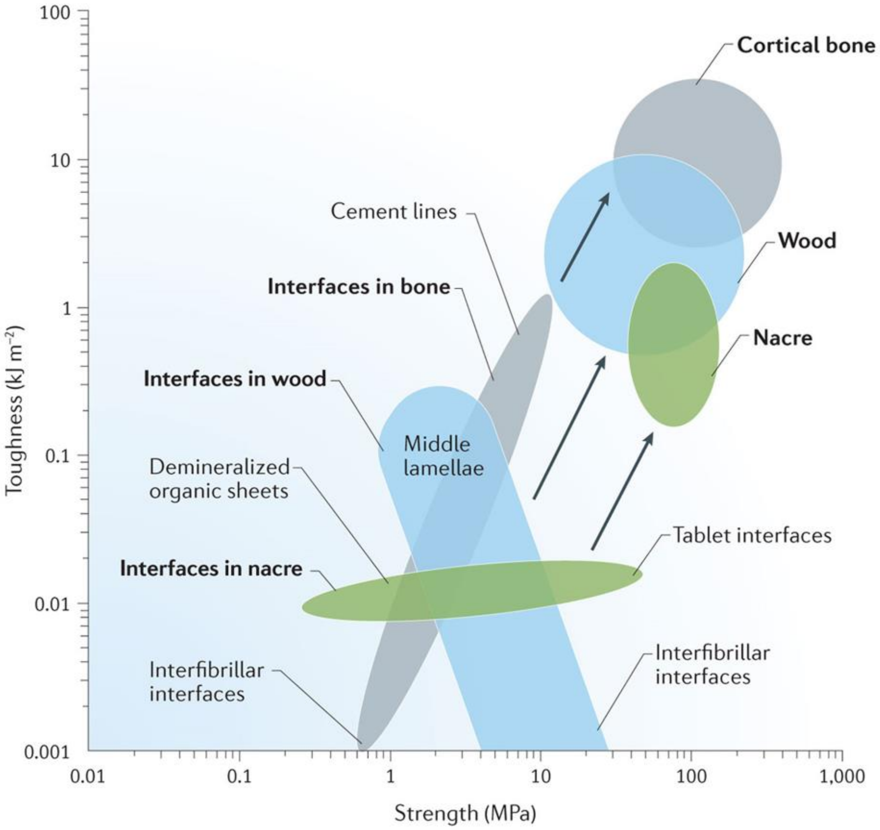

Fig. 2-7: A material properties chart. The toughness and strength for nacre [19, 22, 39], cortical bone [63, 105], wood [149, 150] and their interfaces [16, 22, 63, 105, 128, 129, 150].

Nacre, bone and wood have different types of architectures, building blocks and interfaces, but the mechanical performance of the three materials relies on similar toughening mechanisms. The interfaces generate inelastic deformations at the nanoscale (as seen for bone and wood) or at the microscale (as seen for nacre). Large inelastic deformations redistribute stresses around defects and cracks [155], and reduce the sharpness of crack tips [98]. Inelastic deformations also dissipate mechanical energy that would otherwise be used to propagate cracks. This mechanism is prominent in nacre, and it serves as its main toughening mechanism, with a dissipative process zone in the order of millimetres in size forming around defects and cracks [38]. Other toughening mechanisms that are common to nacre, bone and wood are crack deflection and twisting, as well as crack bridging and fibre or tablet pullout. Interestingly, for bone and wood, ductility is generated at the nanoscale, although the most effective crack deflection and bridging mechanisms occur at the microscale.

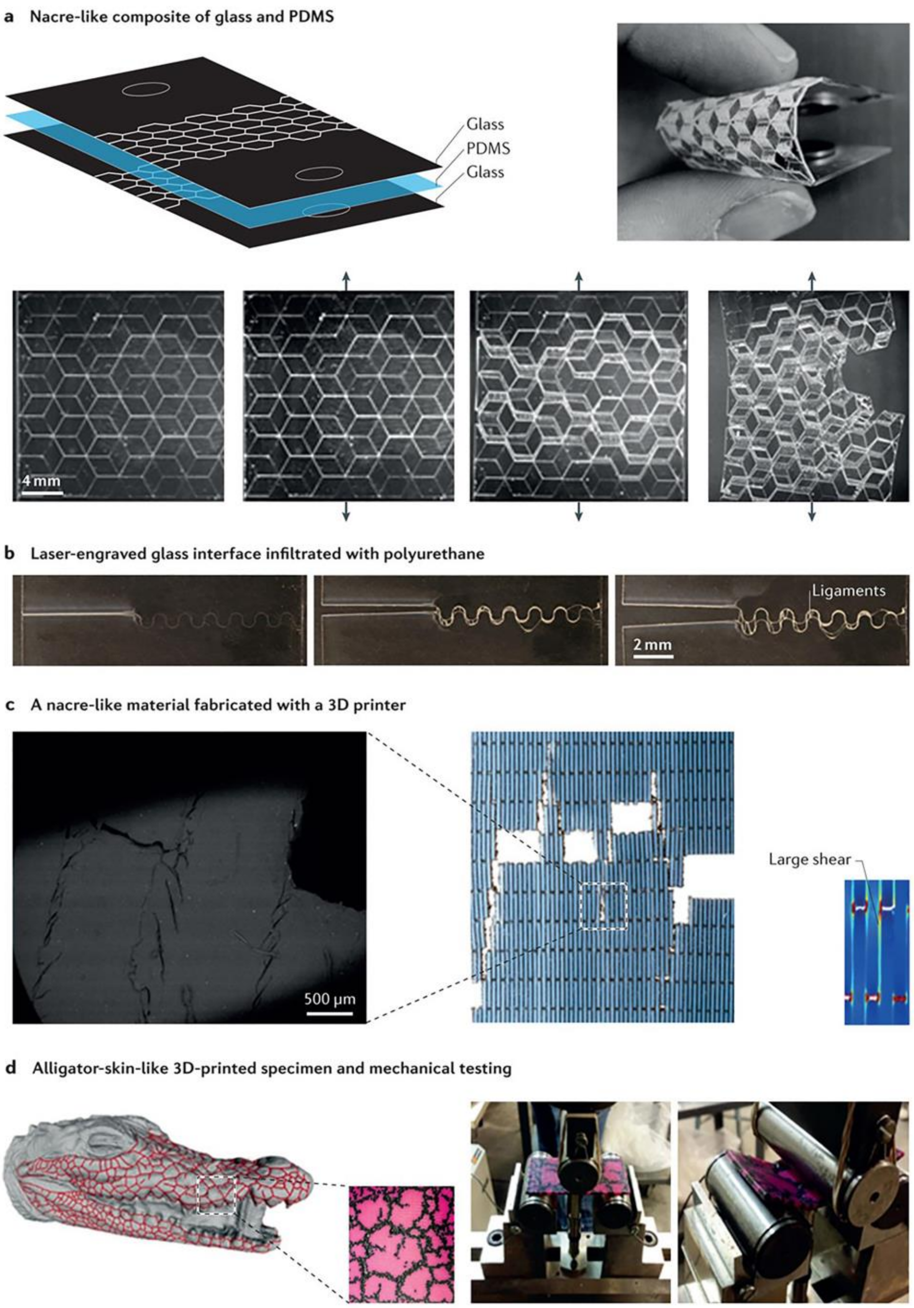

Fig. 2-8: Synthetic materials based on the architectures and interfaces of biological materials. (a) Nacre-like composite of glass and polydimethylsiloxane (PDMS) showing large deformation and progressive failure [30]. (b) A bioinspired laser-engraved suture in glass infiltrated with polyurethane [156]. (c) A nacre-like material fabricated with a multimaterial 3D printer. A stiff polymer is used for the bricks, and a compliant elastomer is used for the mortar [157]. (d) 3D printing can also be used to fabricate bioinspired interfaces with complex morphologies and structural hierarchy, as shown in this alligator-skin-like hard, but flexible, plate. Panel b is from REF. [156], Nature Publishing Group. Panel c is from REF. [157], © IOP Publishing. Reproduced with permission. All rights reserved.

The development of bioinspired composite materials that duplicate the mechanical performance of natural materials has been an active research area for the past two decades [2, 6, 9, 20, 29, 158, 159]. In particular, high performance synthetic composites that mimic the architectures of natural materials have emerged. It is now clear that the performance of these composites relies on interfaces that mirror the attributes of natural interfaces. For example, polymers, such as acrylic foams [26], polymethylmethacrylate [160, 161], polyvinyl alcohol [161, 162] or chitosan [163], were used as interfaces between stiff ceramic layers or platelets to duplicate some of the attributes of the interfaces in nacre — namely, high adhesion, extensibility and energy absorption. To make the most of the ductility and energy absorption capabilities of the ductile polymers, the adhesion to the ceramic inclusions must be very strong, and surface functionalization with (3-aminopropyl)triethoxysilane is sometimes used to form covalent bonds between the polymer and the ceramic [163, 164]. Partially crosslinked polymers or high-molecular-weight uncrosslinked polydimethylsiloxane have also achieved large strains via rheological flow [30] (Fig. 2-8a). In other cases, elastomers were used in combination with glass or rigid polymers in more complex bioinspired architectures [156, 165] (Fig. 2-8b–d). Proteins with sacrificial bonds and the dynamic breaking and healing of hydrogen bonds can be duplicated using polymers with electric charges (polyelectrolytes) [164, 166]. Bioinspired polymers with modular loops that display the same behaviour as proteins, such as lustrin A, were also successfully synthesized [27, 167]. An interesting fabrication route is to use genetics to engineer biopolymeric interfaces with tunable properties [28]. Frictional interaction at the interfaces is also used in composites, most notably in fibre-reinforced composites but also in more recent bioinspired materials [156, 168, 169]. Recent methods, such as 3D laser engraving [156] (Fig. 2-8b) or multi-material 3D printing [165] (Fig. 2-

8a,b), will enable the integration of complex architectures with tunable interface properties. Mechanisms at the interfaces and at the level of the architecture of the material operate in synergy to produce high properties at the macroscale. Capturing these synergies in synthetic materials presents challenges in terms of design and fabrication. Natural materials can inspire new strategies to design interfaces with attractive mechanical responses, which are essential for the design of advanced composite materials.

2.7 References

1. Sarikaya, M. and I.A. Aksay, eds. *Biomimetics, design and processing of Materials*. Polymers and complex materials, ed. AIP. 1995: Woodbury, NY.
2. Mayer, G., *Rigid biological systems as models for synthetic composites.* Science, 2005. **310**(5751): p. 1144-1147.
3. Fratzl, P. and R. Weinkamer, *Nature's hierarchical materials.* Progress in Materials Science, 2007. **52**(8): p. 1263-1334.
4. Barthelat, F., *Biomimetics for next generation materials.* Philosophical transactions. Series A, Mathematical, physical, and engineering sciences, 2007. **365**(1861): p. 2907-2919.
5. Meyers, M.A., et al., *Biological materials: Structure and mechanical properties.* Progress in Materials Science, 2008. **53**(1): p. 1-206.
6. Espinosa, H.D., et al., *Merger of structure and material in nacre and bone - Perspectives on de novo biomimetic materials.* Progress in Materials Science, 2009. **54**(8): p. 1059-1100.
7. Nair , A.K., et al., *Mechanical and interface properties of biominerals: Atomistic to coarse grained modeling," In: Biomineralization Handbook: Characterization of biomineral and biomimetic materials* in *Biomineralization Handbook: Characterization of biomineral and biomimetic materials*, E. DiMasi, Editor. 2014, CRC Press.
8. Ritchie, R.O., *The conflicts between strength and toughness.* Nature Materials, 2011. **10**(11): p. 817-822.
9. Naleway, S.E., et al., *Structural design elements in biological materials: application to bioinspiration.* Advanced Materials, 2015. **27**(37): p. 5455-5476.
10. Barthelat, F., *Architectured materials in engineering and biology: fabrication, structure, mechanics and performance.* International Materials Reviews, 2015. **60**(8): p. 413-430.
11. Ackbarow, T. and M.J. Buehler, *Hierarchical coexistence of universality and diversity controls robustness and multi-functionality in protein materials.* Journal of Computational and Theoretical Nanoscience, 2008. **5(7)**: p. 1193-1204.
12. Buehler, M.J., *Tu(r)ning weakness to strength.* Nano Today, 2010. **5**(5): p. 379-383.
13. Cranford, S. and M.J. Buehler, *Biomateriomics*. 2012, New York: Springer.
14. Dunlop, J.W.C., R. Weinkamer, and P. Fratzl, *Artful interfaces within biological materials.* Materials Today, 2011. **14**(3): p. 70-78.
15. Ritchie, R.O., M.J. Buehler, and P. Hansma, *Plasticity and toughness in bone.* Physics Today, 2009. **62**(6): p. 41-47.

16. Dastjerdi, A.K., R. Rabiei, and F. Barthelat, *The weak interfaces within tough natural composites: Experiments on three types of nacre.* Journal of the Mechanical Behavior of Biomedical Materials, 2013. **19**: p. 50-60.
17. Spivak, D.I., et al., *Category theoretic analysis of hierarchical protein materials and social networks.* Plos One, 2011. **6**(9).
18. Yahyazadehfar, M. and D. Arola, *The role of organic proteins on the crack growth resistance of human enamel.* Acta Biomaterialia, 2015. **19**: p. 33-45.
19. Wang, R.Z., et al., *Deformation mechanisms in nacre.* Journal of Materials Research, 2001. **16**(9): p. 2485-2493.
20. Barthelat, F. and H.D. Espinosa, *An experimental investigation of deformation and fracture of nacre-mother of pearl.* Experimental Mechanics, 2007. **47**(3): p. 311-324.
21. Currey, J.D., *Mechanical properties of mother of pearl in tension.* Proceedings of the Royal Society of London B, 1977. **196**(1125): p. 443-463.
22. Barthelat, F., et al., *On the mechanics of mother-of-pearl: A key feature in the material hierarchical structure.* Journal of the Mechanics and Physics of Solids, 2007. **55**(2): p. 306-337.
23. Weiner, S. and H.D. Wagner, *The material bone: structure mechanical function relations.* Annual Review of Materials Science, 1998. **28**: p. 271-298.
24. Rho, J.Y., L. Kuhn-Spearing, and P. Zioupos, *Mechanical properties and the hierarchical structure of bone.* Medical Engineering & Physics, 1998. **20**(2): p. 92-102.
25. Giesa, T., D.I. Spivak, and M.J. Buehler, *Category theory based solution for the building block replacement problem in materials design.* Advanced Engineering Materials, 2012. **14**(9): p. 810-817.
26. Mayer, G., *New classes of tough composite materials - Lessons from natural rigid biological systems.* Materials Science & Engineering C-Biomimetic and Supramolecular Systems, 2006. **26**(8): p. 1261-1268.
27. Kushner, A.M., et al., *Biomimetic design of reversibly unfolding cross-linker to enhance mechanical properties of 3D network polymers.* Journal of the American Chemical Society, 2007. **129**(46): p. 14110-+.
28. Laaksonen, P., G.R. Szilvay, and M.B. Linder, *Genetic engineering in biomimetic composites.* Trends in Biotechnology, 2012. **30**(4): p. 191-197.
29. Studart, A.R., *Towards high-performance bioinspired composites.* Advanced Materials, 2012. **24**(37): p. 5024-5044.
30. Chintapalli, R.K., et al., *Strain rate hardening: A hidden but critical mechanism for biological composites?* Acta Biomaterialia, 2014. **10**(12): p. 5064-5073.
31. Currey, J.D. and J.D. Taylor, *The mechanical behavior of some molluscan hard tissues.* Journal of Zoology (London), 1974. **173**(3): p. 395-406.
32. Jackson, A.P., et al., *The mechanical design of nacre.* Proceedings of the Royal Society of London. Series B. Biological Sciences, 1988. **234**(1277): p. 415-440.
33. Colfen, H. and M. Antonietti, *Mesocrystals: Inorganic superstructures made by highly parallel crystallization and controlled alignment.* Angewandte Chemie-International Edition, 2005. **44**(35): p. 5576-5591.
34. Rousseau, M., et al., *Multiscale structure of sheet nacre.* Biomaterials, 2005. **26**(31): p. 6254-6262.
35. Marin, F., N. Le Roy, and B. Marie, *The formation and mineralization of mollusk shell.* Frontiers in bioscience (Scholar edition), 2012. **4**: p. 1099-125.

36. Li, X.D., Z.H. Xu, and R.Z. Wang, *In situ observation of nanograin rotation and deformation in nacre.* Nano Letters, 2006. **6**(10): p. 2301-2304.
37. Smith, B.L., et al., *Molecular mechanistic origin of the toughness of natural adhesives, fibres and composites.* Nature (London), 1999. **399**(6738): p. 761-763.
38. Barthelat, F. and R. Rabiei, *Toughness amplification in natural composites.* Journal of the Mechanics and Physics of Solids, 2011. **59**(4): p. 829-840.
39. Rabiei, R., S. Bekah, and F. Barthelat, *Failure mode transition in nacre and bone-like materials.* Acta Biomaterialia, 2010. **6**: p. 4081-4089.
40. Levi-Kalisman, Y., et al., *Structure of the nacreous organic matrix of a bivalve mollusk shell examined in the hydrated state using Cryo-TEM.* Journal of Structural Biology, 2001. **135**(1): p. 8-17.
41. Jackson, A.P. and J.F.V. Vincent, *Application of surface analytical techniques to the study of fracture surfaces of mother-of-pearl.* Journal of Materials Science Letters, 1986. **5**.
42. Menig, R., et al., *Quasi-static and dynamic mechanical response of haliotis rufescens (abalone) shells.* Acta Materialia, 2000. **48**.
43. Lopez, M.I., P.E.M. Martinez, and M.A. Meyers, *Organic interlamellar layers, mesolayers and mineral nanobridges: Contribution to strength in abalone (Haliotis rufescence) nacre.* Acta Biomaterialia, 2014. **10**(5): p. 2056-2064.
44. Shao, C. and S. Keten, *Stiffness enhancement in nacre-inspired nanocomposites due to nanoconfinement.* Scientific reports, 2015. **5**: p. 16452-16452.
45. Barthelat, F., A.K. Dastjerdi, and R. Rabiei, *An improved failure criterion for biological and engineered staggered composites.* Journal of The Royal Society Interface, 2013. **10**(79): p. 20120849.
46. Nabavi, A., et al., *A novel method for net-shape manufacturing of metal–metal sulfide cermets.* Journal of Materials Science, 2014. **49**(23): p. 8095-8106.
47. Huang, Z. and X. Li, *Nanoscale structural and mechanical characterization of heat treated nacre.* Materials Science & Engineering C-Materials for Biological Applications, 2009. **29**(6): p. 1803-1807.
48. Marin, F., et al., *Molluscan shell proteins: Primary structure, origin, and evolution,* in *Current Topics in Developmental Biology, Vol 80*, G.P. Schatten, Editor. 2008. p. 209-276.
49. Shen, X.Y., et al., *Molecular cloning and characterization of lustrin A, a matrix protein from shell and pearl nacre of Haliotis rufescens.* Journal of Biological Chemistry, 1997. **272**(51): p. 32472-32481.
50. Vincent, J.F.V. and U.G.K. Wegst, *Design and mechanical properties of insect cuticle.* Arthropod Structure & Development, 2004. **33**(3): p. 187-199.
51. Schaeffer, T.E., et al., *Does abalone nacre form by heteroepitaxial nucleation or by growth through mineral bridges?* Chemistry of Materials, 1997. **9**(8): p. 1731-1740.
52. Weiss, I.M., *Jewels in the pearl.* Chembiochem, 2010. **11**(3): p. 297-300.
53. Qi, H.J., C. Ortiz, and M.C. Boyce, *Mechanics of biomacromolecular networks containing folded domains.* Journal of Engineering Materials and Technology-Transactions of the Asme, 2006. **128**(4): p. 509-518.
54. Lopez, M.I. and M.A. Meyers, *The organic interlamellar layer in abalone nacre: Formation and mechanical response.* Materials Science & Engineering C-Materials for Biological Applications, 2016. **58**: p. 7-13.

55. Weiss, I.M., et al., *Covalent modification of chitin with silk-derivatives acts as an amphiphilic self-organizing template in nacre biomineralisation.* Journal of Structural Biology, 2009. **167**(1): p. 68-75.
56. Suetake, T., et al., *Chitin-binding proteins in invertebrates and plants comprise a common chitin-binding structural motif.* Journal of Biological Chemistry, 2000. **275**(24): p. 17929-17932.
57. Suzuki, M., et al., *An acidic matrix protein, Pif, is a key macromolecule for nacre formation.* Science, 2009. **325**(5946): p. 1388-1390.
58. Laaksonen, P., et al., *Genetic Engineering of Biomimetic Nanocomposites: Diblock Proteins, Graphene, and Nanofibrillated Cellulose.* Angewandte Chemie-International Edition, 2011. **50**(37): p. 8688-8691.
59. Gent, A.N., J.B. Suh, and S.G. Kelly, III, *Mechanics of rubber shear springs.* International Journal of Non-Linear Mechanics, 2007. **42**(2): p. 241-249.
60. Pascal, J., et al., *Rubber-like adhesive in simple shear - stress-analysis and fracture morphology of a single lap joint.* Journal of Adhesion Science and Technology, 1994. **8**(5): p. 553-573.
61. Song, F., X.H. Zhang, and Y.L. Bai, *Microstructure and characteristics in the organic matrix layers of nacre.* Journal of Materials Research, 2002. **17**: p. 1567-1570.
62. Currey, J.D., *Bones : structure and mechanics*. 2002, Princeton, NJ: Princeton University Press.
63. Wegst, U.G.K. and M.F. Ashby, *The mechanical efficiency of natural materials.* Philosophical Magazine, 2004. **84**(21): p. 2167-2181.
64. Young, M.F., *Bone matrix proteins: their function, regulation, and relationship to osteoporosis.* Osteoporosis International, 2003. **14**: p. S35-S42.
65. Hui, S.L., C.W. Slemenda, and C.C. Johnston, *Age and bone mass as predictors of fracture in a prospective-study.* Journal of Clinical Investigation, 1988. **81**(6): p. 1804-1809.
66. Burr, D.B., *The contribution of the organic matrix to bone's material properties.* Bone, 2002. **31**(1): p. 8-11.
67. Reznikov, N., R. Shahar, and S. Weiner, *Bone hierarchical structure in three dimensions.* Acta Biomaterialia, 2014. **10**(9): p. 3815-3826.
68. Buehler, M.J., *Nature designs tough collagen: Explaining the nanostructure of collagen fibrils.* Proceedings of the National Academy of Sciences of the United States of America, 2006. **103**(33): p. 12285-12290.
69. Uzel, S.G.M. and M.J. Buehler, *Molecular structure, mechanical behavior and failure mechanism of the C-terminal cross-link domain in type I collagen.* Journal of the Mechanical Behavior of Biomedical Materials, 2011. **4**(2): p. 153-161.
70. Shen, Z.L., et al., *Stress-strain experiments on individual collagen fibrils.* Biophysical Journal, 2008. **95**(8): p. 3956-3963.
71. Hassenkam, T., et al., *High-resolution AFM imaging of intact and fractured trabecular bone.* Bone, 2004. **35**(1): p. 4-10.
72. Buehler, M.J., *Molecular nanomechanics of nascent bone: fibrillar toughening by mineralization.* Nanotechnology, 2007. **18**(29).
73. Knott, L. and A.J. Bailey, *Collagen cross-links in mineralizing tissues: A review of their chemistry, function, and clinical relevance.* Bone, 1998. **22**(3): p. 181-187.

74. Launey, M.E., M.J. Buehler, and R.O. Ritchie, *On the Mechanistic Origins of Toughness in Bone*, in *Annual Review of Materials Research, Vol 40*, D.R. Clarke, M. Ruhle, and F. Zok, Editors. 2010. p. 25-53.
75. Ural, A. and D. Vashishth, *Hierarchical perspective of bone toughness - from molecules to fracture.* International Materials Reviews, 2014. **59**(5): p. 245-263.
76. Ritchie, R.O., et al., *A fracture mechanics and mechanistic approach to the failure of cortical bone.* Fatigue & Fracture of Engineering Materials & Structures, 2005. **28**(4): p. 345-371.
77. Thurner, P.J. and O.L. Katsamenis, *The role of nanoscale toughening mechanisms in osteoporosis.* Current Osteoporosis Reports, 2014. **12**(3): p. 351-356.
78. Zimmermann, E.A., et al., *Age-related changes in the plasticity and toughness of human cortical bone at multiple length scales.* Proceedings of the National Academy of Sciences of the United States of America, 2011. **108**(35): p. 14416-14421.
79. Taylor, D., J.G. Hazenberg, and T.C. Lee, *Living with cracks: damage and repair in human bone.* Nature Materials, 2007. **6**(4): p. 263-268.
80. Gupta, H.S., et al., *Fibrillar level fracture in bone beyond the yield point.* International Journal of Fracture, 2006. **139**(3-4): p. 425-436.
81. Fantner, G.E., et al., *Sacrificial bonds and hidden length dissipate energy as mineralized fibrils separate during bone fracture.* Nature Materials, 2005. **4**(8): p. 612-616.
82. Gupta, H.S., et al., *Nanoscale deformation mechanisms in bone.* Nano Letters, 2005. **5**(10): p. 2108-2111.
83. Poundarik, A.A., et al., *Dilatational band formation in bone.* Proceedings of the National Academy of Sciences of the United States of America, 2012. **109**(47): p. 19178-19183.
84. Schwiedrzik, J., et al., *In situ micropillar compression reveals superior strength and ductility but an absence of damage in lamellar bone.* Nature Materials, 2014. **13**(7): p. 740-747.
85. Nalla, R.K., J.H. Kinney, and R.O. Ritchie, *Mechanistic fracture criteria for the failure of human cortical bone.* Nature Materials, 2003. **2**(3): p. 164-168.
86. Fantner, G.E., et al., *Influence of the degradation of the organic matrix on the microscopic fracture behavior of trabecular bone.* Bone, 2004. **35**(5): p. 1013-1022.
87. Hang, F., H.S. Gupta, and A.H. Barber, *Nanointerfacial strength between non-collagenous protein and collagen fibrils in antler bone.* Journal of the Royal Society Interface, 2014. **11**(92).
88. Poundarik, A.A. and D. Vashishth, *Multiscale imaging of bone microdamage.* Connective Tissue Research, 2015. **56**(2): p. 87-98.
89. Hansma, P.K., et al., *Sacrificial bonds in the interfibrillar matrix of bone.* Journal of musculoskeletal & neuronal interactions, 2005. **5**(4): p. 313-5.
90. Gupta, H.S., et al., *Evidence for an elementary process in bone plasticity with an activation enthalpy of 1 eV.* Journal of the Royal Society Interface, 2007. **4**(13): p. 277-282.
91. Seref-Ferlengez, Z., et al., *Structural and mechanical repair of diffuse damage in cortical bone in vivo.* Journal of Bone and Mineral Research, 2014. **29**(12): p. 2537-2544.
92. Thompson, J.B., et al., *Bone indentation recovery time correlates with bond reforming time.* Nature, 2001. **414**(6865): p. 773-776.
93. Fantner, G.E., et al., *Nanoscale ion mediated networks in bone: Osteopontin can repeatedly dissipate large amounts of energy.* Nano Letters, 2007. **7**(8): p. 2491-2498.

94. Thurner, P.J., et al., *Osteopontin deficiency increases bone fragility but preserves bone mass.* Bone, 2010. **46**(6): p. 1564-1573.
95. Tai, K., F.-J. Ulm, and C. Ortiz, *Nanogranular origins of the strength of bone.* Nano Letters, 2006. **6**(11): p. 2520-2525.
96. Bailey, A.J., *Molecular mechanisms of ageing in connective tissues.* Mechanisms of Ageing and Development, 2001. **122**(7): p. 735-755.
97. Tang, S.Y., U. Zeenath, and D. Vashishth, *Effects of non-enzymatic glycation on cancellous bone fragility.* Bone, 2007. **40**(4): p. 1144-1151.
98. Ker, R.F., *Mechanics of tendon, from an engineering perspective.* International Journal of Fatigue, 2007. **29**(6): p. 1001-1009.
99. Puxkandl, R., et al., *Viscoelastic properties of collagen: synchrotron radiation investigations and structural model.* Philosophical Transactions of the Royal Society of London Series B-Biological Sciences, 2002. **357**(1418): p. 191-197.
100. Khayer Dastjerdi, A. and F. Barthelat, *Teleost fish scales amongst the toughest collagenous materials.* Journal of the Mechanical Behavior of Biomedical Materials, 2015. **52**: p. 95-107.
101. Yang, W., et al., *Protective role of Arapaima gigas fish scales: Structure and mechanical behavior.* Acta Biomaterialia, 2014. **10**(8): p. 3599-3614.
102. Ascenzi, M.-G. and A.K. Roe, *The osteon: the micromechanical unit of compact bone.* Frontiers in Bioscience-Landmark, 2012. **17**: p. 1551-1581.
103. Skedros, J.G., et al., *Cement lines of secondary osteons in human bone are not mineral-deficient: New data in a historical perspective.* Anatomical Record Part a-Discoveries in Molecular Cellular and Evolutionary Biology, 2005. **286A**(1): p. 781-803.
104. Burr, D.B., M.B. Schaffler, and R.G. Frederickson, *Composition of the cement line and its possible mechanical role as a local interface inhuman compact-bone.* Journal of Biomechanics, 1988. **21**(11): p. 939-&.
105. Koester, K.J., J.W. Ager, III, and R.O. Ritchie, *The true toughness of human cortical bone measured with realistically short cracks.* Nature Materials, 2008. **7**(8): p. 672-677.
106. O'Brien, F.J., D. Taylor, and T.C. Lee, *Microcrack accumulation at different intervals during fatigue testing of compact bone.* Journal of Biomechanics, 2003. **36**(7): p. 973-980.
107. Bigley, R.F., et al., *Osteon interfacial strength and histomorphometry of equine cortical bone.* Journal of Biomechanics, 2006. **39**(9): p. 1629-1640.
108. Ascenzi, A. and E. Bonucci, *Shearing properties of single osteons.* Anatomical Record, 1972. **172**(3): p. 499-&.
109. Dong, X.N., X. Zhang, and X.E. Guo, *Interfacial strength of cement lines in human cortical bone.* Mechanics & chemistry of biosystems : MCB, 2005. **2**(2): p. 63-8.
110. Zioupos, P. and J.D. Currey, *The extent of microcracking and the morphology of microcracks in damaged bone.* Journal of Materials Science, 1994. **29**(4): p. 978-986.
111. Mellon, S.J. and K.E. Tanner, *Bone and its adaptation to mechanical loading: a review.* International Materials Reviews, 2012. **57**(5): p. 235-255.
112. Ager, J., G. Balooch, and R.O. Ritchie, *Fracture, aging and disease in bone.* Journal of Materials Research, 2006. **21**: p. 1878-1892.
113. Piekarsk, K., *Fracture of bone.* Journal of Applied Physics, 1970. **41**(1): p. 215-&.
114. Hiller, L.P., et al., *Osteon pullout in the equine third metacarpal bone: effects of ex vivo fatigue.* Journal of Orthopaedic Research, 2003. **21**(3): p. 481-488.

115. Buehler, M.J. and T. Ackbarow, *Fracture mechanics of protein materials.* Materials Today, 2007. **10**(9): p. 46-58.
116. Zhang, Z., Y.-W. Zhang, and H. Gao, *On optimal hierarchy of load-bearing biological materials.* Proceedings of the Royal Society B-Biological Sciences, 2011. **278**(1705): p. 519-525.
117. Peterlik, H., et al., *From brittle to ductile fracture of bone.* Nature Materials, 2006. **5**(1): p. 52-55.
118. Zioupos, P., J.D. Currey, and A.J. Sedman, *An examination of the micromechanics of failure of bone and antler by acoustic-emission tests and laser-scanning-confocal-microscopy.* Medical Engineering & Physics, 1994. **16**(3): p. 203-212.
119. Gibson, L.J., *The hierarchical structure and mechanics of plant materials.* Journal of The Royal Society Interface, 2012. **9**(76): p. 2749-2766.
120. Jeronimidis, G.J., *The fracture behavior of wood and the relations between toughness and morphology.* Proceedings of the Royal Society of London B, 1980. **208**: p. 447-460.
121. Gordon, J.E. and G. Jeronimidis, *Composites with high work of fracture.* Phil. Trans. R. Soc. Lond., 1980. **294**: p. 545-550.
122. Lucas, P.W., H.T.W. Tan, and P.Y. Cheng, *The toughness of secondary cell wall and woody tissue.* Philosophical Transactions of the Royal Society B: Biological Sciences, 1997. **352**(1351): p. 341-352.
123. Fratzl, P., *Cellulose and collagen: from fibres to tissues.* Curr. Opin. Colloid Interface Sci., 2003. **8**: p. 145-155.
124. Pilate, G., et al., *Lignification and tension wood.* Comptes Rendus Biologies, 2004. **327**(9-10): p. 889-901.
125. Lichtenegger, H., et al., *Variation of cellulose microfibril angles in softwoods and hardwoods-a possible strategy of mechanical optimization.* Journal of structural biology, 1999. **128**(3): p. 257-269.
126. Jarvis, M., *Cellulose stacks up.* Nature, 2003. **426**(6967): p. 611-612.
127. Sinko, R., X. Qin, and S. Keten, *Interfacial mechanics of cellulose nanocrystals.* Mrs Bulletin, 2015. **40**(4): p. 340-348.
128. Keckes, J., et al., *Cell-wall recovery after irreversible deformation of wood.* Nature materials, 2003. **2**(12): p. 810-814.
129. Fratzl, P., I. Burgert, and J. Keckes, *Mechanical model for the deformation of the wood cell wall.* Zeitschrift Fur Metallkunde, 2004. **95**(7): p. 579-584.
130. Altaner, C.M. and M.C. Jarvis, *Modelling polymer interactions of the 'molecular Velcro' type in wood under mechanical stress.* Journal of Theoretical Biology, 2008. **253**(3): p. 434-445.
131. Salmén, L., *Micromechanical understanding of the cell-wall structure.* Comptes Rendus - Biologies, 2004. **327**(9-10): p. 873-880.
132. Fratzl, P., I. Burgert, and H.S. Gupta, *On the role of interface polymers for the mechanics of natural polymeric composites.* Physical Chemistry Chemical Physics, 2004. **6**(24): p. 5575-5579.
133. Cousins, W.J., *Elasticity of isolated lignin: Young's modulus by a continuous indentation method.* New Zealand Journal of Forestry Science, 1977. **7**(1): p. 107-112.
134. Cave, I., *The anisotropic elasticity of the plant cell wall.* Wood science and technology, 1968. **2**: p. 268-278.

135. Navi, P., et al., *Micromechanics of wood subjected to axial tension.* Wood Science and Technology, 1995. **29**(6): p. 411-429.
136. Spatz, H., L. Köhler, and K.J. Niklas, *Mechanical behaviour of plant tissues: composite materials or structures?* The Journal of experimental biology, 1999. **202**(Pt 23): p. 3269-3272.
137. Köhler, L. and H.-C. Spatz, *Micromechanics of plant tissues beyond the linear-elastic range.* Planta, 2002. **215**(1): p. 33-40.
138. Jin, K., Z. Qin, and M.J. Buehler, *Molecular deformation mechanisms of the wood cell wall material.* Journal of the mechanical behavior of biomedical materials, 2015. **42**: p. 198-206.
139. Adler, D.C. and M.J. Buehler, *Mesoscale mechanics of wood cell walls under axial strain.* Soft Matter, 2013. **9**(29): p. 7138-7144.
140. Liang, L., et al., *A coarse-grain force-field for xylan and its interaction with cellulose.* Carbohydrate Polymers, 2015. **127**: p. 438-450.
141. Saavedra Flores, E.I., et al., *Investigation on the extensibility of the wood cell-wall composite by an approach based on homogenisation and uncertainty analysis.* Composite Structures, 2014. **108**: p. 212-222.
142. Navi, P. and F. Heger, *Combined densification and thermo-hydro-mechanical processing of Wood.* MRS Bulletin, 2004. **29**(05): p. 332-336.
143. Stiernstedt, J., et al., *Friction between cellulose surfaces and effect of xyloglucan adsorption.* Biomacromolecules, 2006. **7**(7): p. 2147-2153.
144. Åkerholm, M. and L. Salmén, *Interactions between wood polymers studied by dynamic FT-IR spectroscopy.* Polymer, 2001. **42**(3): p. 963-969.
145. Wimmer, R. and B.N. Lucas, *Comparing mechanical properties of secondary wall and cell corner middle lamella in spruce wood.* IAWA Journal, 1997. **18**(1): p. 77-88.
146. Whiting, P. and D.A.I. Goring, *Chemical characterization of tissue fractions from the middle lamella and secondary wall of black spruce tracheids.* Wood Science and Technology, 1982. **16**: p. 261-267.
147. Sorvari, J., et al., *Chemical characterization of wood constituents, especially lignin, in fractions separated from middle lamella and secondary wall of Norway spruce (Picea abies).* Wood Science and Technology, 1986. **20**(1): p. 35-51.
148. Thuvander, F. and L.A. Berglund, *In situ observations of fracture mechanisms for radial cracks in wood.* Journal of Materials Science, 2000. **35**(24): p. 6277-6283.
149. Ashby, M.F., et al., *The fracture and toughness of woods.* Proceedings of the Royal Society of London Series a-Mathematical Physical and Engineering Sciences, 1985. **398**(1815): p. 261-280.
150. Forest Products, L., *Wood handbook : wood as an engineering material*. 1974, [Madison]; Washington: The Laboratory ; For sale by the Supt. of Docs., U.S. Govt. Print. Off.
151. He, M.Y. and J.W. Hutchinson, *Crack deflection at an interface between dissimilar elastic-materials.* International Journal of Solids and Structures, 1989. **25**(9): p. 1053-1067.
152. Chan, K.S., M.Y. He, and J.W. Hutchinson, *Cracking and stress redistribution in ceramic layered composites.* Materials Science and Engineering a-Structural Materials Properties Microstructure and Processing, 1993. **167**(1-2): p. 57-64.
153. Gao, H.J., *Application of fracture mechanics concepts to hierarchical biomechanics of bone and bone-like materials.* International Journal of Fracture, 2006. **138**(1-4): p. 101-137.

154. Keten, S., et al., *Nanoconfinement controls stiffness, strength and mechanical toughness of beta-sheet crystals in silk.* Nature Materials, 2010. **9**(4): p. 359-367.
155. Evans, A.G., *Design and life prediction issues for high-temperature engineering ceramics and their composites.* Acta Materialia, 1997. **45**(1): p. 23-40.
156. Mirkhalaf, M., A.K. Dastjerdi, and F. Barthelat, *Overcoming the brittleness of glass through bio-inspiration and micro-architecture.* Nature Communications, 2014. **5**(1): p. 3166.
157. Qin, Z., et al., *Biological materials by design.* Journal of Physics-Condensed Matter, 2014. **26**(7).
158. Sarikaya, M., *An introduction to biomimetics - a structural viewpoint.* Microscopy Research and Technique, 1994. **27**(5): p. 360-375.
159. Wegst, U.G.K., et al., *Bioinspired structural materials.* Nature Materials, 2015. **14**(1): p. 23-36.
160. Munch, E., et al., *Tough, Bio-Inspired Hybrid Materials.* Science, 2008. **322**(5907): p. 1516.
161. Livanov, K., et al., *Tough Alumina/Polymer Layered Composites with High Ceramic Content.* Journal of the American Ceramic Society, 2015. **98**(4): p. 1285-1291.
162. Wang, J., et al., *Synergistic toughening of bioinspired poly(vinyl alcohol)-clay-nanofibrillar cellulose artificial nacre.* ACS Nano, 2014. **8**(3): p. 2739-2745.
163. Bonderer, L.J., A.R. Studart, and L.J. Gauckler, *Bioinspired Design and Assembly of Platelet Reinforced Polymer Films.* Science, 2008. **319**(5866): p. 1069.
164. Cavelier, S., C.J. Barrett, and F. Barthelat, *The mechanical performance of a biomimetic nanointerface made of multilayered polyelectrolytes.* European Journal of Inorganic Chemistry, 2012(32): p. 5380-5389.
165. Dimas, L.S., et al., *Tough Composites Inspired by Mineralized Natural Materials: Computation, 3D printing, and Testing.* Advanced Functional Materials, 2013. **23**(36): p. 4629-4638.
166. Tang, Z.Y., et al., *Nanostructured artificial nacre.* Nature Materials, 2003. **2**(6): p. 413-U8.
167. Guan, Z., *Supramolecular design in biopolymers and biomimetic polymers for properties.* Polymer International, 2007. **56**(4): p. 467-473.
168. Barthelat, F. and D.J. Zhu, *A novel biomimetic material duplicating the structure and mechanics of natural nacre.* Journal of Materials Research, 2011. **26**(10): p. 1203-1215.
169. Bouville, F., et al., *Strong, tough and stiff bioinspired ceramics from brittle constituents.* Nature Materials, 2014. **13**(5): p. 508-514.

Link between Chapter 2 and Chapter 3

In the previous chapter, the hierarchical structures in a set of representative biological materials including nacre, bone and wood are reviewed with emphasis on the composition, structure, properties and mechanics of the organic interfaces. Recent examples of synthetic materials inspired from the mechanics and architecture of natural interfaces are highlighted. It is concluded that having ductile interfaces with local hardening is the key to obtain maximized toughness for biological and bioinspired materials. The next chapter, published in *Acta Biomaterialia* in 2018, these concepts were implemented in a highly deformable and tough bi-layer glass with bioinspired cross-ply architectures. Ethylene-vinyl acetate (EVA), a semi-crystalline copolymer, were used as the polymeric interface in the cross-ply glass. In shear, EVA has low yielding strength and can have large deformation with strain hardening, which is the ideal choice for the interface material. The mechanical behaviors of cross-ply glass under uniaxial tension were evaluated. The cross-ply glass showed large deformation (up to 90% engineering strain) and absorb up to around 100 times more energy than plain laminated glass. Three deformation modes, brittle ply fracture, rotational mode and translational mode, were identified. Finite element models were built to study the mechanics of cross-ply glass. The models used a bi-linear cohesive law to simulate the EVA interface. The simulations showed that the redistribution of shear traction at the interface, caused by ply rotation, is the reason behind the deformability and strain hardening of cross-ply glass. Compact tension fracture tests were also conducted. Compared to plain laminated glass, the cross-ply glass showed up to four times amplification for nominal strength (with notch) and up to 53 times amplification for work of fracture. Three toughening modes, crack deflection, crack channelling and interface shearing, were identified, depending on the ply angle and ply width.

Chapter 3: Tough and deformable glasses with bioinspired cross-ply architectures

Zhen Yin, Ahmad Dastjerdi and Francois Barthelat*

Department of Mechanical Engineering, McGill University, 817 Sherbrooke Street West,
Montreal, QC H3A 2K6, Canada

*corresponding author: (francois.barthelat@mcgill.ca)

3.1 Abstract

Glasses are optically transparent, hard materials that have been in sustained demand and usage in architectural windows, optical devices, electronics and solar panels. Despite their outstanding optical qualities and durability, their brittleness and low resistance to impact still limits wider applications. Here this work presents new laminated glass designs that contain toughening cross-ply architectures inspired from fish scales and arthropod cuticles. This seemingly minor enrichment completely transforms the way laminated glass deforms and fractures, and it turns a traditionally brittle material into a stretchy and tough material with little impact on surface hardness and optical quality. Large ply rotation propagates over large volumes, and localization is delayed in tension, even if a strain softening interlayer is used, in a remarkable mechanism which is generated by the kinematics of the plies and geometrical hardening. Compared to traditional laminated glass which degrades significantly in performance when damaged, our cross-ply architecture glass is damage-tolerant and 50 times tougher in energy terms.

3.2 Introduction

With fast developments in the applications of glass in electronic devices, solar panels and windows for building and vehicles, there are increasing needs for tough and damage tolerant glass materials

[1]. Toughness, which indicates the capability of a material to resist crack propagation and impacts, requires high strength and high deformability. However, strength and deformability are usually mutually exclusive in many traditional engineering materials [2]. Glass is a widely used material because of its hardness, optical properties, thermal and chemical stability, and durability. However, its range of applications is currently severely limited by its low fracture toughness (Fig. 3-1a). Currently, the main two methods used to improve the mechanical performance of glass are tempering and lamination [3]. Tempering consists of generating residual compressive stresses at the surface of glass components by either heat treatment or ion implantation, in order to offset tensile stresses arising from external loading. However, once a crack is initiated in tempered glass, the release of elastic energy produces catastrophic and ‘‘explosive” failures which destroy the entire component into small fragments. Laminating glass is another strategy which consists of intercalating glass layers with softer polymeric layers to keep glass fragments together in case of fracture. However, the impact resistance of laminated glass is not significantly higher than plain glass because the deformability and toughness of the polymer layers are not fully exploited [3]. Recent work has suggested new pathways to transform the mechanics and improve the properties of materials, by creating highly controlled material ‘‘architectures” at length scales intermediate between the micro- scale and the scale of the component.

This approach provides a promising way to exploit the synergies between constituents in a composite material and to achieve new combinations of properties [4]. Since morphological control is high, the shape, size and arrangement of the building blocks can be tailored to maximize overall material properties and generate new and useful combinations of strength and deformability (Fig. 3-1a). Interestingly, nature is well ahead of engineers in making use of architectured materials [4]. Materials such as bone, teeth or mollusk shells are also made of stiff building blocks of well-defined sizes and shapes, bonded by deform- able organic interfaces. The interplay between the building blocks and the non-linear behaviors at the interfaces generate powerful combinations of stiffness, strength and toughness not yet found in synthetic materials [4, 5]. For example, Fig. 3-1b shows the architecture of conch shells, a remarkable material made of >95% vol. of brittle biominerals with a toughness three orders of magnitude higher than that mineral [6]. The architecture of conch shell consists of a series of cross-plies at different length scales [7, 8], where mineral lamellae are separated and adhered by thin organic interfaces. Propagating cracks are deflected and guided by the weaker organic interfaces, which triggers powerful toughening mechanisms such as crack bridging [9, 10]. Cross-ply architecture with similar toughening mechanisms can also be observed in the decussation zone of enamel [11]. The organic content in enamel only represents 1–5 wt% content but it con- tributes substantially to overall toughness [12]. Removing the protein interfaces in enamel can reduce the toughness by 40% [13]. Cross-ply architectures are also found in fish scales [14, 15] and arthropod cuticles [16], generating powerful crack resisting mechanisms such as crack deflection, crack twisting, crack bridging, and process zone toughening [14, 15, 17]. In addition, the interfaces between the fibers in these materials can undergo large deformations [12], so that fibers can rotate and align with the pulling direction, strengthening the material along that direction. While nature presents spectacular examples of cross-ply architectures, attempts to systematically incorporate these bio-inspired designs in synthetic materials have been so far limited [18-20]. Here we combine the concepts of lamination in glass [3], highly controlled material architecture [4], laser-induced weak interfaces [21], highly deformable interlayers [12], and bioinspiration [9, 11, 22] to generate new types of glass with a superior combination of toughness, deformability and damage tolerance. The effect of the architecture on micromechanics of deformation, overall performance, and fracture mechanics are examined by using combinations of experiments and models.

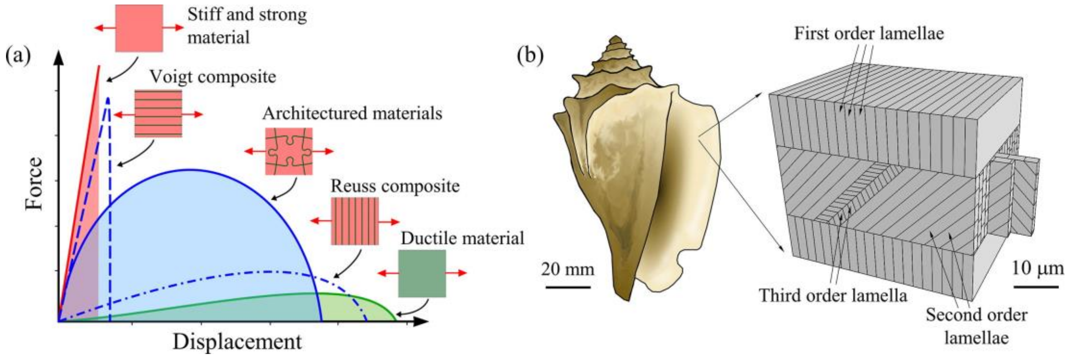

Fig. 3-1: (a) Generic force displacement curve for a stiff and strong (but brittle) material, a low-strength ductile material, and for three possible composites of these materials; (b) Cross-ply architectures in conch shell.

3.3 Fabrication protocol

In this study, 0.22 mm thick standard borosilicate glass sheets (Fisher Scientific, PA, USA) were used as the base material, combined with a continuous, 0.15 mm thick adhesive layer. A critical requirement for the adhesive is to be highly deformable at moderate stress (estimated interfacial shear strength less than 7 MPa [23]) in order to promote interlayer shearing over the fracture of the glass layers. To explore possible adhesives, we conducted single lap shear tests on a selection of adhesives using 1 mm thick borosilicate glass substrates. The adhesives were an ethylene-vinyl acetate (EVA, Caida, Tianjin, China), an ionomer (DuPont Surlyn, DE, USA), a cyanoacrylate (Adhesive System, IL, USA) and an epoxy (BMB Solutions Composites, QC, Canada). Force and displacement were converted to shear stress and shear strain using the surface area and thickness of the adhesive layer (Fig. 3-2). As expected, Cyanoacrylate and epoxy are brittle and have high shear strength (around 8 MPa when leading to the fracture of glass substrates), making them unsuitable for our material. Surlyn show a combination of high shear strength (>10 MPa) and high shear strain at failure (>300%). However, preliminary experiments on the thinner glass slides used in our architectured laminated glass showed extensive damage in glass because Surlyn is too strong. EVA was the most suitable for our material: it is optically transparent, it has strong adhesion on glass, and can undergo large inelastic deformations with energy dissipation. The shear strength of EVA is sufficiently low (~3 MPa) to promote yielding at the interlayer over brittle fracture of the glass substrates. Fig. 3-3 shows the fabrication protocol. A pair of plain glass plates was first covered with a heat resistant polyimide (PI) tape (McMaster-carr, IL, USA) to facilitate the handling of the glass plate after laser engraving. Straight lines were then carved into the glass plates using a laser engraver (Vitro Laser solutions UG, Minden, Germany). These weak interfaces consisted of arrays of microcracks with 10 μm spacing, generated with the focused pulsed UV laser beam (355 nm, 300 mw). These micro- cracks were engraved through the entire thickness of the plates, following a pattern of parallel lines spaced by a distance d and at an angle θ from the long axis of the glass plates (Fig. 3-3b). The individual plies were then mechanically separated along the laser engraved lines, the PI tape holding the plate together for easier handling. A pair of these engraved plates was then assembled with a $\pm\theta$ orientation with the EVA film as interlayer to form a cross-ply architecture (Fig. 3-3c, d). This assembly was pressed with a uniform pressure of 100 kPa and kept at 120 °C in an oven for 1.5 h in order for the EVA layer to develop a strong adhesion to the glass plates (Fig. 3-3e). The assembly was then slowly cooled to room temperature, which produced the final material (Fig. 3-3f). In this study, different architectures were explored with ply angles of $\theta = \pm 45°$, ±60° and ±75° for tensile tests and an additional $\theta = \pm 15°$ for the fracture tests. The ply width was varied from $d = 1$ mm, 2 mm and 3 mm for both tensile and fracture tests. These ply angles and ply widths were chosen because they lead to the wide range of failure modes described below. The process of laser engraving may leave some roughness on the cut surfaces, but the glass faces were not affected and the interfaces between the glass faces and the interlayer remained intact and smooth. For reference, traditional, ‘‘plain” laminated glass plates were also prepared, which were assembled using the same protocol shown on Fig. 3-3, but where the laser engraving step was skipped. Plain and architectured laminated plates were then cut into their final shapes: dogbone specimens for tensile tests, and compact tension specimens for fracture tests.

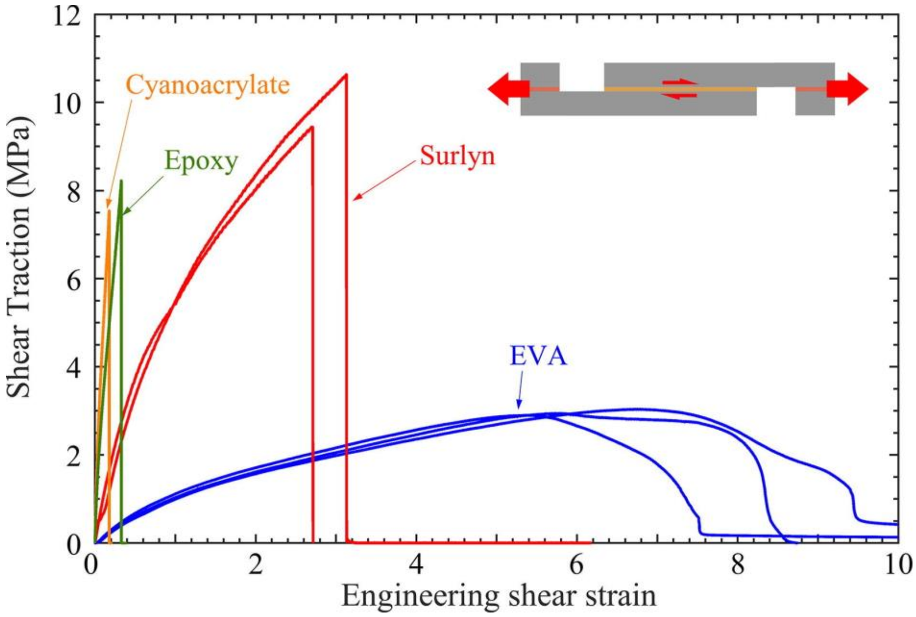

Fig. 3-2: The shear stress-strain curves from the single lap shear tests on EVA, Surlyn, cyanoacrylate and epoxy. The glass substrates failed in the tests of cyanoacrylate, epoxy and Surlyn.

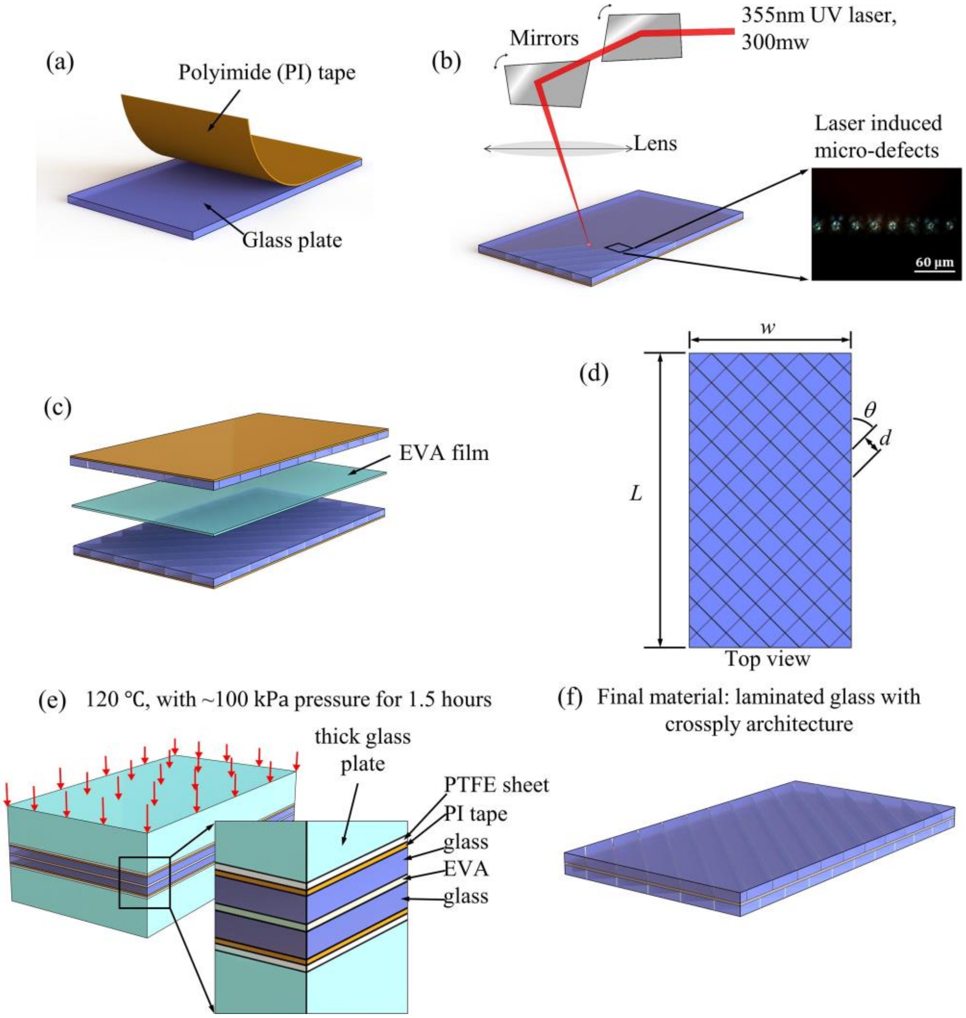

Fig. 3-3: Fabrication steps for the laminated cross-ply samples: (a) A polyimide film is attached to the glass plate; (b) laser engraving of weak interfaces into glass plates to form plies; (c) assembly of the laminated sample with ± θ engraved plates; (d) top view showing the structure of the engraved lines with spacing d and angle ± θ (e) Application of pressure and heat to soften EVA and create adhesion; (f) Final material: plate of architectured cross-ply laminated glass.

3.4 Optical quality

A natural concern for laser engraving features in glasses is their impact on optical quality. Fig. 3-4a shows the results of the light transmittance [24, 25] at different light wavelengths for plain laminated glasses and for cross-ply architectured glasses. Even with a relatively dense ply formation (d = 1 mm, d/w = 0.1), the cross-ply architectured glasses show excellent transmittance in the visible light spectrum (wavelength 380–780 nm). Optical clarity, which is the property of transmitting light without spatial distortions [26], was also assessed. Fig. 3-4b shows our materials in front of a checkered background, showing little effect on contrast and resolution, and no distortion of the pattern viewed through the materials. The impact of laser engraving on the optical quality of the laminated glass panels was therefore not significant (Fig. 3-4a).

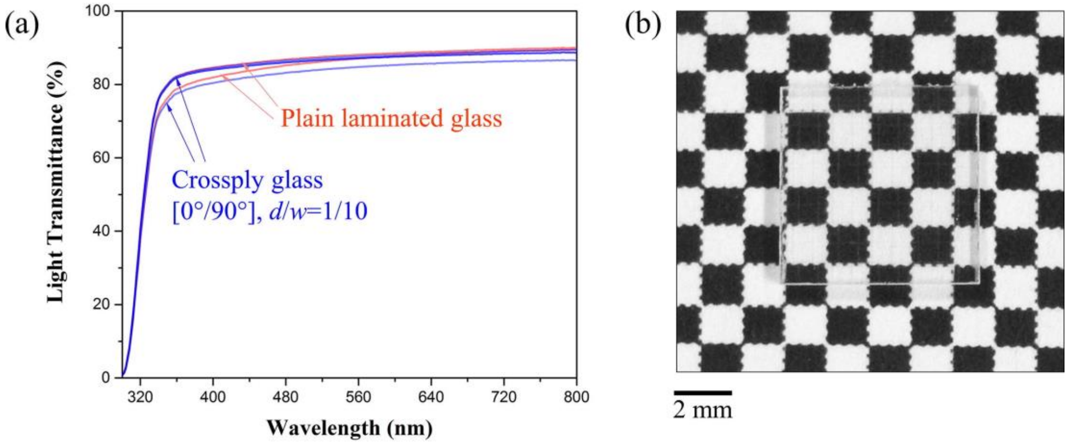

Fig. 3-4: Optical properties of the plain and architectured laminated glasses. (a) light transmittance and (b) optical clarity: No decrease in light transmittance, image distortion or decrease in the appearance of objects was observed for the architectured materials.

3.5 Tensile tests

Tension is the loading configuration where glasses and traditional laminated glasses perform the poorest in term of strength, brittleness and energy absorption. Tensile tests were therefore well suited to highlight how our augmented cross-ply designs can address brittleness in traditional glass materials. For these tests, we prepared dogbone-shaped laminated samples with the dimensions shown on Fig. 3-5a (adapted from ASTM C1273 [27]). Nine combinations of ply width *d* and ply angle θ were explored, and 3–5 samples were tested for each combination. The pictures shown in Fig. 3-5 (and other similar pictures in this paper) were captured with a C-5060 Olympus digital camera using a black background and a bright illumination from an angle that highlighted the engraving lines. In normal conditions of illumination, these lines were barely visible (see optical tests above). The samples were mounted on a miniature loading stage (E. Fullam, NY) and stretched at a constant rate of 10 µm/s. The samples were considered to have failed once the glass architecture had completely collapsed, at which point only the EVA interlayer provided a small tensile force.

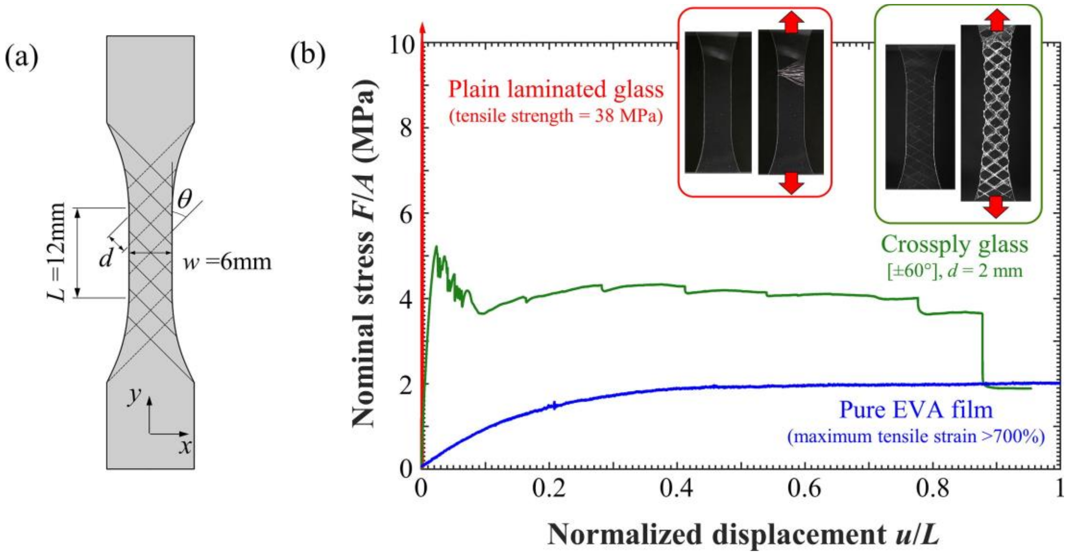

Fig. 3-5: (a) Overview of tensile test samples; (b) typical tensile responses for pure EVA, traditional laminated glass and cross-ply architectured glass.

The characteristic length scale for our architecture (ply width *d* = 1, 2 or 3 mm) is relatively close to the size of the sample (fixed sample width *w* = 6 mm, Fig. 3-5a), so that the usual separation of length scales between microstructure and component size cannot be applied [28]. An important implication is that homogenization of properties is not valid, and that the usual concepts of stress and strains had to be used with caution. For this reason, normalized displacement *u*/*L* was used to characterize deformations, where *u* is the applied displacement and *L* is the effective length of the tensile test specimens (L = 12 mm for all samples, Fig. 3-5a). An ‘‘apparent” nominal stress F/A to characterize internal tractions in the material, where F is the tensile force on the material and A is the cross-sectional area (A = 3.6 mm^2 for all samples). Fig. 3-5b shows typical tensile responses for pure EVA film, traditional laminated glass, and a cross-ply architectured glass. Pure EVA displayed a relatively low nominal tensile strength (~2 MPa), but very large extensions (strain at failure >700%). In contrast the laminated glass was very stiff and strong (strength = 38 MPa) but brittle (strain at failure <0.3%) with multiple catastrophic cracks localized in a small region (Fig. 3-5b). This strong but brittle behavior is typical for laminated glasses. The configuration of the laminated glass in tension corresponds to a ‘‘uniform strain” composite, where the glass layers carry most of the tensile force because they are much stiffer than the EVA interlayer. While the deformable interlayer can hold glass debris together in case of fracture, it generates little improvements in strength, energy absorption or impact resistance [3]. The polymeric interlayer in traditional laminated glasses has a large capacity of absorbing impact energy, but only a small and localized volume fraction of that interlayer is deformed in case of impact and fracture (Fig. 3-5b). The architectured cross-ply glass produced a tensile response which was intermediate between the laminated glass and pure EVA (Fig. 3-5b). Compared to traditional laminated glasses, the architectured glasses have a lower strength, but they are several orders of magnitude more ductile which translated into much larger energy absorption. They also fail progressively and in a more ‘‘graceful” fashion, which contrasts with laminated glass. These large deformations are generated by the separation, sliding and rotation of the plies over large volumes, which involves large shearing deformations in the EVA interlayer (Fig. 3-5b and Fig. 3-6). Ply delamination, sliding, and rotation are common mechanisms in collagen cross-plies in fish scales [14, 15] and chitin Bouligand plies in arthropod cuticles [29, 30]. Fig. 3-6 shows the tensile response for cross-ply architectured glasses with θ = ±45°, ±60° and ±75° and with d = 2 mm, together with snapshots of the samples taken during the tensile tests. Several distinct failure modes were observed depending on ply width and ply angle. Low ply angles (θ = ±45°) lead to the high strength, but some plies failed prematurely, leading to premature strain localization and failure. In these cases, most of the plies did not separate, and most of the interlayer deformed within small strains. The material with a ply angle of θ = ±60° led to a slightly lower strength, but much greater deformations. In these materials, every ply separated and rotated by as much as 10–12° towards the direction of pulling. This ‘‘rotational mode” was prominent in θ = ±60° samples. This mechanism involves the shear deformation of large volumes of the EVA inter- faces, which translates into very high overall deformation and energy absorption. The θ = ±60° samples eventually failed by the brittle fracture of one or more plies, which occurred at tensile deformation of almost 100%. Samples with high ply angle (θ = ±75°) had a slightly lower tensile strength and also displayed early localization of deformations, which in turn led to relatively low deformation at failure and low energy absorption. The plies separated and slid on one another and their rotation was minimal. This ‘‘translational mode” appears to be prominent for high ply angles. Fig. 3-6 shows that the deformation and energy dissipation both increase when the volume of deformed material is larger. The results also show how the geometry of the plies can be tuned to achieved optimum strength (this effect is explored in detail in Section 5 below). The effects of ply width d were also assessed by testing samples with d = 1 mm (corresponding to d/w = 1/6), d =2mm (d/w = 1/3) and d = 3 mm (d/w = 1/2) with ply angles of θ = ±45°, ±60° and ±75° for each width. Fig. 3-7 provides a summary and deformation map for the nine different geometries considered here. Remarkably, it was found that the failure mode was primarily affected by the ply angle but not affected by ply width. For example, all samples with θ = ±75° failed by translational mode, but the failure was much localized for d = 3 mm. The stiffness and the strength of the materials also increased when *d* was increased, because increasing *d* increases the overlap area between the plies, which in turn increases the forces required for ply separation and rotation.

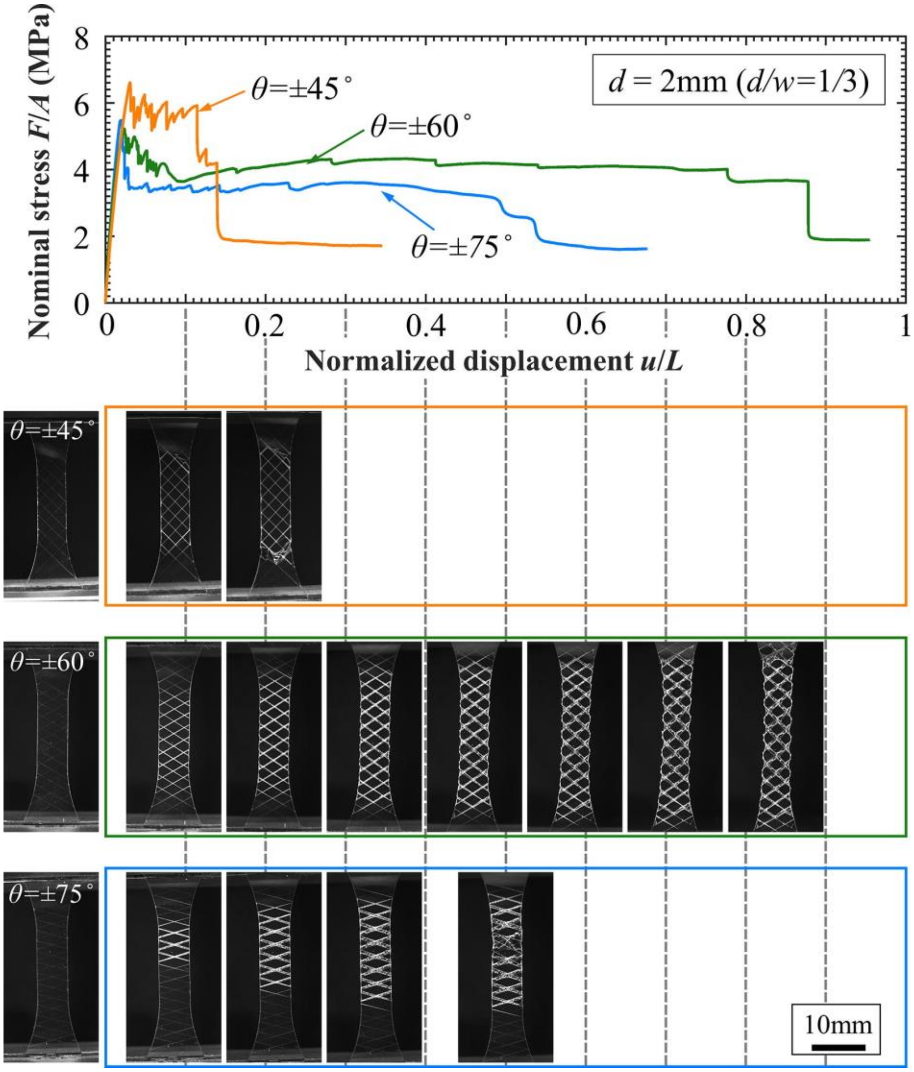

Fig. 3-6: Tensile response and associated deformation mechanisms for cross-ply-architectured glasses with $\theta = 75°$, 60° and 45°. For all configurations $d = 2$ mm (corresponding to $d/w = 1/3$).

The properties obtained for these various cross-ply geometries are summarized on Fig. 3-8. The stiffness of the cross-ply architectured glasses ranges from 0.3 to 0.8 GPa, which is about 20 times lower than plain laminated glass (~15 GPa). However, the strength of the cross-ply architectured glasses is also 100 times higher than plain EVA (~8 MPa), because the cross-ply architecture turns the deformation of the EVA from tension into shear, which grants larger force with the same cross-section area. The cross-ply architectured glasses are about five times weaker than laminated glass in terms of static strength (p-value $p < 0.05$ from a one tailed unpaired sample t-test, Fig. 3-8b), but they can deform up to 400 times more and they can absorb about 100 times more mechanical energy (Fig. 3-8c and d). The progressive failure and large energy absorption of the cross-ply architectured materials is the result of the delocalized deformation induced by the cross-ply architecture. The geometry of the cross-ply has a strong effect on mechanical response, with lower ply angles θ and higher ply width d favoring high stiffness and high strength. However, for energy dis- sipation, intermediate values ($\theta = 60°$ and $d = 2$ mm) led to the best performance. The mechanical response of the architectured laminated glass is the result of a competition between brittle ply fracture, translational ply sliding and ply rotation. As ply width is increased, the overlap between the plies increases and the force transmitted between plies across the interlayer increases. Small ply width ($d = 1$ mm) lead to small overlap, and in general to low strength and energy absorption. In contrast, wider plies ($d = 3$ mm) generate large overlaps and higher strength, but excessive stresses within the plies lead to ply fracture, which limits the amounts of energy absorbed. In this work plies of width $d = 2$ mm provided the best performance in terms of combined strength and energy absorption. This optimum between interface strength, ply strength and overlap is similar to the mechanics and optimization of brick-and-mortar composites [31]. How ply angle affects the results and lead to an optimum of $\theta =60°$ is explored in the next section.

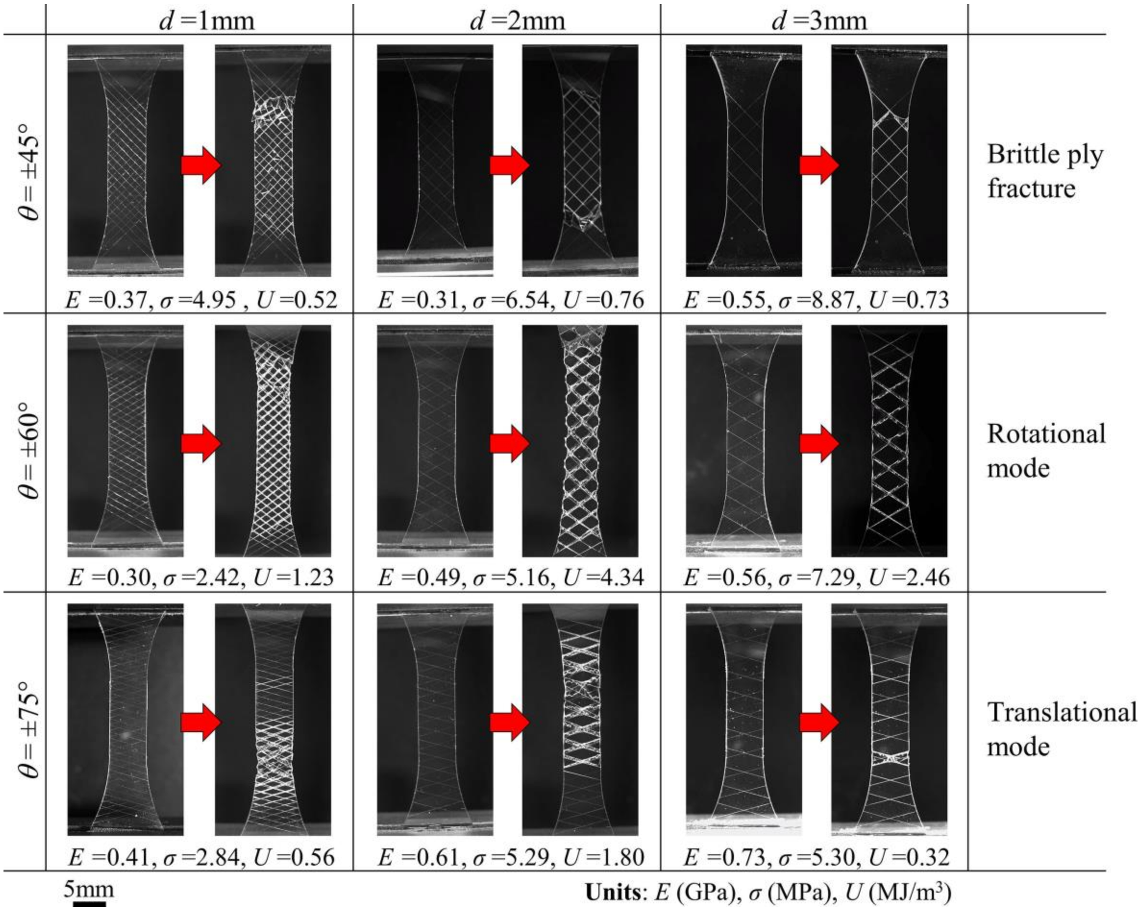

Fig. 3-7: Deformation map showing three tensile deformation and failure modes for cross-ply architectured glasses as function of ply angle and ply width, supplied with stiffness *E*, strength *σ*, and unit volume energy absorption *U* for each configuration.

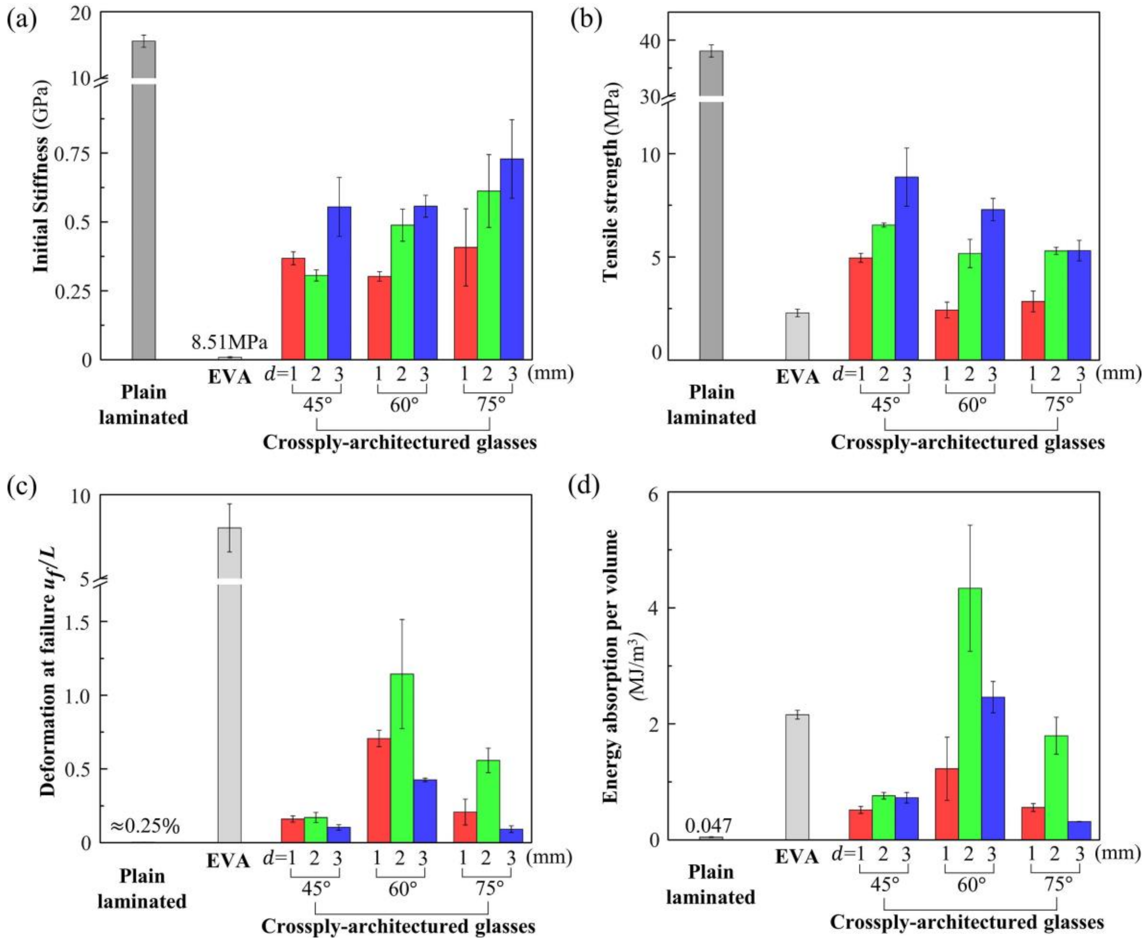

Fig. 3-8: Tensile properties for plain laminated glass, pure EVA and architectured cross-ply glasses: (a) Initial stiffness; (b) tensile strength; (c) deformation at failure and (d) energy absorption based on the failure criterion that the nominal stress drops below the yielding strength of EVA.

3.6 Finite elements model and analysis

For a better understanding of the mechanisms that govern the deformation and failure modes and the overall properties of the cross-plies, the cross-ply architectured samples in tension were modelled using finite elements (ANSYS 16.0, PA, US [32]). The glass plies were modelled using 20-node solid elements SOLID186 and the interface was modelled using 16-node cohesive elements INTER204. The applied displacement was controlled by two master nodes linked to the nodes in upper and bottom faces respectively. Fig. 3-9a shows the 3D geometry and the loading conditions of the finite element model. The glass plies were modeled as linear isotropic elastic with an elastic modulus of 60 GPa and a Poisson's ratio of 0.2. Contact elements were inserted at the interfaces between neighboring plies of the same layer to prevent interpenetration. The EVA interlayer was modelled with nonlinear cohesive elements and a mode-II triangular cohesive law (Fig. 3-9b). The maximum traction of the cohesive law was set to 3.2 MPa, which was obtained from the lap shear tests on the EVA interlayer on glass substrates. A maximum displacement jump of 10 mm was used and the initial slope of the cohesive law was tuned in order to match the tensile response of the $\theta = \pm 75°$, which failed by translational mode of the plies (the $\theta = \pm 75°$ sample was the closest from a shear lap experiment). For all models the mesh was refined to ensure convergence in terms of the force-displacement curves as well as local stresses. Fig. 3-9c shows that the finite element models could successfully captured the experimental trends, but that they overestimated in general the strength of material. This discrepancy was attributed to defects in the physical samples which can decrease their overall properties, and to the simplified failure criteria used in the finite element models. Stiffness and strength both increase when the ply width is increased, or when the ply angle is decreased because higher d and/or lower θ result in an increase of overlap area. In some experiments individual plies fractured, which interrupted the mechanisms of ply rotation and/or sliding and precipitated brittle fracture. The finite element models revealed that the highest stresses in the plies are due to flexion, with maximum stress values at the edges of the plies (Fig. 3-9d). To predict the onset of ply fracture, the maximum principal stresses in the plies were compared with the tensile strength for laser cut borosilicate glasses (70 MPa measured by bending tests no shown here). The predictions in terms of ply fracture and brittle are consistent with the experiments: in samples with lower ply angles ply fracture is the dominant failure mode, which leads to an overall brittle type of failure for the materials. In contrast, the model predicts that the plies of the samples with high ply angle remain intact, which is consistent with the experiments.

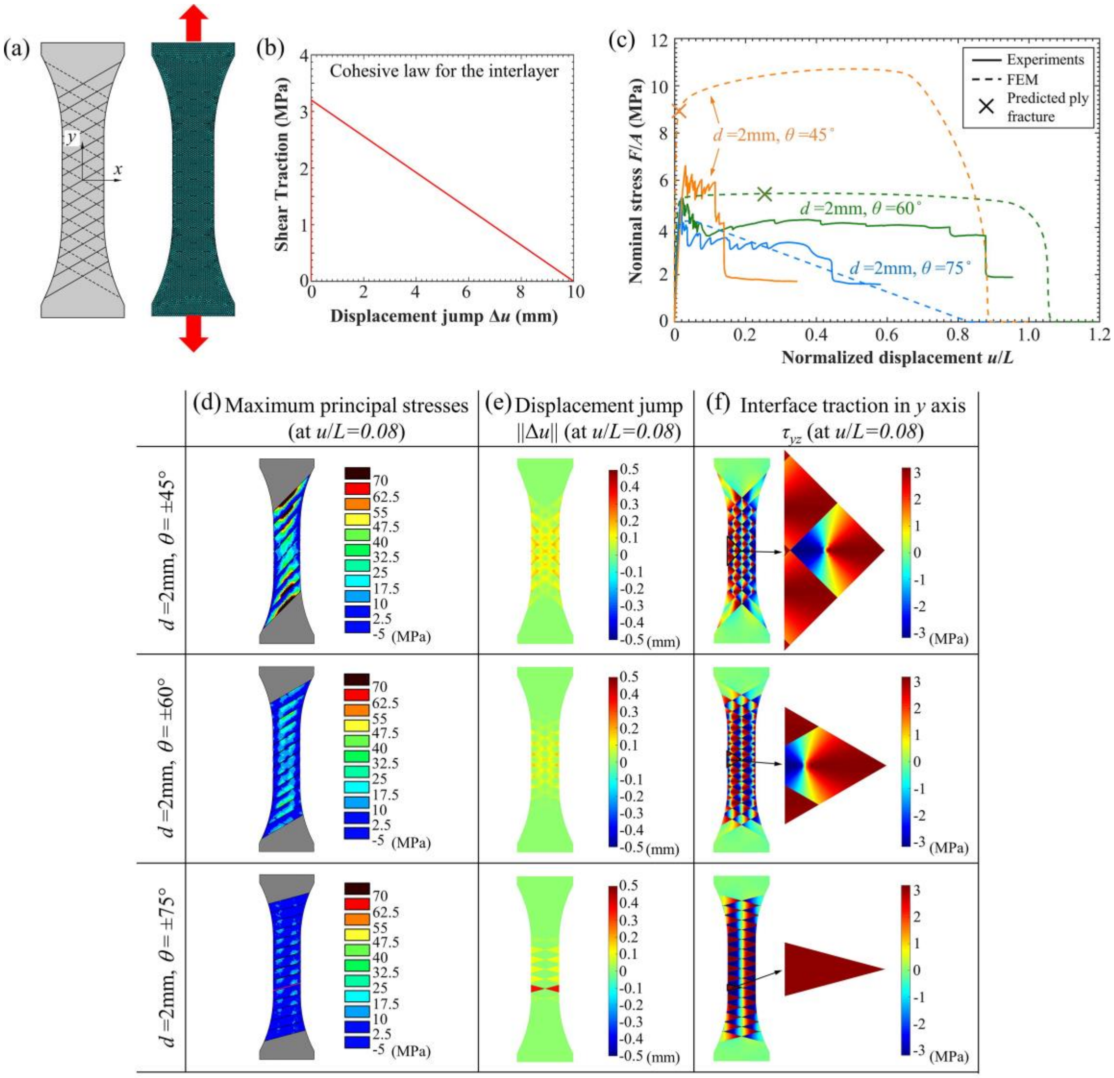

Fig. 3-9: (a) Finite element model setup; (b) Cohesive law simulating the shear response of the EVA interlayer; (c) Experimental and finite elements force-displacement; (d) Maximum first principal stresses in the plies; (e) Displacement jump *Δu* across the layers and (f) distribution of shear tractions at the interlayer.

The model also captures the main trends and deformation modes observed experimentally in the post yield regions. The θ = ±75° cross-plies primarily fail by the translational mode, and the θ = ±45° and θ = ±60° architectures deform and fail by the rotational and brittle ply fracture modes, respectively (Fig. 3-9e). Fig. 3-9f shows that the rotation of plies is prominent for smaller ply angles. At lower ply angles, although the plies can rotate with deformation, the plies carry high bending stresses that make the plies fracture prematurely (Fig. 3-9e).

A striking feature of the architectured glass is its ability to delay strain localization and distribute deformation over large volumes even in the post-yielding stage. This mechanism was explored in depth using our finite element models. Even though the cohesive law softens in the post yield region (Fig. 3-9b), the architectured glass can display constant post-yield tensile stress (θ = ±60°) or even strain hardening (case θ = ±45°, Fig. 3-9c), with the direct effect of delaying strain localization. To explain this phenomenon, the distribution of shear stress was analyzed at the interlayer (Fig. 3-9f). Cases θ = ±60° and θ = ±45° show a non-uniform distribution of shear stresses that results from the rotation of the plies superimposed to the uniform shear stress from ply separation. The profiles display regions where the shear stress is positive, and regions where it is negative. The center of rotation (where $\tau_{xz} = 0$ and $\tau_{yz} = 0$) is slightly off-centered, so that the distribution produces a net tensile force within the material. Fig. 3-10 shows the evolution of the shear distribution for the case d = 2 mm, θ = ±45°. Both series of snapshots were taken in the post-yield region, at $u/L = 0.08$ and $u/L = 0.48$. The region of interest can be conveniently divided into four sectors. Fig. 3-10 shows the net force vector transmitted by the interlayer through each of the sectors, computed from the distribution of shear stresses τ_{xz} and τ_{yz} Three concurrent effects are visible as the global deformation is increased: (i) The magnitudes of the traction forces exerted on each of the fours sectors decrease; (ii) the center of rotation shifts towards the left, so that the region that produces tensile traction forces increases in size; (iii) the traction force vectors rotate and align towards the pulling direction. The first effect is due to the inherent softening of the cohesive law, contributing to global softening. This effect is however offset by the second and third effects. As the region producing negative (blue) traction decreases, the net force increases. As all traction vectors align toward the direction of pulling, their projection along that direction increase, which produces an increasing global force even though the magnitude of each of the four traction vector decreases. These results demonstrate how architecture and large rotational kinematics can produce strain hardening from strain softening materials. This unique mechanism provides the cross-ply glasses with a nearly 100 times amplification of deformability and energy absorption compared to plain laminated glass. The case $\theta = \pm 75°$ does not produce any ply rotation so that these effects are completely absent. As a result, this case produces materials which soften with deformation and when localize deformation prematurely.

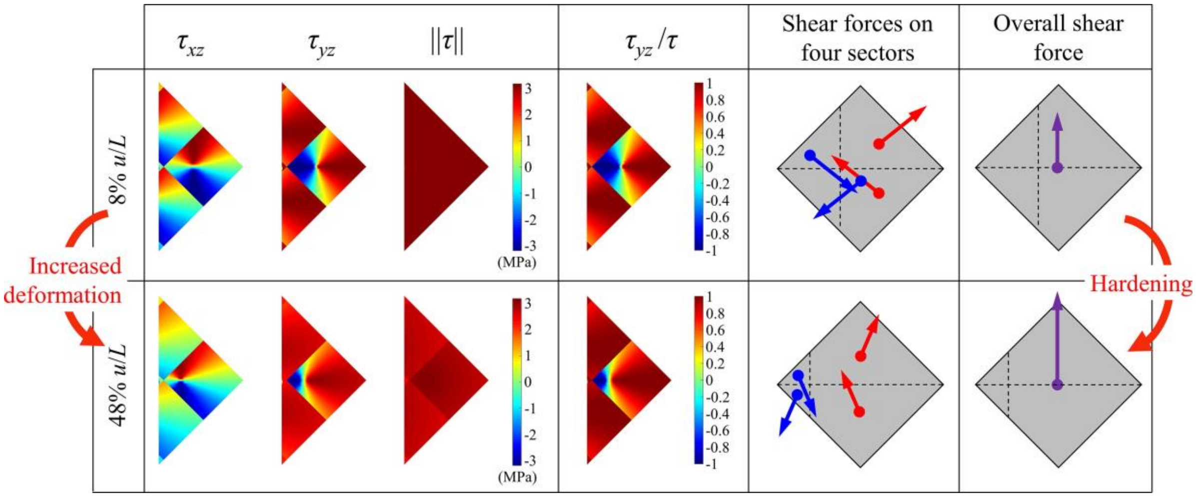

Fig. 3-10: Local shear stresses τ_{xz}, τ_{yz}, magnitude of shear stress τ, distribution of τ_{yz}/τ, schematic showing the change of magnitude and direction of force vectors on four different sectors at the interlayer and resulting overall force. Each data is given at two level of deformation in post yield regime. These results demonstrate how global strain hardening can be attained from a softening interface.

3.7 Notch performance and toughness

Fracture toughness and notch performance of our architectured cross-ply glasses were finally assessed. These properties can be interpreted as their tensile performance in the presence of a severe stress concentration, which is critical for robustness and damage tolerance. Mode-I fracture tests were performed on compact tension samples on both the plain laminated samples and the cross-ply samples, with geometry and dimensions shown on Fig. 3-11a. The overall geometry of the sample (including in-plane dimensions, notch depth and thickness) was kept identical across all samples. The notch was cut using the 355 nm UV laser at a power of 400 mw with a defect spacing of 5 µm. Since the defects generated by the laser consist of microcracks [21], the tip of the initial notch was perfectly sharp. Both plain laminated glass (Fig. 3-11b) and cross-ply architectured glass (Fig. 3-11c) were tested using the same loading stage as for the tensile tests, at a rate of 5 µm/s.

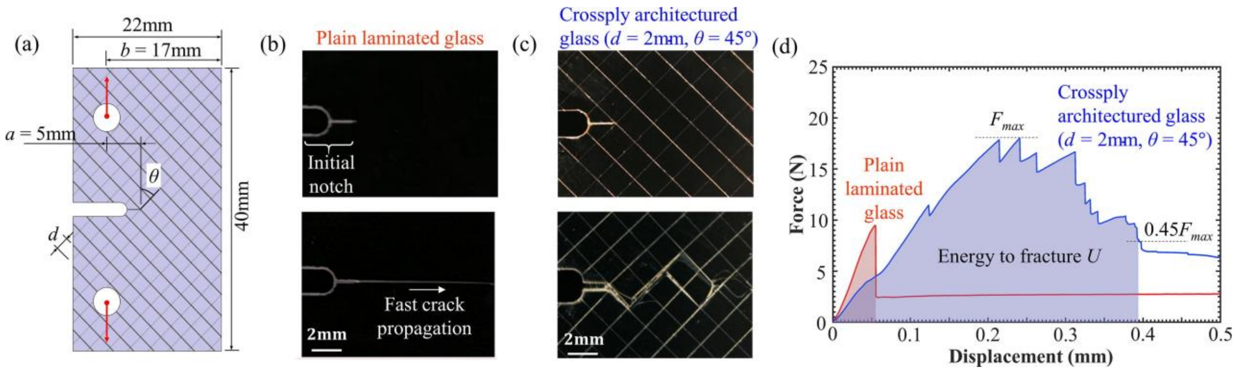

Fig. 3-11: (a) Dimensions of fracture test samples; (b) Straight and rapid crack propagation in plain laminated glass; (c) progressive and twisted crack propagation in cross-ply architectured glass; (d) typical tensile notched force-displacement curves for plain laminated glass and for cross-ply architectured glass.

Fig. 3-11d shows typical force-displacements for regular and architectured glasses. As expected, plain laminated glass performed poorly in the presence of a notch, with a greatly reduced tensile strength. Crack propagation was rapid and straight, and the overall response was brittle. In contrast, the crack path in the architectured glass was convoluted, with multiple deflections and crack twisting and large energy to fracture. Crack propagation was stable, and the force-displacement curve had a general bell curve with multiple drops in the softening region. The peak force F_{max} marked the point where crack propagation commenced, although some inelastic activity was usually observed on the loading part of the curve. The force required to initiate cracking F_{max} in the architectured glass was 1.4 to 4 times higher than in plain laminated glass ($p < 0.05$, Fig. 3-12a). This result demonstrates that powerful toughening mechanisms such as crack blunting of the crack, twisting of the crack front, mixed mode and inelastic deformations ahead of the crack operate to resist the onset of crack propagation. Nominal strength of the materials with and without the presence of a notch was also compared, in order to determine their tolerance to stress concentration. Fig. 3-12b shows the ratio between the nominal strength from a notched sample to the tensile strength from an un-notched tensile test. The ratio for traditional laminated glass is less than 0.05 which is expected, these materials do not tolerate damage well and damaged laminated windows or windshields must be replaced as soon as a small amount of damage is detected. The cross-ply architectured glasses performed much better, with a strength ratio ranging from 0.4 to 1. This result clearly demonstrates how the micromechanics associated with the cross-ply architecture can mitigate or even entirely suppress the effects of stress concentrations from sharp geometrical features, defects or cracks. Extremely tough materials can even become notch insensitive, which mean that they completely suppress stress concentrations by way of inelastic deformations (Fig. 3-12c).

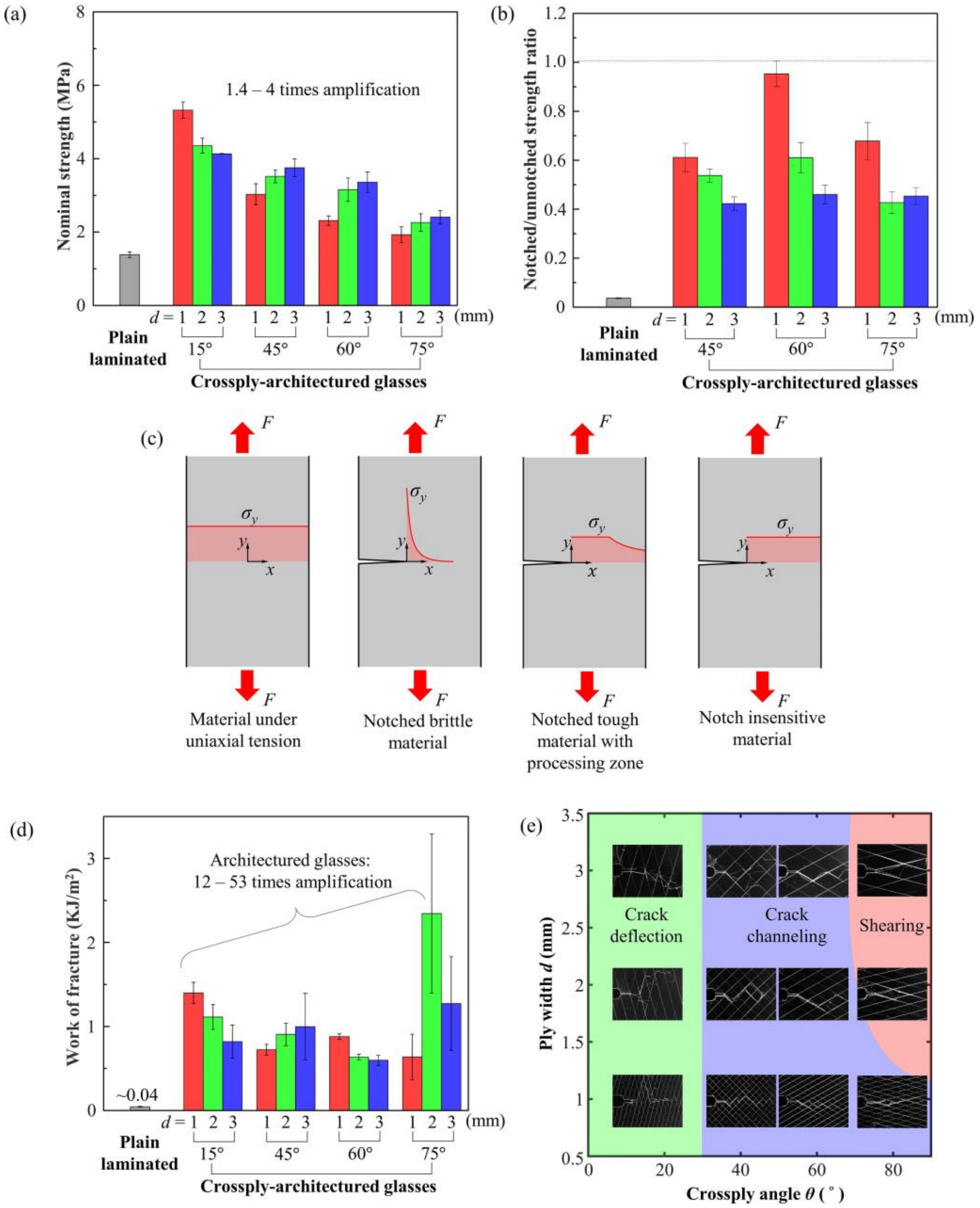

Fig. 3-12: (a) Nominal strength of the notched samples for different configurations; (b) Ratio of notched and unnotched strength (a ratio of 1 means that the material is notch insensitive); (c) Illustration showing how tough and deformable materials redistribute stresses at a notch; (d) Work of fracture for different laminated glass designs; (e) Failure mode map as function of ply angle θ and ply width d.

The resistance to fracture of the material was finally assessed, by estimating the energy required to completely fracture the samples. Since the ductile interlayer maintained a nonzero force even after the glass architecture has collapsed, for the purpose of computing U, it was assumed that the sample had failed when the force had decreased to $0.45F_{max}$ (Fig. 3-12d). To compare the different materials in terms of notch tolerance and toughness, a nominal strength defined as: $F_{max}/(b - a)t$ and the work of fracture defined as $U/(b - a)t$ were used, where $(b - a)t$ is the cross sectional area of the ligament (Fig. 3-11a). Fig. 3-12b shows the work of fracture for the configurations tested here. The work of fracture of traditional laminated glass obtained from the force-displacement curves is very small (~0.04 kJ/m2), because once the crack propagates there is no significant toughening mechanisms in that material. In the cross-ply architectured glasses the work of fracture was 12 to 53 times higher than that of the plain laminated glasses. In addition, because crack propagation in traditional laminated glass is sudden and brittle, a large portion of the energy accumulated prior to fracture may be dispelled in dynamic effects instead of by creating new fracture surfaces. For brittle materials, the real work of fracture may represent as little as half of the strain energy stored in the sample at the onset of fracture [33]. With this correction for dynamic energy considered, the work of fracture of our architectured glass may have been up to 100 times higher than plain laminated glass. Within the results for architectured glass, a simple trend of the work of fracture with ply angle θ and ply width d was not observed, which we attributed this effect to different failure modes observed across these designs. Fig. 3-12e shows the three fracture modes identified for the cross-ply architectured glasses, as function of ply angle and ply width. The snapshots of that figure and in-situ observations showed that in general, when the crack reaches an interface between the plies, it is either deflected by the interface or it penetrates through the plies. When the crack was deflected its path was different in each layer, which triggered additional toughening mechanisms such as crack bridging by the plies and plastic deformation of the inter-layer, improving energy absorption and impeding crack propagation. In general, fracture of individual plies was therefore detrimental to overall toughness. The first mode is the crack deflection mode, which was prominent for low ply angle. In this mode the cracks were deflected along the weak interface, which stabilized crack propagation and increased toughness in a way similar to multilayered ceramics [34]. Fracture of individual plies was however also prominent in that mode. In this particular mode, it was found that the work of fracture was higher for smaller ply width d, because there were more weak interfaces to deflect the crack. At intermediate ply angles, crack channeling mode prevailed, where crack deflection was accompanied by shearing of the interfaces. The dominant toughening mechanism in this mode is the crack bridging by the plies, and the effect of ply width on work of fracture was minimal.

The third fracture mode was the shearing mode that was observed for the highest ply angle (θ = 75°). In this fracture mode crack deflection was prominent, with a crack path which was different in the two layers so that fracture resistance was mostly generated by the shear deformation of the interlayer. In the third fracture mode, the intermediate ply width d = 2 mm achieved the highest work of fracture ($p < 0.05$). For a lower ply width d =1 mm, the overlap area was too small to provide enough resistance and energy absorption. For a higher ply width (d = 3 mm), the over- lap areas were loo large which caused the premature failure of individual glass plies. The optimal failure mode depends on the working environment and the potential applications of the material. The shearing mode has a more progressive crack propagation and the most work of fracture but it produces a relatively low nominal strength in general. The crack deflection mode has the highest nominal strength but its work of fracture is not always the most optimal. In most of cases, the crack deflection mode should probably be promoted due to its stable performances and the balance between nominal strength and work of fracture.

3.8 Conclusions

Conch shells, fish scales or arthropod shells [14-16] demonstrate how the cross-ply architecture generates powerful toughening mechanisms that include crack deflection, twisting and crack bridging [17]. The toughest of these materials also rely on large deformations at the interfaces between plies or fibers, which generates large strains, energy dissipation and fiber rotation towards the axis of pulling [15, 35]. Here biological cross-ply architectures and their associated mechanisms were duplicated in a new laminated glass designs that generate new combination of toughness, deformability, and damage tolerance. The main conclusions are as follows:

(i) The laser engraving approach generates cross-plies and interfaces in laminated glass that can guide and channel cracks and deformation, with little impact on surface hardness and optical quality. The cross-ply architecture can be finely tuned to change the micromechanics of deformation, the overall performance and the mechanisms of fracture.

(ii) Remarkably, it shows that strain hardening and delocalization of strains can be achieved from large rotation of the plies, even if a softening interlayer is used. Our results also emphasize the idea that weak but deformable adhesive are preferable as interlayer over stronger but more brittle adhesives.

(iii) Overall our best cross-ply design has a strength which is 4 times lower than laminated glass in uniaxial tension of intact samples, but it can absorb up 100 times more energy by controlled inelastic deformation of the interlayer. In the presence of a severe stress concentration, our materials perform much better than traditional laminated glasses, demonstrating a high capability for damage tolerance. These results demonstrate how the interplay between hard materials with controlled architectured and soft interlayers can produce outstanding properties.

(iv) The nature of architectured materials creates theoretical difficulties with implications in the laboratory: (1) the size of the architecture approaches the size of the entire sample, so that separation of length scales is not possible and (2) for most architectured samples the size of the inelastic region also approached the size of the sample. For these reasons the principle of autonomy (a cornerstone of predictive fracture mechanics) was not valid for the samples tested [36] and we did not attempt to use measures of fracture resistance such as K_{IC}, G_C or J integrals for our materials. In this work work of fracture was used instead, and only to evaluate the resistance to cracking of our architectured glasses in comparison with regular laminated glasses tested using the same sample geometry and conditions.

This new type of bioinspired laminated glass has therefore potential in architectural glass, glass curtain walls, electronic device and solar panels. Generally, our material also demonstrates how material architectures at intermediate length scales (mm) can completely change the behaviour of material and can generate high performance. In particular, the architecture can be finely tuned to fully exploit the synergies between very hard (but brittle) and very soft (but deformable) components, leading to large amplifications of properties. With this approach superior materials can be synthesized even with inferior base materials, which further expands the design space of the conventional materials. Future studies on this material include models for fracture so that the exact fracture mode map can be refined, effects of strain rate (including strain rate hardening), and mechanical response under combined loading as done for staggered composites [37].

3.9 Acknowledgement

This research was supported by a NSERC Strategic Grant. Z.Y. was partially supported by a McGill Engineering Doctoral Award. The author also thanks Rob Botmann from Glassopolis (Toronto, ON Canada) for valuable discussions and feedback.

3.10 References

1. Burrows, K. and V. Fthenakis, *Glass needs for a growing photovoltaics industry.* Solar Energy Materials and Solar Cells, 2015. **132**: p. 455-459.
2. Ritchie, R.O., *The conflicts between strength and toughness.* Nature Materials, 2011. **10**(11): p. 817-822.
3. Norville, H.S., W. King Kim, and L. Swofford Jason, *Behavior and Strength of Laminated Glass.* Journal of Engineering Mechanics, 1998. **124**(1): p. 46-53.
4. Barthelat, F., *Architectured materials in engineering and biology: fabrication, structure, mechanics and performance.* International Materials Reviews, 2015. **60**(8): p. 413-430.
5. Wegst, U.G.K., et al., *Bioinspired structural materials.* Nature Materials, 2015. **14**(1): p. 23-36.
6. Kuhn-Spearing, L.T., et al., *Fracture mechanisms of the Strombus gigas conch shell: implications for the design of brittle laminates.* Journal of Materials Science, 1996. **31**(24): p. 6583-6594.
7. Menig, R., et al., *Quasi-static and dynamic mechanical response of Strombus gigas (conch) shells.* Materials Science and Engineering: A, 2001. **297**(1): p. 203-211.
8. Meyers, M.A., et al., *Biological materials: Structure and mechanical properties.* Progress in Materials Science, 2008. **53**(1): p. 1-206.
9. Kamat, S., et al., *Structural basis for the fracture toughness of the shell of the conch Strombus gigas.* Nature, 2000. **405**(6790): p. 1036-1040.
10. Kamat, S., et al., *Fracture mechanisms of the Strombus gigas conch shell: II-micromechanics analyses of multiple cracking and large-scale crack bridging.* Acta Materialia, 2004. **52**(8): p. 2395-2406.
11. Yahyazadehfar, M., D. Bajaj, and D.D. Arola, *Hidden contributions of the enamel rods on the fracture resistance of human teeth.* Acta Biomaterialia, 2013. **9**(1): p. 4806-4814.
12. Barthelat, F., Z. Yin, and M.J. Buehler, *Structure and mechanics of interfaces in biological materials.* Nature Reviews Materials, 2016. **1**(4): p. 16007.
13. Yahyazadehfar, M. and D. Arola, *The role of organic proteins on the crack growth resistance of human enamel.* Acta Biomaterialia, 2015. **19**: p. 33-45.
14. Zhu, D., et al., *Structure and Mechanical Performance of a "Modern" Fish Scale.* Advanced Engineering Materials, 2012. **14**(4): p. B185-B194.
15. Yang, W., et al., *Protective role of Arapaima gigas fish scales: Structure and mechanical behavior.* Acta Biomaterialia, 2014. **10**(8): p. 3599-3614.
16. Bouligand, Y., *Twisted fibrous arrangements in biological materials and cholesteric mesophases.* Tissue and Cell, 1972. **4**(2): p. 189-217.
17. Suksangpanya, N., et al., *Twisting cracks in Bouligand structures.* Journal of the Mechanical Behavior of Biomedical Materials, 2017. **76**: p. 38-57.
18. Karambelas, G., S. Santhanam, and Z.N. Wing, *Strombus gigas inspired biomimetic ceramic composites via SHELL—Sequential Hierarchical Engineered Layer Lamination.* Ceramics International, 2013. **39**(2): p. 1315-1325.
19. Grunenfelder, L.K., et al., *Bio-inspired impact-resistant composites.* Acta Biomaterialia, 2014. **10**(9): p. 3997-4008.
20. Chen, L., et al., *Bioinspired micro-composite structure.* Journal of Materials Research, 2007. **22**(1): p. 124-131.

21. Mirkhalaf, M., A.K. Dastjerdi, and F. Barthelat, *Overcoming the brittleness of glass through bio-inspiration and micro-architecture.* Nature Communications, 2014. **5**(1): p. 3166.
22. Weaver, J.C., et al., *The Stomatopod Dactyl Club: A Formidable Damage-Tolerant Biological Hammer.* Science, 2012. **336**(6086): p. 1275.
23. Barthelat, F., *Designing nacre-like materials for simultaneous stiffness, strength and toughness: Optimum materials, composition, microstructure and size.* Journal of the Mechanics and Physics of Solids, 2014. **73**: p. 22-37.
24. D1746-15, A., *Standard Test Method for Transparency of Plastic Sheeting*. 2015, ASTM International: West Conshohocken, PA.
25. Becerril, H.A., et al., *Evaluation of Solution-Processed Reduced Graphene Oxide Films as Transparent Conductors.* ACS Nano, 2008. **2**(3): p. 463-470.
26. Pukánszky, B., *Optical clarity of polypropylene products*, in *Polypropylene: An A-Z reference*, J. Karger-Kocsis, Editor. 1999, Springer Netherlands: Dordrecht. p. 554-560.
27. C1273-18, A., *Standard Test Method for Tensile Strength of Monolithic Advanced Ceramics at Ambient Temperatures*. 2018, ASTM International: West Conshohocken, PA.
28. Ostoja-Starzewski, M., *Material spatial randomness: From statistical to representative volume element.* Probabilistic Engineering Mechanics, 2006. **21**(2): p. 112-132.
29. Raabe, D., C. Sachs, and P. Romano, *The crustacean exoskeleton as an example of a structurally and mechanically graded biological nanocomposite material.* Acta Materialia, 2005. **53**(15): p. 4281-4292.
30. Chen, P.-Y., et al., *Structure and mechanical properties of crab exoskeletons.* Acta Biomaterialia, 2008. **4**(3): p. 587-596.
31. Barthelat, F., A.K. Dastjerdi, and R. Rabiei, *An improved failure criterion for biological and engineered staggered composites.* Journal of The Royal Society Interface, 2013. **10**(79): p. 20120849.
32. Research, A.A., *Release 16.1*.
33. Barinov, S.M. and M. Sakai, *The work-of-fracture of brittle materials: Principle, determination, and applications.* Journal of materials research, 1994. **9**(6): p. 1412-1425.
34. Clegg, W.J., et al., *A simple way to make tough ceramics.* Nature, 1990. **347**(6292): p. 455-457.
35. Khayer Dastjerdi, A. and F. Barthelat, *Teleost fish scales amongst the toughest collagenous materials.* Journal of the Mechanical Behavior of Biomedical Materials, 2015. **52**: p. 95-107.
36. Zehnder, A.T., *Fracture Mechanics*. Lecture Notes in Applied and Computational Mechanics. 2012: Springer Netherlands.
37. Slesarenko, V., N. Kazarinov, and S. Rudykh, *Distinct failure modes in bio-inspired 3D-printed staggered composites under non-aligned loadings.* Smart Materials and Structures, 2017. **26**(3): p. 035053.

Link between Chapter 3 and Chapter 4

The previous chapter presented a type of bi-layer glass designs with bio-inspired cross-ply architectures, which were highly deformable and tough in tension. The deformation and toughen mechanisms of the cross-ply glass were studied. However, the performances under bending, puncture and impact are more critical for glass. The next chapter, published in *Science*, 2019, presents a nacre-like glass that is deformable and impact resistant under transverse loading (bending, puncture and weight-drop impact). The fabrication protocol was designed to generate very well aligned tablets that gave the nacre-like high transparency evaluated by the light transmittance tests. The nacre-like glass successfully duplicated the large-scale tablet sliding that is often observed in natural nacre but was absent in nacre-inspired materials. As a result of the large-scale table tablet sliding, the nacre-like glass was two to three times more impact resistance than tempered glass and laminated glass. In the chapter, the performances of nacre-like glass beams under four-point bending were evaluated with variations on the tablet size. The microscopic images revealed the large-scale tablet sliding that granted the nacre-like glass beams high deformability. Nacre-like glass panels were tested under quasi-static puncture and weight-drop impact. The micro-CT images of damaged nacre-like glass panels showed that tablet sliding spread to a large volume. The amount and type of shear deformation ("sliding") at the interface were quantified and the energy absorption based on it was calculated, which matched with the energy absorption directly measured from the force-displacement curves in the puncture tests. Our study also showed that the energy absorption of nacre-like glass optimized at an intermediate tablet size. Tablet size being too small led to low strength while tablet being too large led to brittle tablet fracture.

Chapter 4: Impact resistant nacre-like transparent materials

Zhen Yin, Florent Hannard and Francois Barthelat*

*Department of Mechanical Engineering, McGill University, 817 Sherbrooke Street West,
Montreal, QC H3A 2K6, Canada*

*corresponding author: (francois.barthelat@mcgill.ca)

4.1 Abstract

Glass has outstanding optical properties, hardness, and durability, but its applications are limited by its inherent brittleness and poor impact resistance. Lamination and tempering can improve impact response but do not suppress brittleness. We propose a bioinspired laminated glass that duplicates the three-dimensional "brick-and-mortar" arrangement of nacre from mollusk shells, with periodic three-dimensional architectures and interlayers made of a transparent thermoplastic elastomer. This material reproduces the "tablet sliding mechanism," which is key to the toughness of natural nacre but has been largely absent in synthetic nacres. Tablet sliding generates nonlinear deformations over large volumes and significantly improves toughness. This nacre-like glass is also two to three times more impact resistant than laminated glass and tempered glass while maintaining high strength and stiffness.

4.2 Introduction, results and discussions

Glass is a widely used material because of its optical properties, hardness, durability, and thermal and chemical stability. However, glass has no large deformation or toughening mechanism at ambient temperature, and as a result, its tensile strength is compromised by the slightest defects or damage [1], and it has poor impact resistance. A strategy to improve strength and impact resistance is tempering, in which compressive stresses are created at the surface of the component to hinder crack initiation, increasing strength to two to five times that of annealed glass [2]. However, fracturing tempered glass results in catastrophic failures that release the elastic energy stored during tempering, destroying the entire component in an “explosive” fashion. Another strategy consists of intercalating glass sheets with softer polymeric layers to form laminated glass. In case of fracture, the polymeric interlayer holds the glass fragments together, but the overall impact resistance is not otherwise improved significantly [3]. Tempering and laminating can be used simultaneously, but these methods do not truly increase fracture toughness, and glass components remain by far the weakest structural elements in vehicles, buildings, and electronic devices.

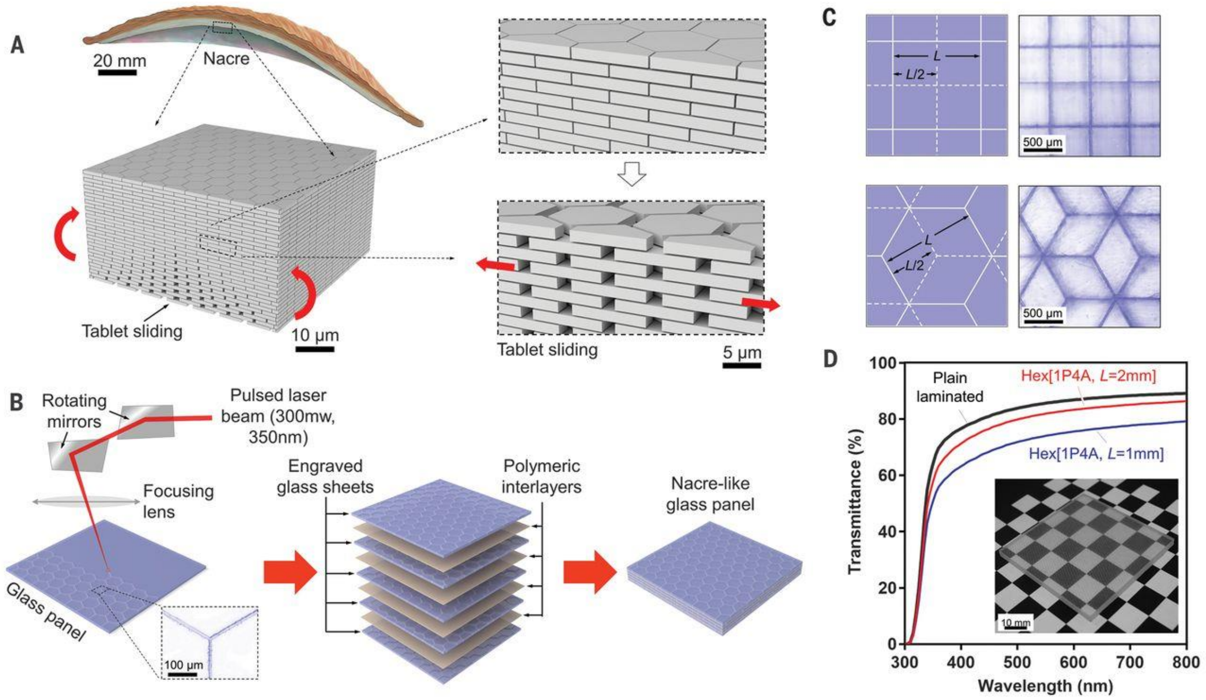

Fig. 4-1: Design and fabrication of nacre-like glass panels. (a) Natural nacre is made of 95 volume % of mineral tablets bonded by a softer organic mortar. Nacre can deform, stop cracks, and absorb impact energy by the sliding of the microtablets on one another and over large volumes. (b) Fabrication protocol for nacre-like glass panels (scale bar: 100 μm). (b) Details of tablet geometry and overlap structure (scale bar: 500 μm). (d) Light transmittance of nacre-like glass panels compared with plain laminated panels. (Inset) Optical clarity of a typical engraved panel (scale bar: 10 mm).

Biological materials can inspire new alleys to overcome brittleness. Now a model for bioinspiration, nacre from mollusk shells is a highly regular three-dimensional brick-and-mortar assembly of microscopic mineral tablets bonded by biopolymers. Under tensile forces, millions of tablets can slide on one another over large volumes (~1 mm^3) [4-6], a mechanism mediated by the shearing of the interfaces (Fig. 4-1a). The sliding mechanism dissipates large amounts of mechanical energy, which makes nacre deformable and tough despite its very high mineral content (95 volume %) [7-9]. Despite three decades of research efforts, fabricating large volumes of microscopic nacre-like "brick walls" remains a major challenge [10-15]. Fracture toughness is increased significantly in existing nacre-like materials, but mainly from crack deflection and crack bridging [14, 16] (mechanisms that are also used in multilayered ceramics [17, 18]). Ductility can be achieved in nacre-like nanocomposites, but at the expense of stiffness and strength [11, 19]. Some of these nacre-like materials are transparent, but they only come in the form of thin films [20, 21]. Large-scale tablet sliding, which is the critical mechanism in natural nacre (Fig. 4-1a), has been largely absent in synthetic nacres because the requirements for this mechanism are stringent: (i) hard tablets with a high aspect ratio to transfer shear stresses, but not too high to prevent tablet fracture [8, 9], (ii) strong adhesion of the interface material to the mineral [22], (iii) interfaces that are orders of magnitude more compliant than the tablets to achieve a near- uniform shear stress transfer [23], (iv) interface highly deformable in shear to maximize deformability [7], (v) strain hardening at the interface to delay strain localization and maximize the spreading of nonlinear deformations [5], and (vi) size and arrangement of the tablets as uniform as possible to delay strain localization and maximize energy dissipation [24]. The "synthetic nacres" that could fulfill these requirements were fabricated at millimeter scales, allowing high control over material architecture [25-27]. These materials achieved extensive tablet sliding but only in one plane, along one direction, and under simple, uniaxial loading.

This paper reports a three-dimensional synthetic nacre-like material that embodies the requirements for tablet sliding and overcomes the inherent brittleness of glass. The contours of the tablets were first engraved on 220-μm-thick borosilicate glass sheets by using a focused pulsed laser beam [28] (Fig. 4-1b). The engraved lines were sufficiently strong to enable the handling of individual glass sheets without separating the tablets, yet weak enough so that individual tablets were separated in a controlled fashion at later stages in the lamination process [28]. Five engraved glass sheets were laminated with ~125-μm-thick polymeric interlayers. During assembly, the glass sheets were carefully aligned so that the tablets formed a three-dimensional staggered arrangement akin to natural nacre (Fig. 4-1b). Nacre-like panels were fabricated based on square tablets and based on hexagonal tablets (Fig. 4-1c) of different sizes [length (L) = 1 mm, 1.5 mm, 2 mm, and 4 mm]. These dimensions were chosen to create tablets with an aspect ratio in the order of 10, which is close to the mineral tablets in natural nacre. A critical step was to identify synthetic polymers with mechanical attributes similar to the interfaces in nacre [22]. Most of the transparent polymers tested in shear were too brittle (resulting in poor energy absorption) and/or too strong (resulting in unwanted fracture of the glass tablets) [28]. Ethylene-vinyl acetate (EVA) was eventually selected as the interface material because of its relatively low strength, very high deformability in shear (>800%), strain hardening, and high energy absorption. EVA is also more resistant to ultraviolet light than polyvinyl butyral [29], another transparent polymer that is used in standard laminated glass. Nacre-like EVA-glass beams were deformed by large-scale sliding of the tablets (fig. S4), with an estimated work of fracture of 7200 J/m^2 (28) (more than three times higher than the work of fracture of synthetic nacres made by freeze casting [13, 14]).

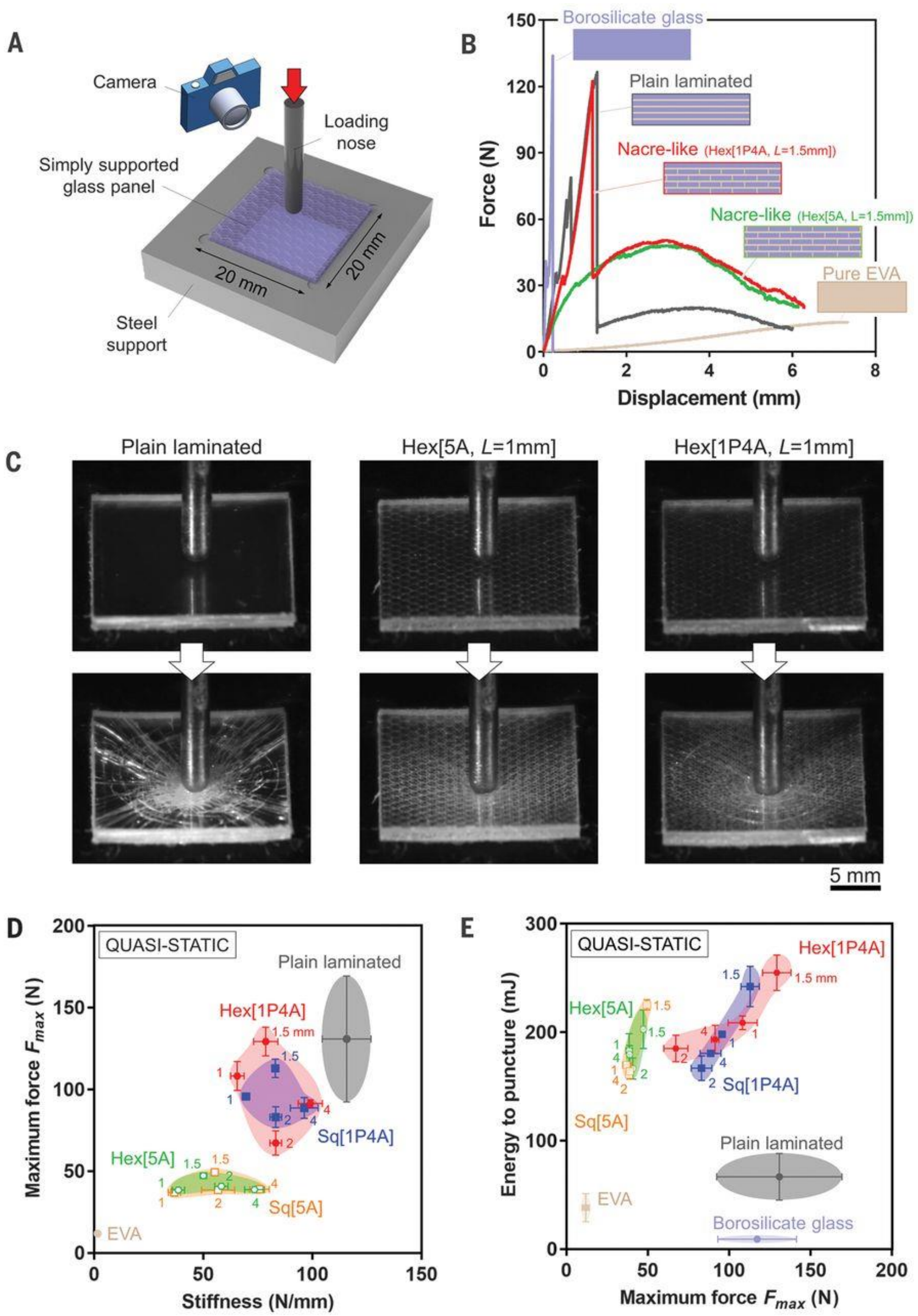

Fig. 4-2: Puncture of small nacre-like glass panels. (a) Experimental setup: A simply supported glass panel is punctured with a loading nose at a quasi-static rate. (b) Puncture force–displacement curves for pure borosilicate glass and pure EVA panels, plain laminated panels, and nacre-like panels with [5A] and [1P4A] layer configurations. (c) Plain laminated and nacre-like panels before and during puncture (at a displacement = 3 mm). The lighting and background were chosen to highlight the engraving patterns. Scale bar: 5 mm. (d and e) Property maps showing (d) maximum

force (strength) versus stiffness and (e) energy to puncture versus maximum force for different materials and designs.

Visually, nacre-like panels are transparent materials that generated relatively little blurring, little haze, and no image distortion (Fig. 4-1d). Light transmittance in the visible light range was about 10% lower than the transmittance of regular laminated glasses (Fig. 4-1d). Puncture tests on simply supported (20 mm by 20 mm by 1.6 mm) panels of different designs (Fig. 4-2a) showed that borosilicate glass and plain laminated glass have a high strength but fail in a brittle fashion (Fig. 4-2b), with multiple catastrophic cracks emanating from the loading point to the edge of the panel (Fig. 4-2c). The strength of these materials showed large variability because it is governed by weakest-link (Weibull) statistics [30]. In the laminated glass panels, the fragments were held by the EVA interlayers, which produced a small but non-negligible residual puncture force. This mechanism, typical of traditional laminated windows and windshields, only involves a small volume fraction of the EVA interlayer, and therefore the deformation and energy-absorbing capabilities of the interfaces were largely underused. By contrast, the nacre-like panels produced a more ductile response with large deformations and high energy to puncture (area under the force-displacement curve). The mechanical response of the nacre-like glass was more repeatable than in plain and laminated glasses because it is governed by tablet sliding, a well-controlled deterministic mechanism. Damage was overall much less visible compared to with regular laminated glass, but a large homogenous and plastic deformation developed around the puncture site (Fig. 4-2c). Because of their segmented architecture, the stiffness and the strength of the initial all-engraved designs [5A] were about half of the stiffness and strength of laminated glass (Fig. 4-2d). An improved design with a plain glass sheet used as front layer (designs [1P4A]: Fig. 4-2b) increased the initial strength and stiffness to levels only 10 to 15% below plain laminated glass (Fig. 4-2d).

(Similarly, the strength and stiffness of natural nacre are lower than that of the individual aragonite tablets [22], and the nacreous layer is covered by a harder and stiffer layer of prismatic calcite [31].). The homogenous front glass layer also provides high surface hardness, durability, dimensional stability, and waterproofness. In terms of energy to puncture, plain borosilicate glass performed the worst (Fig. 4-2e). Laminated glass had an improved (sixfold) energy to puncture, but the nacre-like designs were the toughest, “amplifying” the energy to puncture by another factor of 2.5 to 4 compared with laminated glass. Short tablets (L = 1 mm) ensured tablet sliding without tablet failure. By contrast, longer tablets (L = 2 mm and L = 4 mm) led to higher stiffness, but excessive fracture of individual tablets limited strength and energy absorption. The best nacre-like panels design in terms of high energy to puncture and high strength was the [1P4A] layer configuration with L = 1.5- mm hexagonal tablets (Fig. 4-2e).

Micro-computed tomography (micro-CT) of the punctured panels [28] provided a comprehensive picture of the micromechanics of deformation in laminated glass and in the nacre-like panels (Fig. 4-3). We were particularly interested in quantifying the amount and type of shear deformation (“sliding”) at the interfaces between the glass layers, because it is the main mechanism for energy dissipation [28]. The sliding distribution in the lowermost interlayer in the panel (Fig. 4-3b) shows relatively small interfacial sliding distances in the plain laminated glass, except near large cracks. By contrast, the sliding distances in the nacre-like panels were much larger and more homogenously distributed. On the basis of the sliding distance distributions, we computed the square of the sliding distance integrated over the entire interface, a quantity that scales with energy absorption. The integrated values for the nacre-like panel were about 2.4 times greater than those of the plain laminated glass, in agreement with the puncture tests in which the energy to puncture in the nacre-like panels was 2 to 3 times larger than that of the plain laminated glass. The shear deformation of the interfaces is therefore the main source of toughness in the nacre-like panels. A sliding mechanism index (SMI) [28], a normalized version of the local divergent of the sliding displacements vector field (Fig. 4-3d), was also computed. In plain laminated glass, sliding was mostly uniform (SMI ~ 0), except in localized regions across the cracks, where SMI ~ 0.5 (uniaxial separation of fragments). By contrast, the deformation in the nacre-like panels was dominated by unidirectional and biaxial sliding (0.5 < SMI < 1), providing quantitative evidence that these panels properly duplicated the nacre-like sliding mechanism over large volumes (Fig. 4-3c).

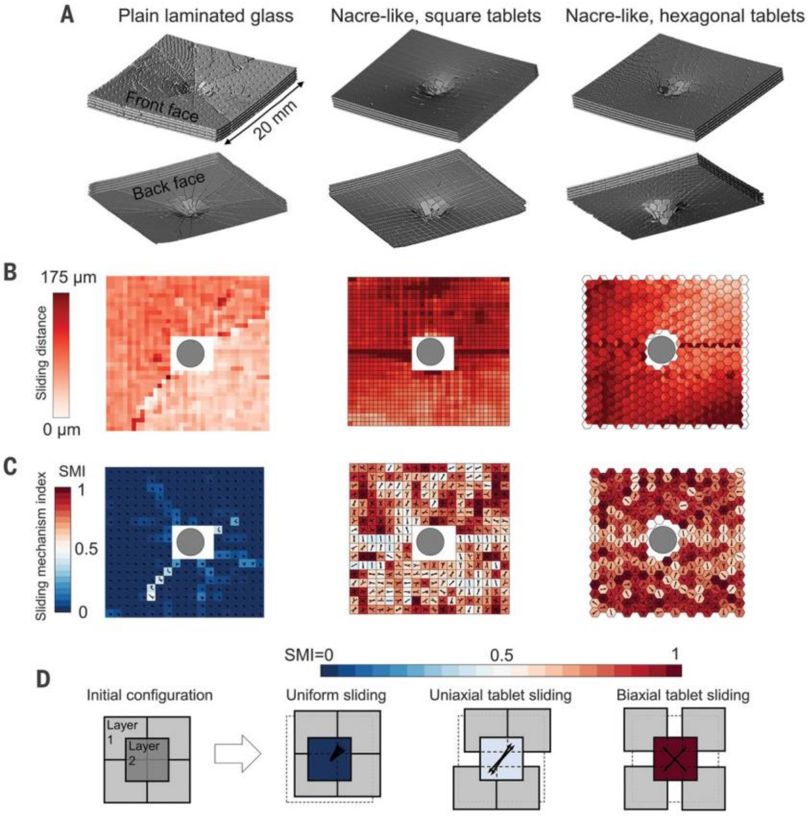

Fig. 4-3: Micro-CT scans and analysis for plain laminated and nacre-like panels. (a) Three-dimensional microtomography perspectives of punctured samples (for plain laminated glass, arrays of microdots were engraved on the surface of the layers to track their relative sliding). (b) Maps of the sliding distance in the lowermost interlayer, showing larger and more distributed sliding in the nacre-like designs. (c) Maps of the SMI in the lowermost interlayer in the panel, also showing sliding vectors. (d) Schematic showing three sliding mechanisms corresponding to three values of the SMI. Tablet sliding was generally more bidirectional and isotropic in panels based on hexagonal tablets.

Larger panels (50 mm by 50 mm by 3 mm) were finally tested for impact resistance [28]. Poly(methyl methacrylate) (PMMA) (Plexiglas) was the lightest of the materials tested, but it also had the lowest impact resistance (energy to puncture) (Fig. 4-4b). This transparent polymer is brittle at high loading rates, and the panel fractured into four to five large fragments (Fig. 4-4c). Pure borosilicate glass is about twice as dense as PMMA, with a slightly higher impact resistance but also a brittle fracture. The two types of tempered glasses tested had an improved impact resistance; failure was catastrophic and explosive, with multiple small fragments. Laminated glass performed better than the tempered glasses in terms of impact resistance, because of the large number of layers used (N = 10) and the high deformability of the EVA interlayers. The damage pattern was, however, the same as in the quasi-static regime, with extensive damage in the form of long radial and circumferential cracks and fragments held together by the EVA interlayer. Finally, nacre-like panels based on hexagonal tablets (L = 1.5 mm) and with a [2P8A] configuration (two plain layers were used on the front face of the 10-layer panel to match the composition of the [1P4A)] design) had the highest impact resistance, about double that of the tempered glasses. The nacre-like panels also failed by a graceful mode with large inelastic deformations and no shards (Fig. 4-4c).

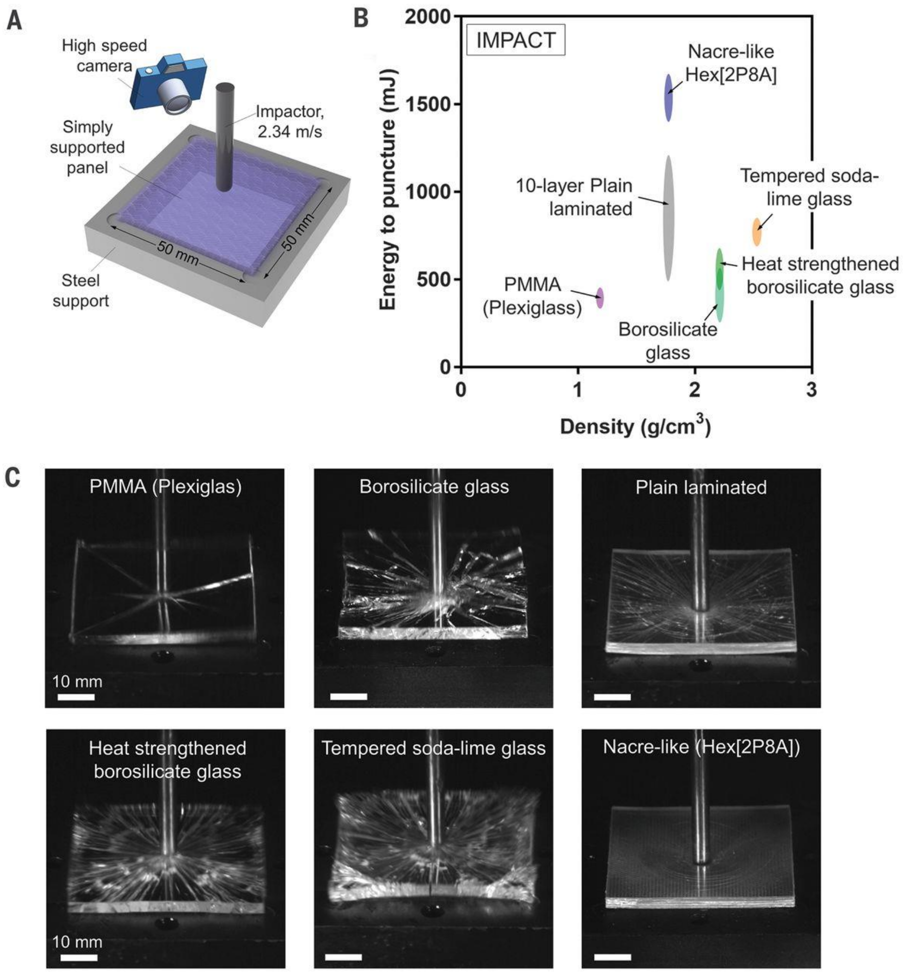

Fig. 4-4: Impact tests on large nacre-like panels and other transparent materials. (a) Experimental setup: A simply supported (50 mm by 50 mm by 3 mm) panel is impacted at a velocity of 2.34 m/s. (b) Energy to puncture versus mass density property map for the six designs and materials tested in impact (all had the same overall dimensions). (c) Corresponding snapshots from high-speed photography. Scale bar: 10 mm.

Our transparent glass duplicates the large-scale sliding of individual tablets in three dimensions and over large volumes, even when subjected to a concentrated force. This mechanism is mediated by the shearing of the interlayers, which absorbs large amounts of mechanical energy, providing the material with toughness, superior impact resistance, graceful failure, and damage tolerance. These nacre-like panels also illustrate how an architecture with relatively large size but with high order and periodicity can be preferable to smaller but more disordered microstructures, which is consistent with recent models and other recent bio-inspired materials [24, 32]. Finally the laser engraving and lamination fabrication methods are inexpensive, and relatively easy to implement into the large-scale production of impact-resistant nacre-like glass panels for a wide range of applications, including protective structures, windows, photovoltaic systems, building materials, and electronic devices.

4.3 Appendix

4.3.1 Materials and methods

Glass laser engraving and mechanical separation: The nacre-like glasses were made with 0.22 mm thick borosilicate glass plates (fisher scientific Hampton, NH, USA) which were engraved using a laser engraver (Model Vitrolux, Vitro Laser Solutions UG, Minden, Germany) with a pulsed UV beam (355 nm, 0.5 W cw pumped, 4 kHz repetition rate, 4–5 ns pulse duration). The laser engraver carved arrays of 20 µm wide micro-defects through the thickness of the glass plate. The power was set at 300 mw and the defect spacing was set to 10 µm. The positions for each defect was generated in MATLAB (Fig. 4-5a) and stored in the form of three-dimensional coordinates and sequence of engraving. The engraving process left weak interfaces in the glass and ~40 µm deep trenches on the glass surface from laser ablation (Fig. 4-5a-e). A polyimide tape (Dupont) was then glued to the engraved glass plate, and the tablets were separated by gently bending the glass plate using a 6 mm diameter cylindrical roller (Fig. 4-5c).

Multi-layered glass lamination: The lamination process started with a two-layer lamination. A pair of engraved glass plates were first laminated with 90 µm or 250 µm thick EVA thermoplastic film (CAIDA, Tianjin, China) as the interlayer. Two rigid plates were applied on each side of the pre-laminate to ensure even pressure. Rigid confining frame elements were installed on the four sides of the two-layer pre-laminates to prevent tablet misalignment during the lamination process. The two-layer pre-laminates were then placed in a vacuum oven (Model No: 1410M, Shel Lab) under a 100 kPa pressure for 1.5 hours. The polyimide tape was then peeled off. The interlayer thickness after pressured lamination decreased by about 50% from the initial film thickness. The two-layer materials were then laminated again using the same procedure for the fabrication of multi-layered (N>2) materials.

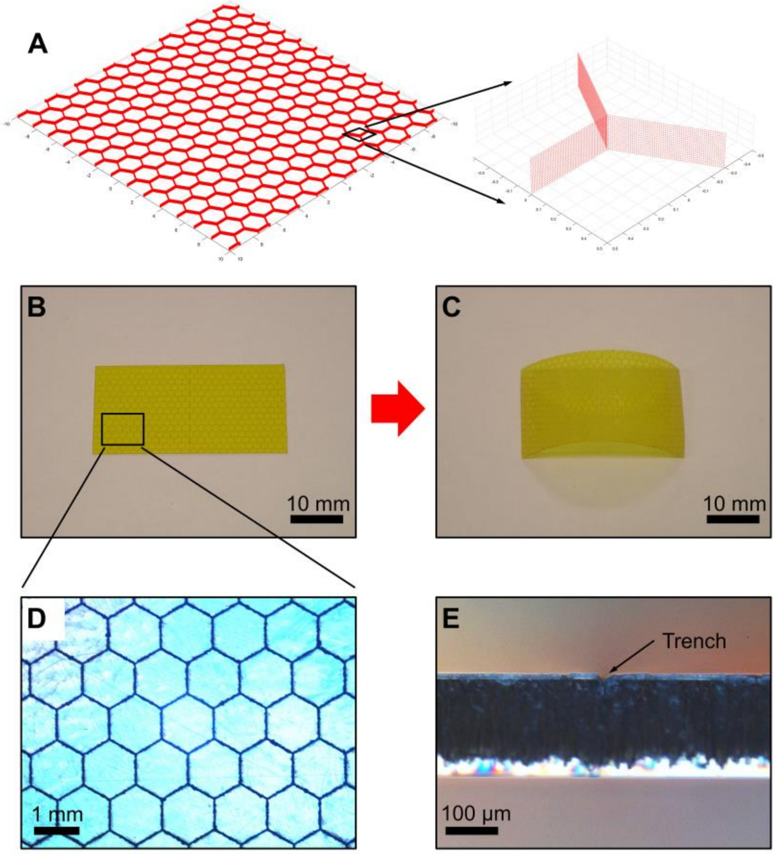

Fig. 4-5: Preparation of individual glass layers. (a) Example of point clouds used as input for laser engraving. (b) The glass plate was engraved with this hexagonal pattern and was taped with a polyimide film. Scale bar: 10 mm. (c) Individual glass tablets were mechanically separated using controlled bending. Scale bar: 10 mm. (d) Micrograph of the engraved layer showing a close-up view of the hexagonal pattern. Scale bar: 1 mm. (e) Side view of an engraved glass plate, showing a trench on the surface of the glass plate, that resulted from laser ablation in the laser engraving process. Scale bar: 100 µm.

Shear lap tests: The test setup used ASTM C961 as a reference. 50 micrometer thick layer of polymers were deposited over a 25 mm by 2 mm overlap area between pairs of borosilicate glass substrates. The samples were then loaded in tension using a universal testing machine (model: eXpert 5000, ADMET, Norwood, MA, USA) at a displacement rate of 10 µm/s, to induce a state of simple shear in the polymer. Shear stress-strain curves were computed from the force-displacement curves obtained from these experiments. Three samples were tested for each polymer.
Quasi-static puncture tests: The test setup used ASTM F3007 as a reference. The samples used for the quasi-static puncture tests were 20×20 mm panels. For each design, 4-10 samples were tested. The samples were simply supported at their periphery on a 2 mm wide shoulder machined in a steel frame. The puncture tests were conducted on a universal testing machine (model: eXpert 5000, ADMET, Norwood, MA, USA). A loading nose with a spherical tip (radius =3 mm) was driven into the center of the simply supported panel at a quasi-static rate of 10 µm/s and until failure. The puncture force and puncture displacement were collected during the test, and the energy to puncture of each panel was determined by computing the area under the force-displacement curves. In the cases where failure was brittle, only a small fraction of the area under the curve is actually absorbed by the material [33]. Excess energy is dissipated as stress waves in the system, phonons, or kinetic energy in the fragments. For case where failure was “graceful” with a progressive decrease on force, most of the energy to puncture was actually absorbed by the visco-plastic shearing of the interlayers within the panels.

Weight-drop impact tests: The test setup used ASTM 3007 as a reference. All panels tested for impact had a dimension of 50×50 mm and a thickness of 3 mm, and they were simply supported at their periphery. For each design, 3-7 samples were tested. The laminated glass and nacre-like samples contained 10 glass layers. In the nacre-like panel, two plain layers were used as front layers so that the fraction of plain glass layer was the same in the [1P4A] and [2P8A] designs. The weight-drop impact tests were conducted on an instrumented drop tower (model CEAST 9310 drop tower impact system, Instron, Norwood, MA, USA) mounted with a rod-like impactor with rounded tip (diameter = 5mm). The tests used a drop mass of 0.75 kg and an impact velocity of 2.34 m/s, which provided ample kinetic energy to puncture the samples. First a force-displacement curve was computed from the force-time curve, and then the impact resistance (in energy terms) was measured by calculating the area under the force-displacement curve.

<u>Light transmittance tests</u>: The test setup used ASTM D1746 as a reference. The light transmittance tests were conducted on a multi-mode microplate reader (model: SpectraMax M5, Molecular Devices). The sample fabricated for light transmittance tests were five-layer nacre-like panels with dimensions of 20×10×1.6 mm^3. The microplate reader was used to measure the light absorbance of the material at the spectrum ranging from 300 to 800 nm. The absorbance measured was then converted to transmittance using the following equation:

$$\%T = 10^{(2-A+A_{bg})}$$

where $\%T$ is the transmittance, A is the absorbance measured for the sample and A_{bg} is the background absorbance measured.

<u>Imaging of the nacre-like glasses</u>: The pictures of the nacre-like glass panels of Fig. 4-2 and Fig. 4 in the main text were taken by a digital camera (model: C-5060, Olympus, Shinjuku, Tokyo, Japan) under natural daylight. The snapshots of nacre-like glass panels under quasi-static puncture tests were captured using a pair of high-speed cameras (model: IL-5, Fastec Imaging, San Diego, CA, USA). The two cameras were synchronized to capture the deformation of nacre-like panels simultaneously. The images were taken every 5 seconds. 3D digital image correlation was

conducted using the software vic-3D (version: 2012, correlated solutions, Irmo, SC, USA) to obtain the surface deformation of nacre-like glass panels under puncture. The camera setup was the same for weight-drop impact tests, but the acquisition rate was wet to 1000 frames/s.

<u>Micro-CT analysis of the nacre-like panels</u>: The samples were scanned using a Zeiss Xradia Versa 520 scanner with an accelerating voltage of 60 kV and a power of 82 mA. The scans were carried out with 0.4x objective lens with 1 bin, resulting in pixel size of 11.35 μm in 2000 × 2000 pixels images. The source-to-sample and the detector-to-sample distances were 42mm and 85mm, respectively. 1601 projections were acquired during a 180 degree rotation of the sample with high aspect ratio tomography mode and the exposure time was 3.75 s. The tablets in the reconstructed grayscale images were segmented with a 3D multiple seeded region growing algorithm. This procedure was implemented in MATLAB and was adapted from a single seeded region growing algorithm [34]. For each reconstructed volume of the glass panel, the analysis started by isolating each glass layer within the panel. A seed point was then placed approximately at the centroid of each tablet (as illustrated in 2D in Fig. 4-6a for clarity). Volumetric regions were then iteratively grown from these seed points by voxel aggregation. At each iteration, the difference between the average intensity of a region and the intensity value of each neighboring voxel to this region was calculated. For each region, the voxel with the smallest difference of intensity was aggregated and the iterative process was stopped when the difference between the region average intensity and the new voxel intensity became larger than a given threshold. A typical result of the region growing procedure is shown in Fig. 4-6b. Each 3D region (i.e. each group of connected voxels) corresponds to one 3D tablet. To improve the accuracy of the analysis, each of these 3D regions was then fitted with a geometrical representation of a 3D tablet (i.e. a 3D object with the exact tablet shape). The

position and orientation of each tablet in the panel were then computed from the reconstructed CT scan (Fig. 4-6c).

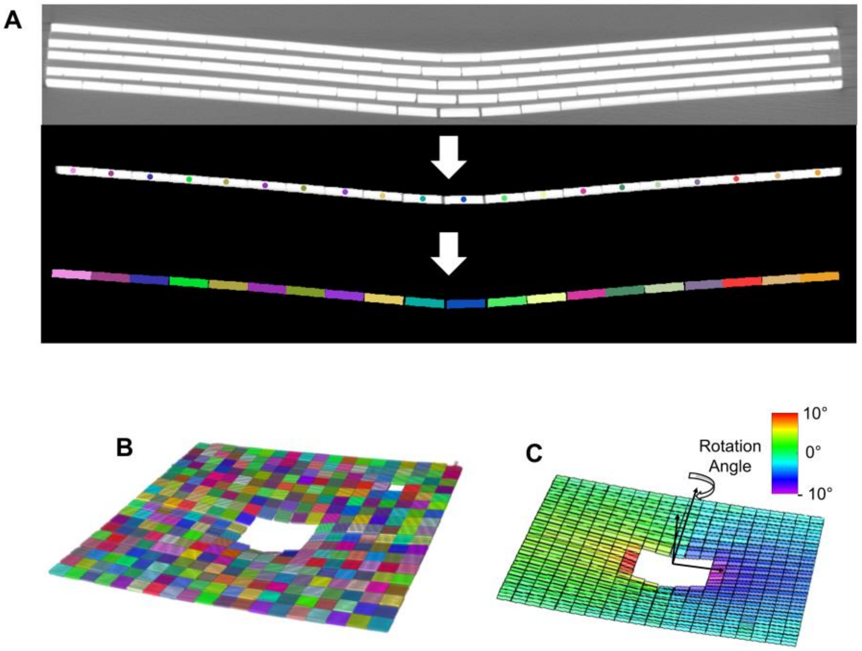

Fig. 4-6: Micro-CT analysis of the nacre-like panels. (a) Cross section of an X-ray microtomography for a nacre-like the glass panel. After processing, the position of the center and the rotation of each tablet is computed (reconstructed tablets are colored). (b) Entire glass layer reconstructed with position of each tablet (c) The procedure can also be used to measure the rotation of individual tablets.

For the case of plain laminated glass, laser engraving was used to generate arrays of micro-markers on the surface of each layer to track the relative motion of the layer from micro-CT imaging. The depth of these markers was large enough to be clearly resolved within the CT scanner but small enough to avoid failure from stress concentrations (it was verified that the mechanical property and failure mode of the laminated glass panels were not affected by this array of micro-markers).

Fig. 4-7a shows 3D microtomography perspective of punctured architectured glass panel (with square tablets configuration). Fig. 4-7c shows a contour map of the sliding distance within each interlayer of this panel. Since the shearing of the interface is the main energy absorbing mechanism, energy absorption scales with the square of the sliding distance integrated over the entire interface. Fig. 4-7b shows this integrated value for each interlayer of the square nacre-like panel. The energy distribution indicates that the top interlayer (i.e. on the impact side) contribution is very limited (approx. 10%). This explains why replacing the top architectured layer with a plain glass sheet increases the initial strength without losing the energy absorption capacity of the nacre-like panels.

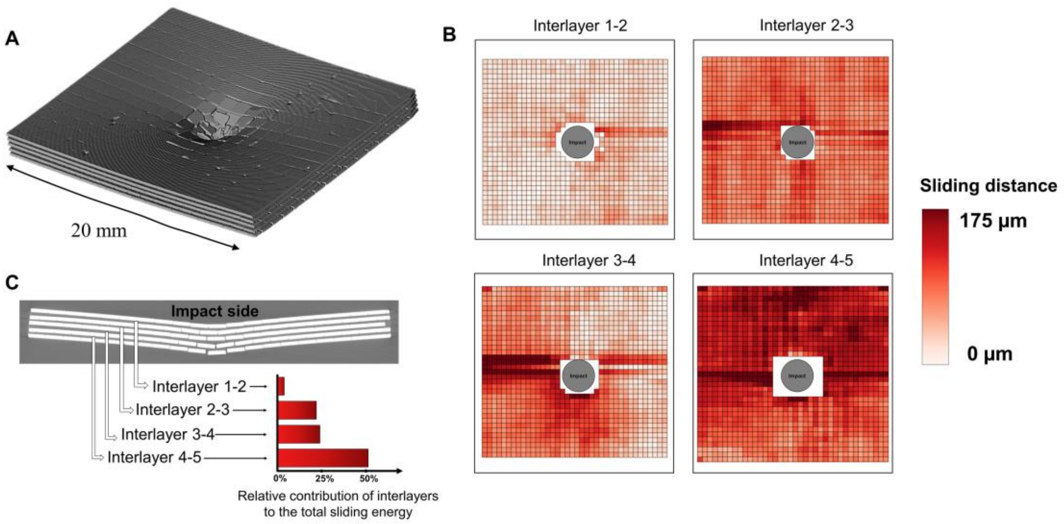

Fig. 4-7: Energy absorption analysis based on micro-CT analysis. (a) Full 3D microtomography of a punctured sample. (b) Maps of the sliding distance within each of the four interlayers in the panel (each colored area corresponds to an overlap between two tablets) (c) The sliding distances are squared and integrated over the surface of each interlayer. This procedure is used to estimate the relative contribution of each interlayer to the total energy absorption. The lowermost interlayer accounts for 50% of the total energy absorbed in the panel.

4.3.2 Selection of a synthetic polymer as the interfacial material

Thermoplastic polymers are particularly well suited for nacre-like interfaces, because they combine elastomeric response with large inelastic deformations. Surlyn and ethylene-vinyl acetate (EVA) were selected as two possible candidates. Surlyn is a thermoplastic carboxylate ionomer and a copolymer of ethylene and methacrylic acid, neutralized with alkali metals or zinc [35, 36]. The addition of acid monomer reduces the long chain branching and the overall degree of crystallinity. The absence of light scattering large-scale crystalline superstructures result in the high clarity of Surlyn that makes it suitable for glass lamination. The microstructure of Surlyn contains crystalline and ionic phases connected by a matrix of soft hydrocarbon chains, resulting in a combination of relatively high strength, high deformability and high toughness [36]. As opposed to covalent bonds, ionic crosslinks can break and reform as the material is deformed, which can generate very large inelastic deformations in shear (up to about 300%) accompanied with energy dissipation. This type of dynamic crosslinks and sacrificial bonds are also found in the proteins and polysaccharides at the interfaces of bone, nacre and wood, and they are critical to their deformability and toughness [22]. Surlyn was however too strong, which led to excessive damage to the glass tablets in our composites. EVA is another type of copolymer made of copolymerizing ethylene with vinyl acetate by high pressure processing. The crystallinity of polyethylene is decreased by the vinyl acetate comonomer incorporated into the polyethylene backbone chains [37]. The hard and soft phases existing in the thermoplastic copolymers produce a strain hardening effect, increased toughness and deformability than homopolymers [38]. EVA combines the mechanical properties of an elastomer (large deformations), with the properties of a thermoplastic polymer (yield point followed by plastic flow). It also has a relatively low melting temperature (90 ºC) which facilitated fabrication. Other adhesives were also tested in single lap shear tests (Fig. 4-8). Cyanoacrylate and epoxy are too brittle to make nacre-like interfaces that can dissipate energy. These adhesives are also too strong to channel deformations and deflect cracks, and nacre-like glass-polymer composites made with these polymers failed by cracking of the glass tablets with little deformation at the interfaces. Silicone, a covalently crosslinked elastomer, was also considered because it is highly deformable in tension. However, under shear stress this type of covalently crosslinked elastomer has a linear response with limited deformability and limited dissipative capabilities [39, 40].

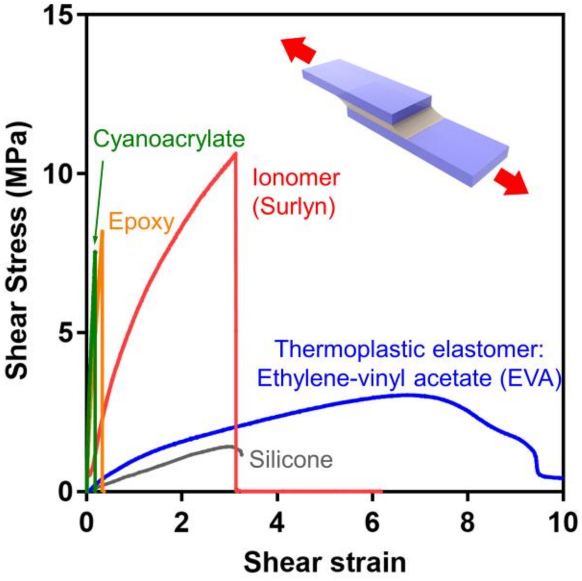

Fig. 4-8: Single lap shear tests on a selection of synthetic adhesives. In shear, cyanoacrylate and epoxy are too strong and brittle to make good nacre-like interfaces. Ionomer (Surlyn) provides some ductility, but it is too strong and leads to excessive damage in nacre-like panels. Silicone has a linear elastic response in shear with little energy dissipation. EVA has relatively low strength, but very high deformability in shear (>800%) accompanied with strain hardening. EVA was used as nacre-like interfaces for our materials.

4.3.3 Flexural tests on nacre-like glass beams

As the preliminary experiments prior to the puncture and impact tests, flexural tests on nacre-like beams were performed to validate the feasibility and observe the effects of large-scale tablet sliding directly. Flexural tests were also used to evaluate the optimal tablet size and to measure an estimated work of fracture. The flexural properties of nacre-like beams (Fig.S5A) were assessed using a four-point bending configuration (ASTM D7264) to screen and optimize different designs, and for in-situ observations of the micro-mechanisms of deformation and fracture. The samples were five-layer nacre-like beams with dimensions of 20 mm x 2 mm (width) x 1.3 mm (thickness). The thickness of the EVA interlayers was 50 microns. Four-point bending tests were conducted on a miniature loading machine (Ernest F. Fullam Inc., Latham, NY, USA) with a 10 lbs load cell, at a displacement rate of 10 μm/s. Snapshots of the nacre-like glass beams were acquired during the test under an optical microscope (model: BX51M, Olympus, Shinjuku, Tokyo, Japan) using a digital CCD camera (model: Retiga 2000R, QImaging, Surrey, BC, Canada), with a side illumination to highlight the micro-architecture of the beams. Fig. 4-9b shows the flexural responses of different designs, together with snapshots showing the failure mechanisms (Fig. 4-9c). The plain laminated glass produced an elastic response followed by brittle fracture at small deformations. Failure was highly localized and only a small volume fraction of the EVA interface deformed plastically. This failure, typical of traditional laminated windows or windshields, only involves a small volume fraction of the EVA interlayer and therefore the deformation and energy absorbing capabilities of this material is not used to the fullest. Once the glass layers fractured, the EVA interlayers produced some cohesion to the material, which illustrates the main function of the interlayer in traditional laminated glass: to hold the glass fragments together once the glass layers have fractured. In comparison, the nacre-like beams with tablet size L=1.5 mm (aspect ratio=6.8) had a lower flexural strength but showed more deformability. This particular design however showed localization and relatively brittle failure, because the long overlaps between the tablets resulted in overstressing the tablets in tension and in the premature tablet fracture, with limited energy dissipation (Fig. 4-9b). The nacre-like beams with tablet size L=1 mm (aspect ratio = 4.55) had a lower strength but it could also withstand larger deformations (Fig. 4-9b). Its deformation and failure mode were also different from the other two designs: the tablets remained intact, and sled on one another in the entire gage region of the beam. Localization was delayed and tablet sliding occurred over the entire volume of the stressed region because of a combination of lower aspect ratio of the tablets, near perfect periodicity in the architecture (*30*), and strain hardening provided by the EVA interlayer (Fig. 4-8). This large-scale sliding of the glass tablets on one another, mediated by the shearing of the soft interlayer is the nacre-like mechanism that we sought in our designs. Similar mechanism is found in nacre-like beams with L=0.75 mm (aspect ratio = 3.41) but at a lower strength (Fig. 4-9b).

The energy dissipated in this nacre-like beam was about 15 times higher than for the plain laminated beams for L = 1 mm. For L = 0.75 mm, the amplification factor was only about 5 because of the reduced strength. For L = 1.5 mm and L = 2 mm the energy absorption was even smaller and down to levels similar to plain laminated beams because of little tablet sliding brittle fracture. No attempt was made to measure the fracture toughness of this material, because the size of the inelastic region is comparable to the size of the sample, so even large-scale plasticity theories for fracture mechanics do not hold. However, a work of fracture (w.o.f.) could be estimated based on the energy required to completely fail the beam, by interpreting the junctions between the tablets in the lower layer as an initial dominant crack. Using this procedure, the w.o.f. of our nacre-like glass beams was estimated at up to 7200 J/m^2 (SD = 2.7 J/m^2, N = 4).

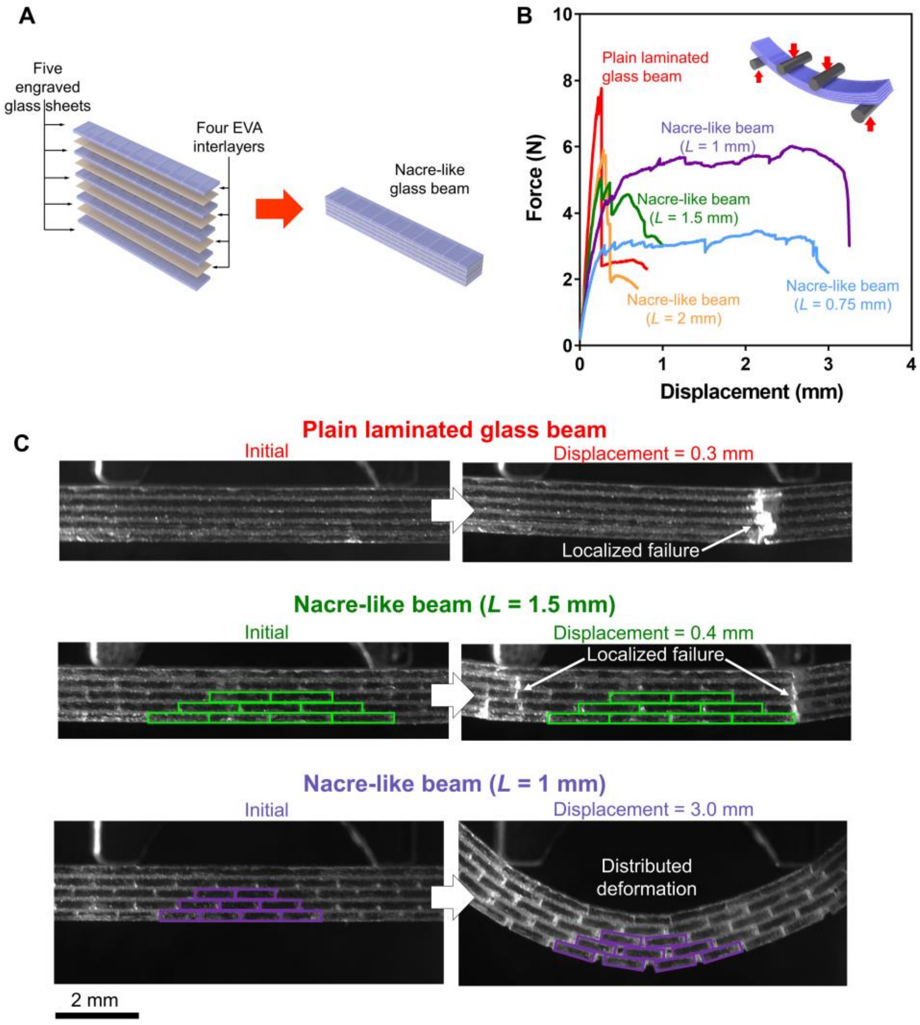

Fig. 4-9: Flexural tests on nacre-like glass beams. (a) Fabrication of nacre-like glass beams. (b) Flexural force-displacement curves of plain laminated glass beams and nacre-like glass beams (four-point bending tests). (c) Snapshots of the plain laminated glass and nacre-like beams showing initial and deformed configurations. The contours of some tablets is highlighted to show their relative displacements and rotations. Scale bar: 2 mm.

4.3.4 Effects of interface thickness on the performances of nacre-like panels

Puncture tests were conducted on five-layer 20 mm by 20 mm hexagon patterned nacre-like glass panels with interface thickness $t_i = 50$ µm and $t_i = 125$ µm. Fig. 4-10a shows the force-displacement curves of nacre-like panels with tablet size $L = 1$ mm and $L = 1.5$ mm. Thinner interfaces produced responses with a higher initial stiffness, but the energy to puncture was also significantly reduced (Fig. 4-10b). Thinner interfaces also produced panel with less deformability, where damage to the tablets was extensive (Fig. 4-10c). For impact resistant designs, thicker interfaces (t_i = 125 µm) was chosen to promote energy to puncture and deformability. The reduced stiffness was partially offset by choosing the highest possible length for the tablets (*L* = 1.5 mm) while preventing fracture of the tablets.

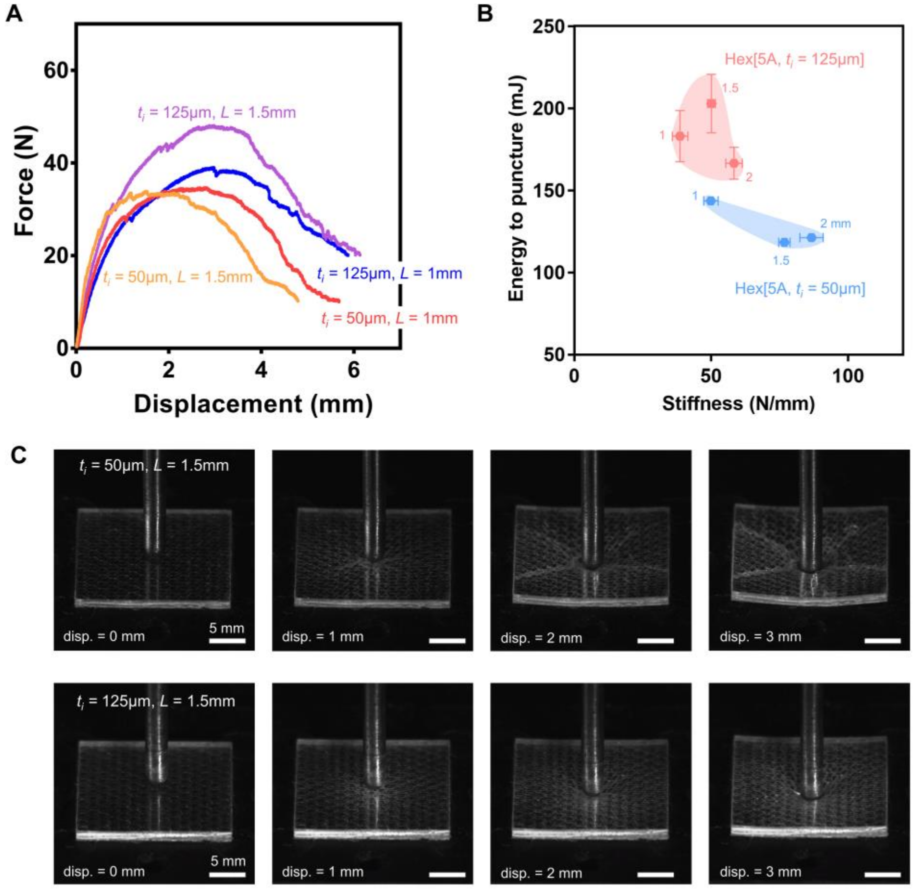

Fig. 4-10: Comparison between nacre-like glass panels with 50 µm and 125 µm thick interfaces. (a) Force-displacement curves of hexagon patterned nacre-like glass panels with *L* = 1 mm and *L* =1.5 mm with two different interface thicknesses (b) Energy to puncture vs. stiffness map for the data showed on (a). Thinner interfaces produced stiffer panels, but at the expense of energy to puncture. (c) Snapshots of the hexagon patterned nacre-like glass panels (L = 1.5 mm) taken during the puncture test. For t_i = 50 µm, there is extensive tablet fracture and the panel fails by a few

radial cracks. For t_i = 125 µm, the tablets remain largely intact and the deformation is distributed over a large volume near the puncture site. Scale bar: 5 mm.

4.4 Acknowledgement

We thank R. Botman (Glassopolis) for discussions on current challenges and opportunities in glass technologies and R. Tahara (Redpath Museum) for assistance with the micro-CT scans. Funding: This work was supported by a Strategic Grant (STPGP 479137–15) from the Natural Sciences and Engineering Research Council of Canada. Z.Y. was supported by a McGill Engineering Doctoral Award. The micro-CT facility was acquired from a CFI Innovation Grant (33112) awarded to J. Vogel and the Integrated Quantitative Biology Initiative. Author contributions: Z.Y. and F.B. designed the nacre-like glass panels, the fabrication protocol, and the experiments. Z.Y. fabricated and tested the materials. F.H. developed the analysis protocol and data processing codes for the micro-CT scans. Z.Y., F.H., and F.B. analyzed the experimental results, prepared the figures, and wrote the manuscript. F.B. is an inventor (with A. K. Dastjerdi and S. M. Mirkhalaf) on U.S. patent applications (US2017197873-A1 and US2015274587-A1) submitted by McGill University that cover the fabrication methods used in this article. Competing interests: None declared. Data and materials availability: All data needed to evaluate the conclusions of the paper are present in the paper or the supplementary materials.

4.5 References

1. Zhong, Z.W., Y.B. Tian, and T.G. Xie, *Investigation of subsurface damage of ground glass edges.* The International Journal of Advanced Manufacturing Technology, 2016. **87**(9): p. 3261-3269.
2. Carré, H. and L. Daudeville, *Load-bearing capacity of tempered structural glass.* Journal of Engineering Mechanics, 1999. **125**(8): p. 914-921.
3. Norville, H.S., W. King Kim, and L. Swofford Jason, *Behavior and Strength of Laminated Glass.* Journal of Engineering Mechanics, 1998. **124**(1): p. 46-53.
4. Wang, R.Z., et al., *Deformation mechanisms in nacre.* Journal of Materials Research, 2001. **16**(9): p. 2485-2493.

5. Barthelat, F., et al., *On the mechanics of mother-of-pearl: A key feature in the material hierarchical structure.* Journal of the Mechanics and Physics of Solids, 2007. **55**(2): p. 306-337.
6. Jackson, A.P., et al., *The mechanical design of nacre.* Proceedings of the Royal Society of London. Series B. Biological Sciences, 1988. **234**(1277): p. 415-440.
7. Barthelat, F. and R. Rabiei, *Toughness amplification in natural composites.* Journal of the Mechanics and Physics of Solids, 2011. **59**(4): p. 829-840.
8. Begley, M.R., et al., *Micromechanical models to guide the development of synthetic 'brick and mortar' composites.* Journal of the Mechanics and Physics of Solids, 2012. **60**(8): p. 1545-1560.
9. Barthelat, F., *Designing nacre-like materials for simultaneous stiffness, strength and toughness: Optimum materials, composition, microstructure and size.* Journal of the Mechanics and Physics of Solids, 2014. **73**: p. 22-37.
10. Behr, S., et al., *Large-scale parallel alignment of platelet-shaped particles through gravitational sedimentation.* Scientific Reports, 2015. **5**(1): p. 9984.
11. Das, P., et al., *Nacre-mimetics with synthetic nanoclays up to ultrahigh aspect ratios.* Nature Communications, 2015. **6**(1): p. 5967.
12. Bonderer, L.J., A.R. Studart, and L.J. Gauckler, *Bioinspired Design and Assembly of Platelet Reinforced Polymer Films.* Science, 2008. **319**(5866): p. 1069.
13. Munch, E., et al., *Tough, Bio-Inspired Hybrid Materials.* Science, 2008. **322**(5907): p. 1516.
14. Bouville, F., et al., *Strong, tough and stiff bioinspired ceramics from brittle constituents.* Nature Materials, 2014. **13**(5): p. 508-514.
15. Erb, R.M., et al., *Composites Reinforced in Three Dimensions by Using Low Magnetic Fields.* Science, 2012. **335**(6065): p. 199.
16. Morits, M., et al., *Toughness and Fracture Properties in Nacre-Mimetic Clay/Polymer Nanocomposites.* Advanced Functional Materials, 2017. **27**(10): p. 1605378.
17. Clegg, W.J., et al., *A simple way to make tough ceramics.* Nature, 1990. **347**(6292): p. 455-457.
18. Livanov, K., et al., *Tough Alumina/Polymer Layered Composites with High Ceramic Content.* Journal of the American Ceramic Society, 2015. **98**(4): p. 1285-1291.
19. Zhu, B., et al., *Hierarchical Nacre Mimetics with Synergistic Mechanical Properties by Control of Molecular Interactions in Self-Healing Polymers.* Angewandte Chemie International Edition, 2015. **54**(30): p. 8653-8657.
20. Ebina, T. and F. Mizukami, *Flexible Transparent Clay Films with Heat-Resistant and High Gas-Barrier Properties.* Advanced Materials, 2007. **19**(18): p. 2450-2453.
21. Liu, Y., S.-H. Yu, and L. Bergström, *Transparent and Flexible Nacre-Like Hybrid Films of Aminoclays and Carboxylated Cellulose Nanofibrils.* Advanced Functional Materials, 2018. **28**(27): p. 1703277.
22. Barthelat, F., Z. Yin, and M.J. Buehler, *Structure and mechanics of interfaces in biological materials.* Nature Reviews Materials, 2016. **1**(4): p. 16007.
23. Barthelat, F., A.K. Dastjerdi, and R. Rabiei, *An improved failure criterion for biological and engineered staggered composites.* Journal of The Royal Society Interface, 2013. **10**(79): p. 20120849.

24. Abid, N., M. Mirkhalaf, and F. Barthelat, *Discrete-element modeling of nacre-like materials: Effects of random microstructures on strain localization and mechanical performance.* Journal of the Mechanics and Physics of Solids, 2018. **112**: p. 385-402.
25. Espinosa, H.D., et al., *Tablet-level origin of toughening in abalone shells and translation to synthetic composite materials.* Nature Communications, 2011. **2**(1): p. 173.
26. Valashani, S.M.M. and F. Barthelat, *A laser-engraved glass duplicating the structure, mechanics and performance of natural nacre.* Bioinspiration & Biomimetics, 2015. **10**(2): p. 026005.
27. Dimas, L.S., et al., *Tough Composites Inspired by Mineralized Natural Materials: Computation, 3D printing, and Testing.* Advanced Functional Materials, 2013. **23**(36): p. 4629-4638.
28. *Materials and methods are available as supplementary materials*.
29. Serafinavičius, T., et al., *Long-term Laminated Glass Four Point Bending Test with PVB, EVA and SG Interlayers at Different Temperatures.* Procedia Engineering, 2013. **57**: p. 996-1004.
30. Lawn, B., *Fracture of Brittle Solids*. 2 ed. Cambridge Solid State Science Series. 1993, Cambridge: Cambridge University Press.
31. Taylor, J.D. and M. Layman, *The mechanical properties of bivalve (Mollusca) shell structures.* Palaeontology, 1972. **15**(1): p. 73-87.
32. Yin, Z., A. Dastjerdi, and F. Barthelat, *Tough and deformable glasses with bioinspired cross-ply architectures.* Acta Biomaterialia, 2018. **75**: p. 439-450.
33. Barinov, S.M. and M. Sakai, *The work-of-fracture of brittle materials: Principle, determination, and applications.* Journal of materials research, 1994. **9**(6): p. 1412-1425.
34. Kroon, D.-J., *Region Growing*. 2008, MATLAB Central File Exchange.
35. Tant, M.R., K.A. Mauritz, and G.L. Wilkes, *Ionomers: Synthesis, structure, properties and applications*. 2011: Springer Netherlands.
36. Longworth, R. and D.J. Vaughan, *Physical Structure of Ionomers.* Nature, 1968. **218**(5136): p. 85-87.
37. Salyer, I.O. and A.S. Kenyon, *Structure and property relationships in ethylene–vinyl acetate copolymers.* Journal of Polymer Science Part A-1: Polymer Chemistry, 1971. **9**(11): p. 3083-3103.
38. Parker, A.J. and J. Rottler, *Molecular Mechanisms of Plastic Deformation in Sphere-Forming Thermoplastic Elastomers.* Macromolecules, 2015. **48**(22): p. 8253-8261.
39. Wang, Z.-Y., et al., *Shear behaviour of structural silicone adhesively bonded steel-glass orthogonal lap joints.* Journal of Adhesion Science and Technology, 2018. **32**(24): p. 2693-2708.
40. Mooney, M., *Stress—Strain Curves of Rubbers in Simple Shear.* Journal of Applied Physics, 1964. **35**(1): p. 23-26.

Link between Chapter 4 and Chapter 5

In this previous chapter presented an impact resistant nacre-like glass with high transparency. The high energy absorption was caused by the large-scale tablet sliding and maximized at an intermediate tablet size. We also proposed and evaluated the design that can compensate the loss on strength and stiffness by placing a plain layer at the front. However, the general design principle towards simultaneously improved stiffness, strength, deformability and toughness is still unclear for glass and for architectured materials in general. In the next chapter, to address this question, we explored various types of bioinspired designs including the continuous-ply designs with cross-ply and Bouligand architectures, the segmented designs with segmented Bouligand and nacre-like architectures, and the hybrid designs where plain layer(s) and architectured layers were combined. The performances of the designs were evaluated by glass panels under quasi-static puncture tests. The continuous-ply designs tended to have brittle ply fracture that led to localized damage. The brittle behaviours and the localized damage limited the strength, deformability and energy absorption of the glass panels. In the segmented designs, brittle fracture of building blocks was suppressed, and energy could be absorbed through interface shearing. Both strength and toughness were improved in the segmented designs. However, the stiffness of segmented designs was reduced compared to the continuous-ply designs. The hybrid designs, by combining one or more plain layers with the architectured layers (nacre-like architectures), was able to further improve the stiffness and strength of the best segmented designs by up to 520% and 133%, respectively. The general design principle is that to have simultaneously improved stiffness, strength and toughness, the optimal design should approach a critical point where the brittle fracture of building blocks can be just suppressed, and local architecture should be design in a way based on the local stress state. It can be realized simply through adjusting the size and arrangement of building blocks.

Chapter 5: Stiff, strong and tough laminated glasses with bio-inspired designs

Zhen Yin[1] and Francois Barthelat[1,2]*

[1] *Department of Mechanical Engineering, McGill University, 817 Sherbrooke Street West,*
Montreal, QC H3A 2K6, Canada
[2] *Department of Mechanical Engineering, University of Colorado, 427 UCB, 1111 Engineering*
Dr, Boulder, CO 80309, United States

* Correspondence to: francois.barthelat@colorado.edu

Keywords: Tough glass; Bio-inspired; Bouligand; Cross-ply; Nacre-like; Architectured materials

5.1 Abstract

Glass is an attractive material with outstanding transparency, hardness, durability and chemical stability. However, the inherent brittleness and low toughness of glass limit its applications. Overcoming the brittleness of glass will help satisfy the rapidly increasing demands of glass in building materials, optical devices, electronics and photovoltaic systems, but it has been a challenge to create glass that is stiff, strong and tough while maintaining its transparency. This study explores how the basic design of laminated glass can be enriched with bio-inspired architectures generated with laser engraving. The performance of designs is assessed based on continuous plies (90° cross plies, Bouligand) and finite glass blocks (segment Bouligand, nacre-like brick-and-mortar). The mechanical performance of these various designs is assessed and compared using puncture tests on panels. It shows that stiffness, strength and toughness can be simultaneously improved by tailoring the size, geometry and arrangement of the building blocks, and by combining continuous, plain glass layers with architectured layers. Overall the designs based on finite size glass blocks were more successful than designs based on continuous plies. As

a general rule, the architecture should be adjusted to promote shear of the interface over brittle fracture of the glass building blocks.

5.2 Introduction

Glass is a material with high demand in mechanical, biomedical, electronic and photovoltaic applications because of its outstanding optical properties, hardness, durability and chemical stability. However, at ambient temperature, glass is a brittle material with little deformability, poor reliability and low damage tolerance, which still limits the range of its applications. The tensile strength of glass is compromised by the slightest defects or damage, and it has poor impact resistance [1]. Thermal or chemical tempering can increase the strength of glass two to five-fold through creating residual compressive stresses to offset the tensile stresses arising from external loadings [2]. However, if a crack initiates in tempered glass, the entire component is immediately destroyed in a catastrophic and “explosive” manner. While tempered glass has a higher strength that regular glass, its resistance to crack propagation (toughness) is not improved. Laminating glass is another strategy where glass layers are intercalated with softer polymeric layers. The polymeric interlayer holds the glass fragment together in case of fracture which is advantageous in terms of safety, but does not improve impact resistance significantly [3]. Overcoming glass brittleness remains a difficult challenge. Solving the problem will lead glass to a broader range of applications, meeting current industry demands.

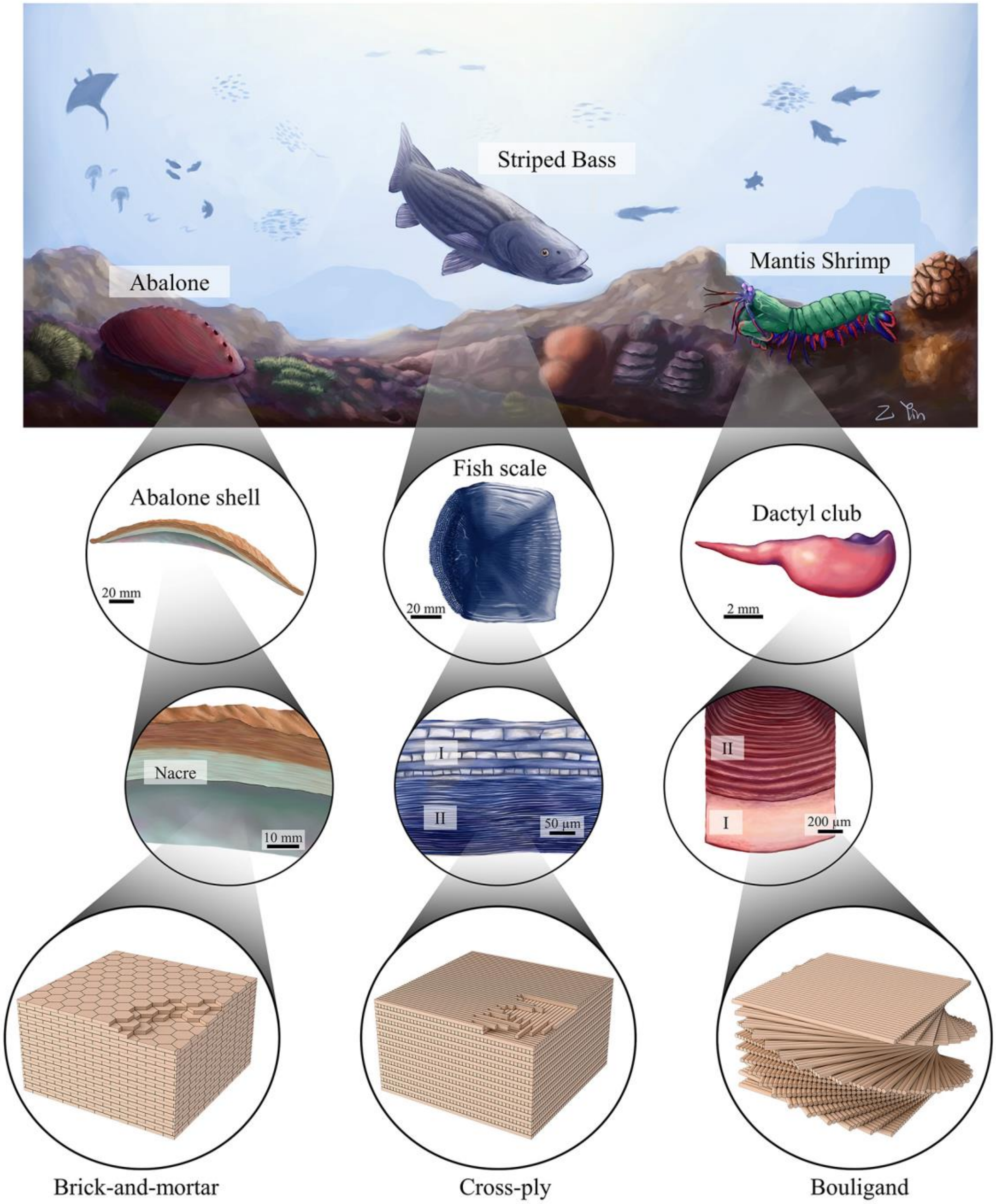

Fig. 5-1: The hierarchical structure of biological materials in three marine animals. The inner layer of abalone shells, nacre, are in the form of well-organized brick-and-mortar structures [4]. Fish scales from striped bass are made of two layers: (I) bony layer and (II) collagen layer. The collagen layer are collagen fibers forming 90º cross-ply architectures [5]. The dactyl club of the mantis shrimp consists of (I) impact region, (II) periodic region and striated region. In the periodic region, the mineralized chitin fibers form a helicoidal structure (Bouligand structure) [6].

Interestingly, nature has been “solving” issues associated with material brittleness for millions of years (Fig. 5-1). Many hard biological materials such as mollusk shells and teeth are made of hard but brittle minerals, but their toughness can be thousands of times higher than their fragile constituents [7-10]. This unique combination of toughness, stiffness and strength originates from intricate material architectures at the microscopic scale [7, 11]. The microarchitectures of these biological materials generally consist of regular hard building blocks and more deformable bio-polymeric interfaces [10]. These building blocks can take a wide variety of size, geomertry and arrangement. For example, cross-ply structures can be found in fish scales [5, 12, 13], teeth [14-16] and conch shells [17-20], formed by hard mineralized fibers or lamellae (Fig. 5-1). In the cuticles of many arthropod species, mineralized chitin fibers form in a twisted-ply (Bouligand) structure [6, 21] (Fig. 5-1). Nacre from mollusk shells has a microstructure with highly organized three-dimensional brick-and-mortar assembly of microscopic mineral tablets bonded by biopolymeric interfaces [22-24] (Fig. 5-1). These highly organized microstructures trigger toughening mechanisms such as crack deflection, crack bridging and tablet sliding that contributes to the toughness of biological materials [23]. These biological materials therefore provide interesting models as bioinspiration for toughened glasses and ceramics [25, 26]. Fabricating large volumes of bio-inspired materials with well controlled material architectures has been a major challenge for decades [7, 10, 27]. There have been some attempts to introducing bio-inspired architectures into glass in recent years [4, 28-30], and it has been especially challenging to achieve high combinations of hardness, stiffness, strength and toughness as well as maintaining the transparency of glass [4, 30]. A glass with nacre-like microarchitectures was developed recently through compacting and sintering glass flakes infiltrated with refractive-index matching polymer. It had high strength and was toughened through crack deflection [30]. Another nacre-inspired glass with highly controlled architectures was also developed recently through high precision three-dimensional laser engraving and lamination [4]. The nacre-inspired glass duplicated the toughening mechanisms of crack deflection and large-scale tablet sliding, showing high toughness, high deformability and high transparency with little loss on stiffness and strength compared to laminated glass [4]. Bio-inspired glasses are usually based on nacre, and few studies systematically studied the effects of material architectures and the geometry of building blocks on the mechanical performances [31]. Nacre-like, cross-ply or Bouligand structure have intricate 3D architecture so that crack propagation and failure can be difficult to capture in models. This work took an experimental approach to assess and compare the mechanical performance of glass panels with various bio-inspired material architectures. General design strategies are proposed in this paper to guide the design of stiff, strong, tough and deformable glass based on hard building blocks and soft interfaces.

5.3 Design, fabrication and testing

The designs explored in this study were based on a multilayered architecture where glass layers are alternated with polymeric layers, so as to generate cross-ply, Bouligand and nacre-like architectures. Ten 220 μm thick standard borosilicate glass sheets (Lightingglass, Guangzhou, China) were laminated with nine 50 μm thick adhesive layers for a total laminated glass panel thickness of 2.65 mm. Ethylene-vinyl acetate (EVA) (Caida, Tianjin, China) was selected as the adhesive interface materials for its high optical transparency, strong adhesion to glass, relatively low shear strength to promote interface yielding and large inelastic deformations with energy dissipation [4]. Fig. 5-2a shows the general fabrication protocol. The contours of the tablets were first engraved on individual borosilicate glass sheets using a focused pulsed laser beam (Model Vitrolux, Vitro Laser Solutions UG, Minden, Germany). The engraved glass sheets were then laminated with EVA films at a temperature of 120 ºC and under a uniform compression of 100 kPa. During the process, the glass sheets were carefully aligned to achieve the well-controlled three-dimensional architectures considered in this study (Fig.2b). For continuous ply designs, the patterns created within each glass layer were parallel lines to create 90° Cross-ply and Bouligand architectures (Fig. 5-2b). For each of these designs, three different ply widths were considered: $w = 1$, 2 and 3 mm. For the cross-ply architecture, the relative ply angle between two consecutive layers was 90° (Fig. 5-2b). For the Bouligand architecture, the angle between consecutive layers was 18 degree (Fig. 5-2b), which was to achieve a complete 180-degree twist of the plies through the thickness of the panel. In addition to Bouligand and cross-plies based on continuous plies, segmented designs were studied where the glass elements were squares or rectangles with finite size and arranged in 3D to create segmented Bouligand and nacre-like architectures (Fig.2b). The segmented Bouligand architecture had rectangular tablets with width w and length s, arranged in a way similar to the continuous Bouligand architecture (Fig. 5-2b). The nacre-like panels had square-shape tablets with size $L \times L$ with $L = 1$, 2 and 3 mm. The puncture performances of hybrid designs were finally investigated, where plain glass layers and architectured layers were combined. All the designs explored in this study had the same overall dimensions (20 mm × 20 mm × 2.65) and the same composition (10 glass layers alternated with 9 EVA interlayers). The mechanical performance of the different architectured glass panel designs was assessed using puncture tests on a simply supported configuration. The panel was placed in a custom-made steel frame to support its periphery, and a steel indenter with a 3 mm diameter spherical tip was driven through the center of the panel (Fig. 5-2c) at a rate of 10 µm/s (a quasi-static loading condition) until complete puncture of the panel. The test was performed using a universal test machine (model: eXpert 5000, ADMET, Norwood, MA, USA). The energy absorption capability of the panel was determined by computing the area under the force-displacement curves. Stereo-imaging was also used to monitor the deflection of the panel in-situ (pair of synchronized cameras model IL-5, Fastec Imaging, San Diego, CA, USA). The deflection of the upper surface of the sample during puncture was reconstructed using 3D scene reconstruction methods (VIC 3D, correlated solutions, Irmo, SC, USA).

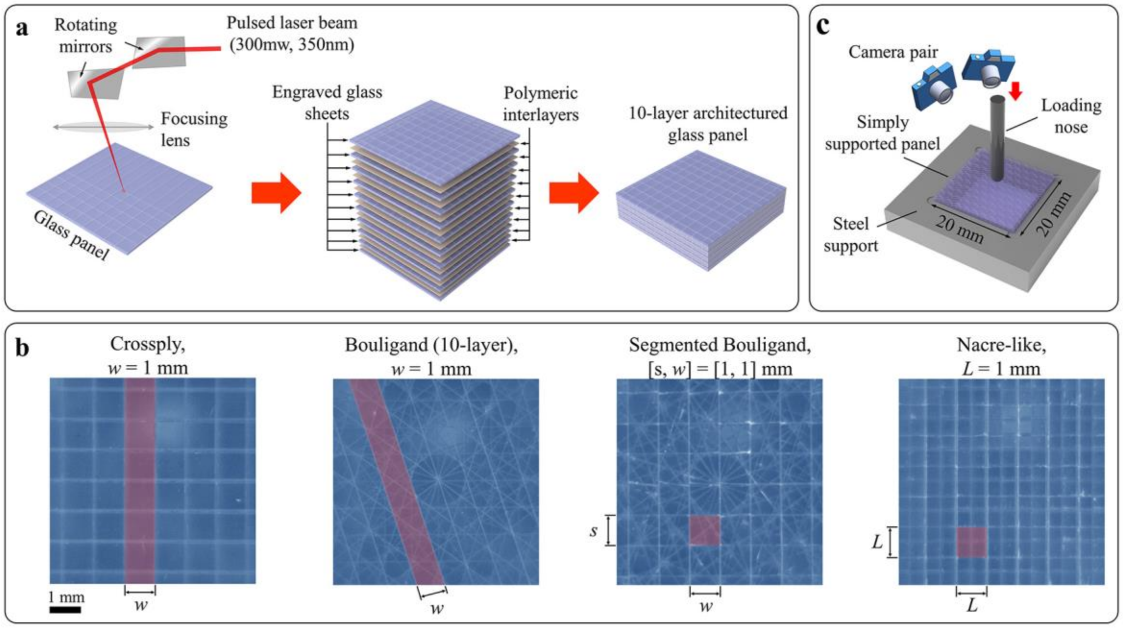

Fig. 5-2: Design, fabrication and testing of multi-layer architectured glass panels: (a) Fabrication protocol for the architectured glass panels. (b) Design and arrangement of material architectures: cross-ply, Bouligand, segmented Bouligand and nacre-like (square, 50% overlap). (c) Experimental setup for the puncture tests.

5.4 Continuous ply designs: 90° Cross-ply and Bouligand

Fig. 5-3a shows typical puncture force-displacement curves obtained from the 90° cross-ply and the Bouligand designs, with ply width *w* = 1 mm and *w* =2 mm. In general, the curves initially showed a relatively stiff linear region, followed by a drop in force and softening associated with the fracture and sliding of individual glass plies (Fig. 5-3a). In all cases the failure was progressive and "graceful", in contrast to plain glass where puncture failure is catastrophic and accompanied by a sharp drop in puncture force [4]. The 90°cross-ply and Bouligand panels showed similar deformations (Fig. 5-3b): large deflections and heavy damage were concentrated near the puncturing site, and most of the panels remained intact except for a few cracks emanating from the puncture site.

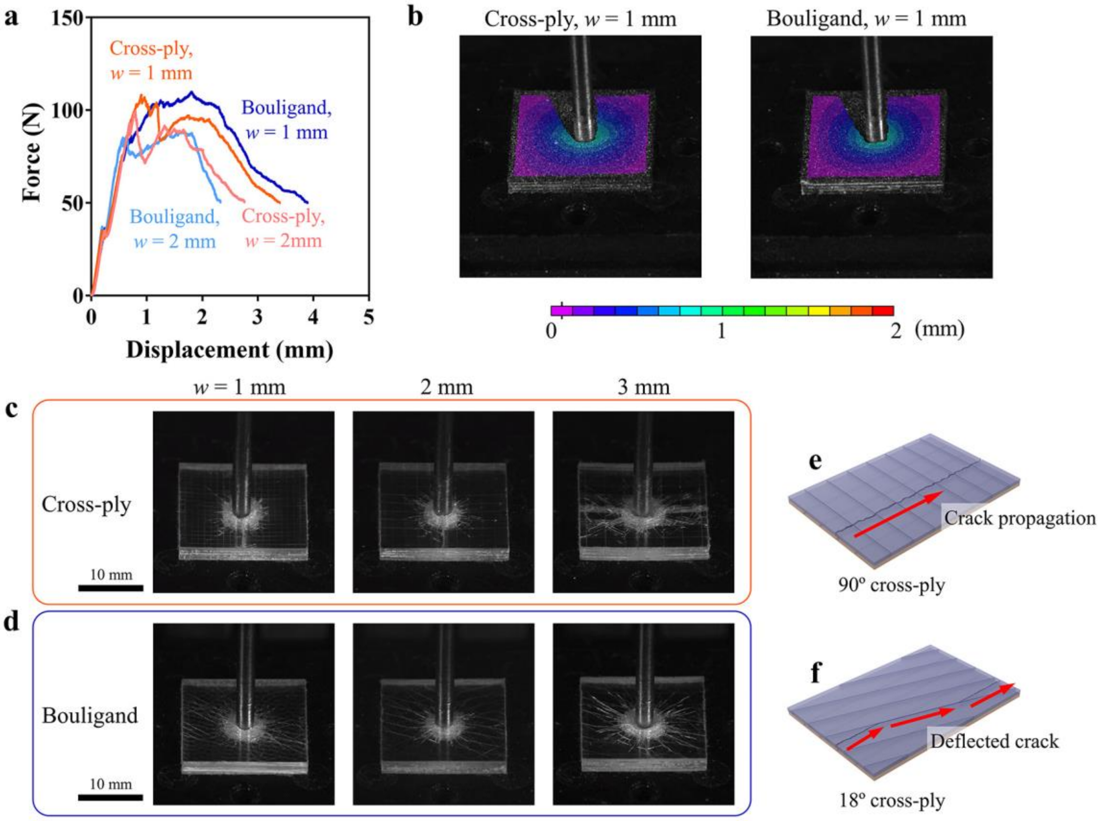

Fig. 5-3: Puncture tests of 10-layer glass panels with cross-ply and Bouligand architectures. (a) Force-displacement curves for cross-ply and Bouligand panels; (b) 3D digital image correlation results showing the deflection of the glass panels at displacement = 2 mm; Fracture of (c) cross-ply and (d) Bouligand glass panels with ply width *w* = 1 mm, 2 mm and 3 mm, at displacement = 2 mm; (e) In-plane crack propagation in the 90° cross-ply structure and (f) 18° cross-ply (Bouligand) structure.

Failure occurred by brittle fracture of individual plies from flexural stresses (Fig. 5-3c, d). In the 90°cross-ply designs, most of the cracks followed a 0°/ 90° orientation parallel to the direction of the plies (Fig. 5-3c), with the longest of these cracks splitting the panel in half (Fig. 5-3c). Within some layers the cracks propagated along the interface between the plies, and in the adjacent layers the cracks propagated through the plies. There was no deflection along the plies because of the relatively large ply angles (Fig. 5-3c, e) [29]. The 90°cross-ply panels were more deformable in the case of w = 1 mm because the sliding of plies along one another was more extensive. For the Bouligand design, cracks were more uniformly distributed along the radial direction (Fig. 5-3d). Fewer in-plane radial cracks were observed (Fig. 5-3d) and these radial cracks tended to be shorter. For Bouligand panels with w = 1 mm, the in-plane cracks propagating from the puncture site were usually deflected by the interfaces between the plies within the same layer (Fig. 5-3d, f) because of the low ply angles (18 degree) between the adjacent layers and dense interfaces between the plies within a layer. The shear deformation in the polymeric interlayers, caused by the difference of the crack propagation directions between the neighboring layers, also contributed to the energy absorption of the panel [29]. Therefore, there was no sudden force drop for the w = 1 mm case and the energy absorption was increased. When w = 2 mm and 3 mm, the panels showed more limited deformability compared to the case of w = 1 mm (Fig. 5-3a). Some of the in-plane radial cracks propagating in the glass layer were not deflected by the interfaces between the plies (Fig. 5-3d). Overall, continuous ply designs showed relatively limited deformability and energy absorption due to localized damage. Decreasing the ply width could increase the deformability but the improvement was limited. Despite distinct failure patterns, the 90° cross-ply and Bouligand panels showed generally similar stiffness, strength and energy absorption.

5.5 Segmented designs: Segmented Bouligand and nacre-like panels

In both the 90°cross-ply and the Bouligand panels, brittle fracture of individual plies was observed, which led to localization and relatively limited deformability under puncture. A possible approach to better control deformation and failure in these designs is to partition the plies into segments of well-defined lengths. We explored this route in “Segmented” Bouligand designs where the plies were segmented into individual segment of length *s*. Another way to consider this design is that of finite glass plates of size $w \times s$ arranged in regular array within a layer, but rotated by 18° to the next layer (Fig. 5-4a). Another type of segmented designs explored in this study is the nacre-like brick-and-mortar architecture based on square tablets of size $L \times L$ arranged in a staggered fashion in three dimensions [4]. When the ply width *w* equals to the plate length *s* for segmented Bouligand panels, the only difference between the segmented Bouligand and nacre-like panels is the tablet arrangement: The Bouligand architecture has a helix ply arrangement while the nacre-like is staggered (Fig. 5-1 and Fig. 5-2b).

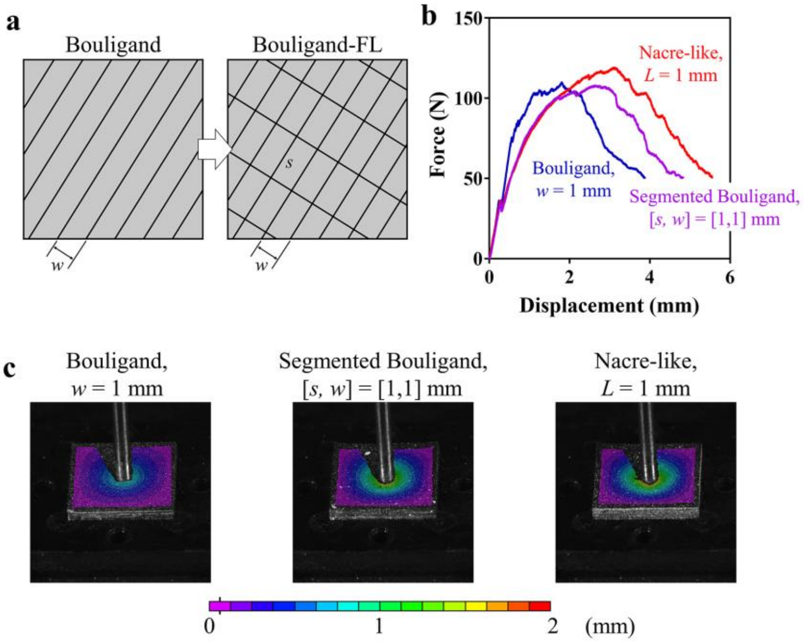

Fig. 5-4: Design and puncture mechanical response of segmented Bouligand and nacre-like panels. (a) Design of segmented Bouligand panels compared to regular Bouligand panels; (b) Force-displacement curves of segmented Bouligand panels (ply width w = 1 mm, ply length s = 1 mm) compared to regular Bouligand panels with the same ply width and nacre-like panels with the same tablet size (L = 1 mm); (c) Comparison of surface deflection between regular Bouligand, segmented Bouligand and nacre-like panels, at the displacement of 2 mm.

Fig. 5-4b shows typical puncture force-displacement curves for a segmented Bouligand design (w = s = 1 mm) and for a nacre-like design (L = 1 mm). Both of these designs showed an initially linear region, followed by gradual softening and an overall bell shape indicating a graceful failure. 3D surface reconstructions revealed that the deformations of the segmented Bouligand and nacre-like panels were more distributed over the panel, with less abrupt ply fracture compared to the continuous designs (Fig. 5-4c). The length of the segments was varied using s = 1 mm, 2 mm and 3 mm, with a ply width kept to w = 1 mm (best value for continuous-ply based designs). The length of the segments had a significant impact on performance. The segmented Bouligand panels were about 25% less stiff than the continuous ply-based panels ($s = \infty$), because the abilities of individual plies to carry stresses along their axis is reduced by the segmentation. Segmented Bouligand panels were however also significantly stronger and more deformable than the continuous design. In particular, the segmented Bouligand panels with s = 1 mm and 2 mm were stronger and more deformable than the ones with s = 3 mm and $s = \infty$ (continuous plies) because sudden ply fracture was avoided, ply to ply sliding being dominant instead (Fig. 5-5a, c). In contrast the segmented Bouligand panels with s = 3 mm fractured in a way similar to the regular Bouligand panels, with damage localized near the puncture site (Fig. 5-5c). Segmented panels with intermediate ply length (s = 2 mm) had a higher puncture strength than the panels with s = 1 mm, without sacrificing deformability. It is found that nacre-like panels with L = 1 mm were more deformable and as strong as segmented Bouligand panels (Fig. 5-5b), with a better distributed deformation and damage compared to the other designs. Small cracks on the top layer were also observed occurring at large displacement, which could be caused by the compressive stresses in the tablets and the shear stresses transferred from the polymeric interface [4]. Larger tablet size (L = 2 mm and L = 3 mm) led to premature brittle tablet fracture that greatly limited deformability and strength (Fig. 5-5b, d). For L = 2 mm and 3 mm, the cracks formed a cross or a "number sign" (#) pattern because the in-plane crack propagation within a layer tended to follow the interfaces between the tablets. The results show that for fixed material properties for the hard and soft phases, deformation and failure modes as well as mechanical performance are very sensitive to the size of the building blocks. Therefore, fabrication protocols with precise control on the geometry of the building blocks are required to reach the optimal configuration of architectured glass.

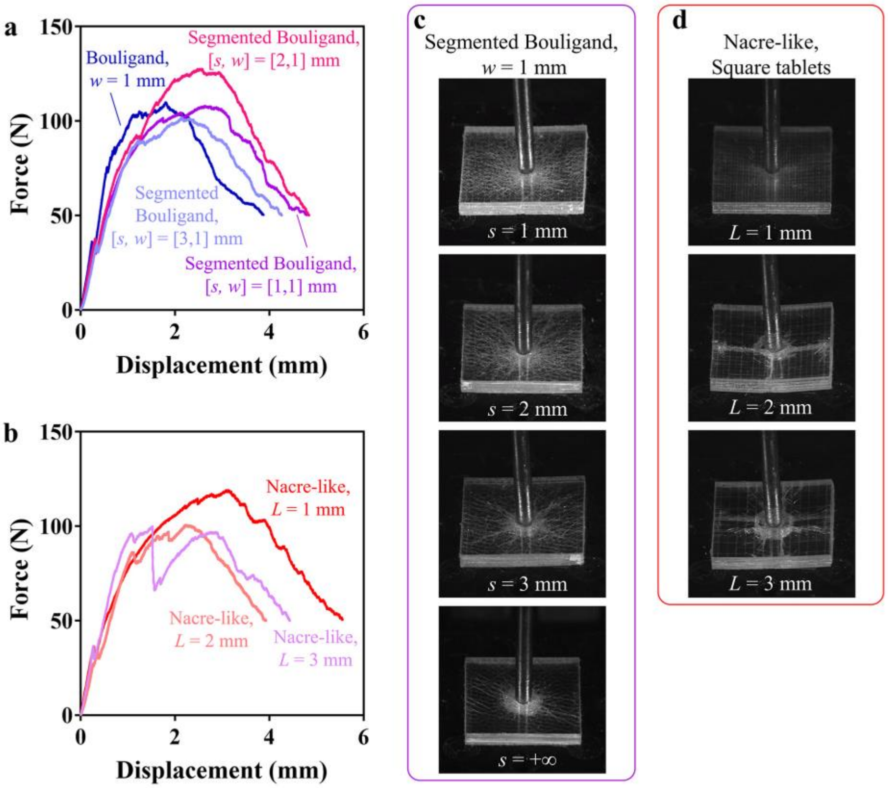

Fig. 5-5: Behaviour of glass panels with finite-plate designs under puncture. Force-displacement of (a) finite-length Bouligand panels with various ply width and (b) nacre-like panels with various tablet size. The deformation snapshots of (c) segmented Bouligand of $[s, w] = [1, 1]$ mm, ([2, 1] mm and [3, 1] mm and regular Bouligand panels, and (d) nacre-like panels with tablet size $L = 1$, 2 and 3 mm, at a displacement of 2 mm.

5.6 Hybrid laminated designs mixing plain and architectured glass layers

The results presented so far show how the energy absorption, damage tolerance and deformability of multilayer architectured glasses are significantly increased compared to the monolithic and laminated glasses, but that this improvement comes at the expense of stiffness and strength [4]. One way to compensate the loss in stiffness and strength is to use one or more plain, un-engraved glass layer(s) as front layer(s) [4]. This study explored five configurations involving different combinations of plain and architectured layers (Fig. 5-6a), keeping the overall thickness of the panels constant. The architectured layers in all five configurations had square-shape nacre-like architecture with tablet size $L = 1$ mm. The notation $[N_p\mathrm{P}_t N_A\mathrm{A}]$ was used for each configuration, where N_p is the number of plain layers used as front layers, t is the thickness of the individual plain layers (in increments of 220 µm), and N_A is the number of architectured layers. For example, [$2P_18A$] is a design with two front plain layers with a thickness of 220 µm each, with eight architectured layers underneath.

Fig. 5-6b shows representative force-displacement curves for these hybrid designs. In general, the panels initially showed linear elastic deformation until a series of first peak(s) at a relatively high force, corresponding to the sequential failure of the plain front layer(s). Once the front layers were fractured, the underlying architectured layers took over the mechanical response of the panel, producing large deformation and a second peak of maximum force (Fig. 5-6b). Radial and concentric cracks progressively developed in the plain layers as the indenter punctured in (Fig. 5-6c). The different hybrid designs showed distinct mechanical performances depending on the number and thickness of the plain layers. For example, results from the [$1P_19A$], [$2P_18A$] and [$4P_16A$] designs show that increasing the number of plain layers increases stiffness (Fig. 5-6b and Fig. 5-7a). Results from the [$1P_28A$] and [$1P_46A$] designs show that increasing the thickness of the plain layer also substantially improved stiffness. In terms of puncture strength (maximum force), hybrid designs having with the same overall thickness of the plain layers (i.e. [$4P_16A$] and [$1P_46A$]) had similar maximum force. Increasing the number of plain layers (for [$2P_18A$] and [$4P_16A$]) and increasing the thickness of individual plain layers (for [$1P_28A$] and [$1P_46A$]) both improved puncture strength. The strengthening effect of the plain layers could be evaluated by the ratio between the maximum of the first peak(s) generated by the plain layers and the second maximum force generated by the architectured layers (F_{P1}/F_{P2}) (Fig. 5-6d). For [$1P_19A$], F_{P1}/F_{P2} was slightly below one, meaning that the plain layer was too thin to improve the puncture strength of the panels. Increasing the number (for [$2P_18A$] and [$4P_16A$]) and the thickness (for [$1P_28A$] and

[$1P_46A$]) of the plain layer(s) could raise the F_{P1}/F_{P2} up to 1.6 (Fig. 5-6d), corresponding to a 60% improvement in strength. However, the strength improvement by the plain layers was not as pronounced as in our recent work (~100% improvement) [4], probably due to the lower aspect ratio of the panels (width/thickness = 7.55) compared to our previous study (width/thickness = 12.5). In panels with smaller aspect ratios the plain layers were not only under compressive stresses but also transverse shear stresses. In terms of deformability and energy absorption, [$1P_19A$] showed similar force-displacement curves after the failure of plain layers and overall deformability compared to [10A] (Fig. 5-6b). The second maximum force F_{P2} and overall deformability of [$2P_18A$], [$4P_16A$] and [$1P_28A$] were lower than [10A] and [$1P_19A$] (Fig. 5-6b) because of the relatively fewer architectured layers to absorb energy through tablet sliding. Therefore, the energy absorption of these designs was inferior to [10A] and [$1P_19A$] (Fig. 5-7b). For [$1P_46A$], there was a rapid recovery of stiffness when the plain layer failed but the recovery ended shortly with the onset of the delamination between the plain layer and the architectured layers (Fig. 5-6c). The propagation of the delamination resulted in a progressive softening of [$1P_46A$] panels. The energy absorption of [$1P_46A$] panels was relatively limited compared to other hybrid designs because of the early-stage softening caused by delamination (Fig. 5-6b and Fig. 5-7c).

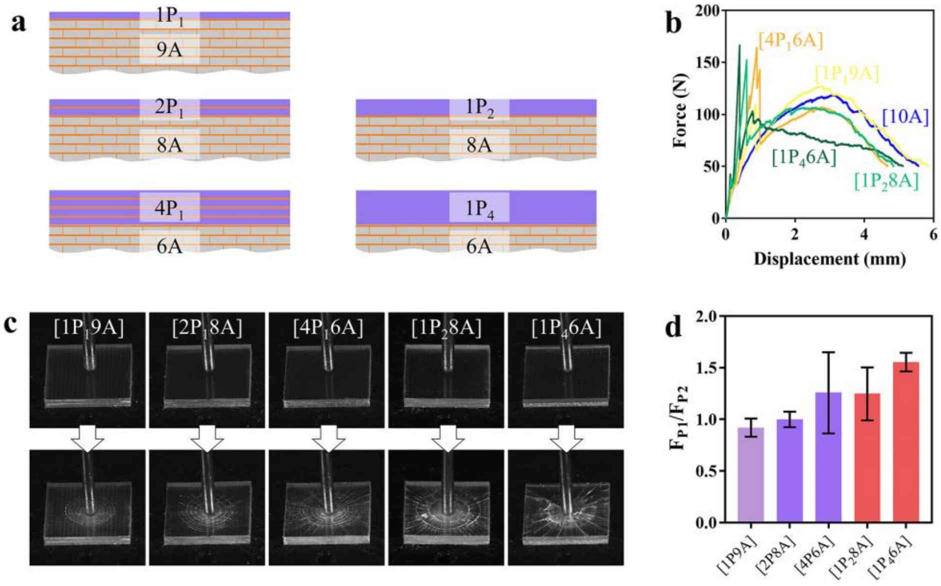

Fig. 5-6: Design and mechanical responses for the hybrid (plain-nacre-like) laminated designs: (a) Schematic of the [$1P_19A$], [$2P_18A$], [$4P_16A$], [$1P_28A$] and [$1P_46A$] designs; (b) Force-displacement curves for [10A], [$1P_19A$], [$4P_16A$], [$1P_28A$] and [$1P_46A$] configurations under puncture (tablet size L =1 mm for all configurations); (c) Deformation and failure of glass panels with [$1P_19A$], [$2P_18A$], [$4P_16A$], [$1P_28A$] and [$1P_46A$] designs, at the displacement of 2 mm. (d) Ratio between the maximum of the first force peak(s) F_{P1} generated by the plain layers and the second maximum force F_{P2} by the architectured layers in the force-displacement curves.

5.7 Comparison of continuous ply, segmented and hybrid designs

The mechanical performances of the different glass panel designs explored in this study were displayed on the property maps showed on Fig. 5-7a-c. The stiffness, maximum force (puncture strength) and energy absorption of the 90° cross-ply and Bouligand panels were within the same range because in these designs the failure of the panels was dominated by the brittle fracture of glass plies (Fig. 5-7a, c). Bouligand panels with w = 1 mm had the highest strength and energy absorption but the lowest stiffness among all three groups of Bouligand panels tested (Fig. 5-7b), which was resulted by the more graceful failure of w = 1 mm (Fig. 5-3a, d). The segmented Bouligand designs in general had around 30% decreased stiffness, 14% increased puncture strength and 60% increased energy absorption compared to regular Bouligand panels (Fig. 5-7b, c). The improvement of strength and energy absorption in the segmented design resulted from the suppression of brittle ply fracture with an adequate size of the building blocks. Both strength and energy absorption of segmented designs (segmented Bouligand and nacre-like) were maximized when the building blocks was at the intermediate size [4, 29] (Fig. 5-7c). When the size of building blocks was too large, strength, deformability and energy absorption of segmented designs were reduced because of the brittle fracture of the plies (or tablets) (Fig. 5-7c). The optimal configuration for deformability, strength and energy absorption should be at the critical point where the brittle fracture of building blocks is just suppressed (the dashed line in the failure mode map in Fig. 5-7d). In the hybrid designs, the plain layers substantially improve the stiffness of nacre-like panels ([10A], L = 1 mm) by up to 520% ([1P$_4$6A]) (Fig. 5-7a-b). The hybrid designs also improved the puncture strength of nacre-like panels ([10A], L = 1 mm) by up to about 33% ([4P$_1$6A] and [1P$_4$6A]). However, replacing the front layers with plain layer did not improve energy absorption compared to nacre-like panels (L = 1 mm). [1P$_1$9A] absorbed slightly more energy than [10A] but other configurations of hybrid designs had lower energy absorption (Fig. 5-7c). The results show that stiff, strong and tough architectured glass can be achieved simply through adjusting the size, geometry and arrangement of the building blocks.

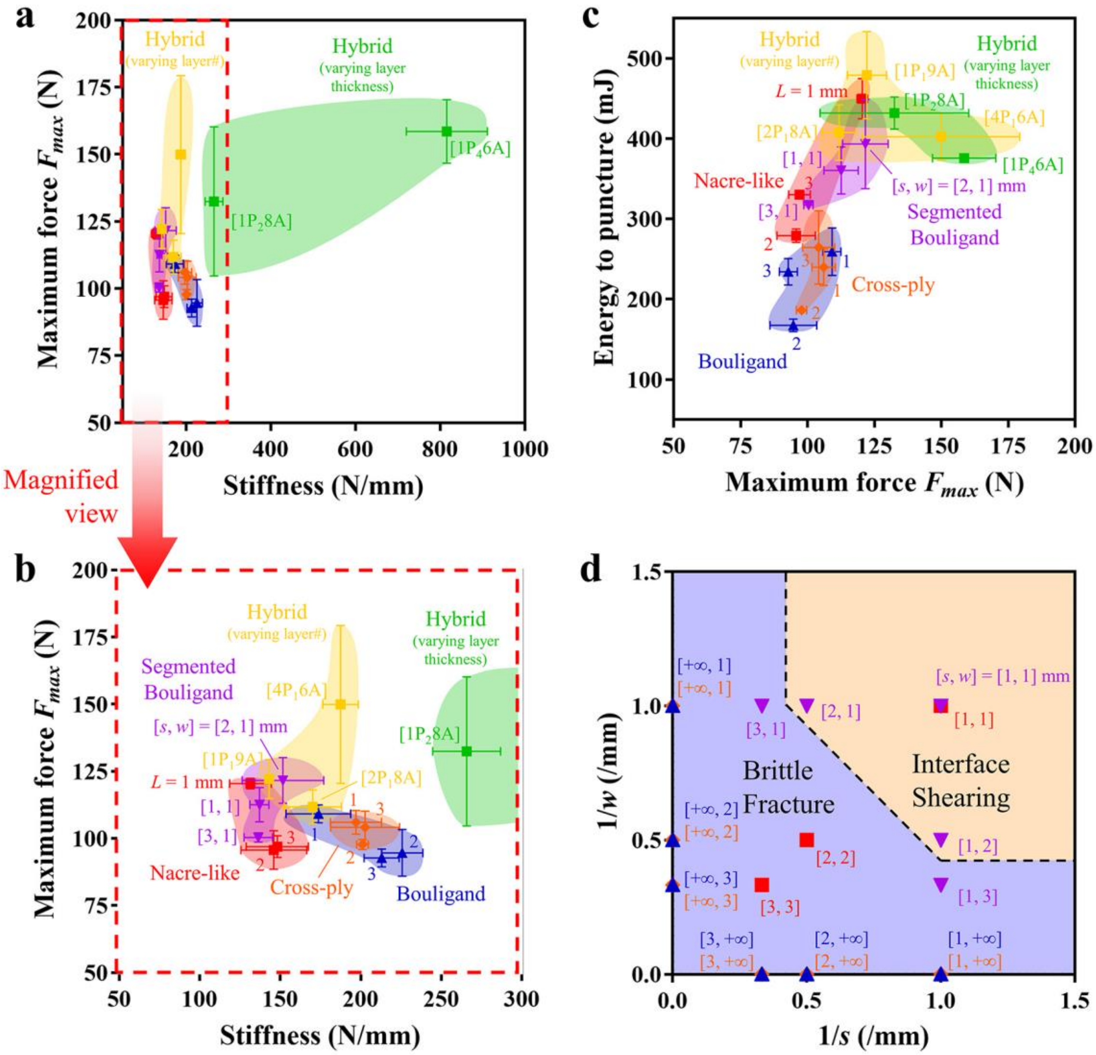

Fig. 5-7: Property maps of the laminated panels explored in this study showing (a) maximum force (puncture strength) vs. stiffness and (b) magnified version showing the low stiffness region; (c) Energy to puncture vs. maximum force. (d) The transition map from brittle fracture of building blocks to interface shearing for rectangular building blocks, as a function of length s and width w. *s* = 1, 2 and 3 mm for continuous designs and *w* = 1, 2 and 3 mm for segmented designs were plot based on geometrical symmetry.

5.8 Summary

This study explored how the basic design of laminated glass can be enriched with bio-inspired architectures generated with laser engraving. Specifically, the puncture performance of bioinspired architectured glass panels with continuous ply designs (cross-ply and Bouligand), segmented designs (segmented Bouligand and square-tablet nacre-like) and hybrid designs (that incorporate plain front glass layers) were assessed. The continuous ply designs showed toughening mechanisms such as crack deflection and ply sliding at some degree, but in general their mechanical performances were limited by the premature fracture of the glass plies. Segmented designs showed delocalized deformation, increased deformability, increased strength and substantially improved toughness provided an adequate size, geometry and arrangement of the glass building blocks that promotes interface shearing over brittle fracture of the blocks. The hybrid designs combining plain layer(s) and architectured layers proved to be a powerful solution for providing high stiffness and high strength, combined with high toughness. This study therefore demonstrates that with an architecture adapted to the loading configuration and precise control on size, geometry and arrangement at the fabrication stage can provide simultaneous improvements on stiffness, strength and toughness. The design principle is to obtain controlled deformation of building block without the disruption of brittle fracture, and to combine different material architectures located in the positions where they can be loaded in their advantageous way.

5.9 Acknowledgments

This work was supported by a Strategic Grant (STPGP 479137 – 15) from the Natural Sciences and Engineering Research Council of Canada and by a Team Grant (191270) from the Fonds de Recherche du Québec – Nature et Technologies. Z.Y. was partially supported by a McGill Engineering Doctoral Award. The authors acknowledge Prof. Luc Mongeau (McGill University) software for 3D digital image correlation.

5.10 references

1. Zhong, Z.W., Y.B. Tian, and T.G. Xie, *Investigation of subsurface damage of ground glass edges.* The International Journal of Advanced Manufacturing Technology, 2016. **87**(9): p. 3261-3269.
2. Carré, H. and L. Daudeville, *Load-bearing capacity of tempered structural glass.* Journal of Engineering Mechanics, 1999. **125**(8): p. 914-921.
3. Norville, H.S., W. King Kim, and L. Swofford Jason, *Behavior and Strength of Laminated Glass.* Journal of Engineering Mechanics, 1998. **124**(1): p. 46-53.
4. Yin, Z., F. Hannard, and F. Barthelat, *Impact-resistant nacre-like transparent materials.* Science, 2019. **364**(6447): p. 1260.
5. Zhu, D., et al., *Structure and Mechanical Performance of a "Modern" Fish Scale.* Advanced Engineering Materials, 2012. **14**(4): p. B185-B194.
6. Suksangpanya, N., et al., *Twisting cracks in Bouligand structures.* Journal of the Mechanical Behavior of Biomedical Materials, 2017. **76**: p. 38-57.
7. Barthelat, F., *Architectured materials in engineering and biology: fabrication, structure, mechanics and performance.* International Materials Reviews, 2015. **60**(8): p. 413-430.
8. Fratzl, P. and R. Weinkamer, *Nature's hierarchical materials.* Progress in Materials Science, 2007. **52**(8): p. 1263-1334.
9. Meyers, M.A., et al., *Biological materials: Structure and mechanical properties.* Progress in Materials Science, 2008. **53**(1): p. 1-206.
10. Barthelat, F., Z. Yin, and M.J. Buehler, *Structure and mechanics of interfaces in biological materials.* Nature Reviews Materials, 2016. **1**(4): p. 16007.
11. Wegst, U.G.K., et al., *Bioinspired structural materials.* Nature Materials, 2015. **14**(1): p. 23-36.
12. Yang, W., et al., *Protective role of Arapaima gigas fish scales: Structure and mechanical behavior.* Acta Biomaterialia, 2014. **10**(8): p. 3599-3614.
13. Yang, W., et al., *Structure and fracture resistance of alligator gar (Atractosteus spatula) armored fish scales.* Acta Biomaterialia, 2013. **9**(4): p. 5876-5889.
14. Bajaj, D. and D. Arola, *Role of prism decussation on fatigue crack growth and fracture of human enamel.* Acta Biomaterialia, 2009. **5**(8): p. 3045-3056.
15. Bajaj, D., et al., *Fracture processes and mechanisms of crack growth resistance in human enamel.* JOM, 2010. **62**(7): p. 76-82.
16. Yahyazadehfar, M., et al., *On the Mechanics of Fatigue and Fracture in Teeth.* Applied mechanics reviews, 2014. **66**(3): p. 0308031-3080319.
17. Menig, R., et al., *Quasi-static and dynamic mechanical response of haliotis rufescens (abalone) shells.* Acta Materialia, 2000. **48**.
18. Kamat, S., et al., *Fracture mechanisms of the Strombus gigas conch shell: II-micromechanics analyses of multiple cracking and large-scale crack bridging.* Acta Materialia, 2004. **52**(8): p. 2395-2406.
19. Kuhn-Spearing, L.T., et al., *Fracture mechanisms of the Strombus gigas conch shell: implications for the design of brittle laminates.* Journal of Materials Science, 1996. **31**(24): p. 6583-6594.
20. Kamat, S., et al., *Structural basis for the fracture toughness of the shell of the conch Strombus gigas.* Nature, 2000. **405**(6790): p. 1036-1040.

21. Weaver, J.C., et al., *The Stomatopod Dactyl Club: A Formidable Damage-Tolerant Biological Hammer.* Science, 2012. **336**(6086): p. 1275.
22. Jackson, A.P., et al., *The mechanical design of nacre.* Proceedings of the Royal Society of London. Series B. Biological Sciences, 1988. **234**(1277): p. 415-440.
23. Barthelat, F., et al., *On the mechanics of mother-of-pearl: A key feature in the material hierarchical structure.* Journal of the Mechanics and Physics of Solids, 2007. **55**(2): p. 306-337.
24. Wang, R.Z., et al., *Deformation mechanisms in nacre.* Journal of Materials Research, 2001. **16**(9): p. 2485-2493.
25. Mayer, G., *Rigid biological systems as models for synthetic composites.* Science, 2005. **310**(5751): p. 1144-1147.
26. Barthelat, F., *Biomimetics for next generation materials.* Philosophical transactions. Series A, Mathematical, physical, and engineering sciences, 2007. **365**(1861): p. 2907-2919.
27. Naleway, S.E., et al., *Structural design elements in biological materials: application to bioinspiration.* Advanced Materials, 2015. **27**(37): p. 5455-5476.
28. Mirkhalaf, M., A.K. Dastjerdi, and F. Barthelat, *Overcoming the brittleness of glass through bio-inspiration and micro-architecture.* Nature Communications, 2014. **5**(1): p. 3166.
29. Yin, Z., A. Dastjerdi, and F. Barthelat, *Tough and deformable glasses with bioinspired cross-ply architectures.* Acta Biomaterialia, 2018. **75**: p. 439-450.
30. Magrini, T., et al., *Transparent and tough bulk composites inspired by nacre.* Nature Communications, 2019. **10**(1): p. 2794.
31. Jia, Z., et al., *Biomimetic architected materials with improved dynamic performance.* Journal of the Mechanics and Physics of Solids, 2019. **125**: p. 178-197.

Chapter 6: Conclusion

6.1 Summary of the accomplishments

Although hard biological materials including mollusk shells, teeth and bone are mostly made of brittle minerals, they achieve a unique combination of stiffness, strength and toughness, resulted from the synergies between their highly organized mineral building blocks and weak organic interfaces. For nacre from mollusk shells, its toughness is around 3000 times higher than the aragonite mineral it is made of while remaining almost as stiff as aragonite. These biological materials provide excellent templates to toughen brittle materials such as glass and ceramics with bio-inspired architectures. However, it has been a challenge to fabricate bio-inspired materials with large volumes of highly organized building blocks, and to duplicate the toughening mechanisms in biological materials. This thesis presents various types of bioinspired glass materials that successfully duplicates the deformation and toughening mechanisms of selected hard biological materials, with original contributions listed below:

- A fabrication protocol for dense architecture materials that can produce large volumes of meso-scale building blocks with well controlled geometry and arrangement: To have delocalized deformation and maximized energy absorption, it is important to have a nearly perfect periodic arrangement of building blocks. To achieve it, high-precision 3D laser engraving is utilized to precisely carve pre-defined contours within each glass sheet. In order to obtain a highly controlled 3D arrangement of building blocks, thin polyimide adhesive films were applied on engraved glass sheets and rigid glass frames around the sides of the pre-laminates to restrain the movement of building blocks in the lamination process. The resulted multi-layer laminates obtained precisely aligned 3D arrangement of building blocks. The nearly perfect alignment of building blocks also granted the laminates high light transmittance.

- <u>A transparent, tough and highly deformable glass with bio-inspired cross-ply architectures</u>: Glass is a brittle material that has very limited deformability and toughness under tension. The cross-ply glass is first kind of glass composites that are transparent and can sustain large deformation (up to 90% engineering strain) in tension. Ethylene-vinyl acetate (EVA) films are used as the interfacial material for the cross-ply glass, for its low strength, high deformability and The deformation and failure mechanisms of glass are completely changed in the cross-ply glass, from catastrophic failure in monolithic and plain laminated glass to inelastic deformation through sliding and rotation of glass plies. The fracture resistance of cross-ply glass is also significantly higher than plain laminated glass, evaluated through mode-I fracture tests. In terms of the critical force where crack propagation commences, cross-ply glass is around 1.4 to 4 times higher than plain laminated glass due to crack blunting. Cross-ply glass also obtains a work of fracture 12 to 53 times higher than plain laminated glass due to various toughening mechanisms triggered by the cross-ply architecture.
- <u>The deformation modes of cross-ply architectures and the dominant influential parameters</u>: The arrangement of glass plies in the cross-ply glass is controlled by the orientation angle (to the loading direction) and width of the glass plies. Our study revealed that the most dominant parameter that influenced the deformation modes of the cross-ply glass was the orientation angle of glass plies. Overall three deformation modes were identified: brittle ply fracture when the orientation angle is relatively low, ply rotation mode when the orientation angle is intermediate and ply sliding mode when the orientation angle is high. Among the three

deformation modes, the ply rotation mode gave the cross-ply glass the highest deformability and energy absorption.

- The unique mechanisms behind the deformability and hardening of cross-ply glass: For the cross-ply glass, most of the deformation is contributed by the deformation of the polymeric interface. Therefore, the mechanical behaviors and deformation modes of the cross-ply glass is essentially controlled by the shear stresses in the polymeric interface. The distribution of shear traction at the polymeric interface were analyzed through finite element simulation. The behaviour of the polymeric interface was represented by a bi-linear cohesive law verified by the shear lap tests of the polymeric adhesive and the tensile tests of the cross-ply glass. Our simulation results revealed that even the polymeric interface was softening everywhere, the apparent mechanical response of the whole structure was still hardening because of the redistribution of interfacial shear traction caused by the rotation of plies. Our finding provides insights and inspiration to design tough and deformable materials through delayed global failure.
- Fracture modes of cross-ply glass and the dominant influential parameters: The fracture modes of cross-ply glass under mode-I fracture depend on the width and orientation angle of plies. There are overall three fracture modes observed. At low ply orientation angle, the dominant fracture mode is the crack deflection mode where the cracks were deflected along the weak interfaces. At intermediate ply angles, crack channeling mode prevailed, where crack deflection was accompanied with interface shearing. Crack bridging is the dominant toughening mechanism in this mode. Shearing mode is triggered at higher ply orientation angles. In this fracture mode crack deflection was prominent, with a crack path which was

different in the two layers so that fracture resistance was mostly generated by the shear deformation of the interlayer.

- An impact resistant transparent nacre-like glass that outperforms tempered glass and laminated glass on energy absorption: It has been a challenge for three decades to produce large volumes of well-organized microscopic nacre-like brick walls and to duplicate the toughening mechanism of large-scale tablet sliding in nacre. High precision laser was used to engrave contours of tablets in glass sheets and assembled well-aligned glass sheets into multi-layer nacre-like brick-and-mortar structure. The nacre-like glass panels show high transparency due to well aligned tablets. Under quasi-static puncture and weight-drop impact tests, the nacre-like glass panels outperformed tempered glass and plain laminated glass in terms of energy absorption by 2-3 times, through large-scale tablet sliding. For nacre-like glass panels made of all architectured layers, though energy absorption is higher, the strength and stiffness are lower than plain laminated glass. Plain glass layer(s) can be placed on the front surface of nacre-like glass panels to compensate the loss on strength and stiffness, without losing toughness. For a five-layer nacre-like glass panels with a plain front layer, the strength and initial stiffness can be increased up to only 10-15% lower than plain laminated glass while more than twice tougher.
- Large-scale tablet sliding to absorb energy in the nacre-like glass: In nacre, one of the most important toughening mechanisms is the sliding of mineral micro-tablets. The local hardening provided the organic interfaces in nacre and the dovetail shape of the tablets helps tablet sliding spread over large volumes. In the nacre-like glass panels, large-scale tablet sliding is realized by the strain hardening of the EVA interfaces. The amount and types of sliding mechanisms were quantified using micro-computed tomography (micro-CT). Overall three types of sliding mechanisms can be observed in the nacre-like glass panels under puncture: uniform sliding

where a layer slides in a uniform direction relative to the adjacent layer, uniaxial sliding where adjacent tablets have uniaxial separation and biaxial tablet sliding.

- The dominant parameters affecting the mechanical behaviours of nacre-like architectures: The mechanical behaviors of nacre-like glass panels are affected by the size and shape of the tablets. For nacre-like panels with square tablets punctured in the center, tablet sliding is more localized at the center lines following the interfaces between tablets. For nacre-like panels with hexagonal tablets, tablet sliding is more isotropic. Tablet size has substantial effects on the mechanical behaviors of nacre-like glass panels. Large tablets lead to brittle fracture that limit the energy absorption and deformability of nacre-like panels. Small tablets lead to low strength and deformation localized near the puncture site. The optimal configuration for energy absorption as well as the deformability is an intermediate tablet size where deformation is delocalized without brittle tablet fracture.
- A comparative study on various bio-inspired glass designs: Few studies have systematically studied the effects of material architectures and geometry of building blocks for bio-inspired glass. This thesis comparatively studied three categories of bio-inspired glass designs: continuous-ply designs with 90° cross-ply and Bouligand architectures, segmented designs with segmented Bouligand and nacre-like (square tablets) architectures, and hybrid designs combining plain layer(s) and architectured layers (nacre-like). Under quasi-static puncture tests, for continuous-ply designs, the glass panels have brittle ply fracture with deformation localized at the puncture site. For a 90° cross-ply panel, a major in-plane radial crack emits from the puncture site, follows the interfaces between the plies in some layers while propagates through the plies in the adjacent layers, and eventually snaps the panel in half. For a Bouligand panel, radial cracks are more uniformly distributed and shorter than those in the cross-ply panels. In-

plane radial crack propagation tends to be deflected along the interfaces between plies within each layer. Overall continuous-ply designs show limited deformability and energy absorption due to brittle ply fracture and localized deformation. Segmented designs suppress brittle ply fracture by finite-size building blocks. Compared to continuous Bouligand panels, segmented Bouligand architectures show suppressed brittle fracture and delocalized deformation, which leads to higher strength, higher deformability and higher energy absorption. Another segmented design, the nacre-like panels, similarly show improved strength, energy absorption and delocalized deformation. Size of the building blocks has great effects on the mechanical behaviors of segmented designs. Building blocks being too large leads to brittle fracture that greatly limits the mechanical performances of segmented designs. Compared to monolithic and plain laminated glass, the improvements on deformability and energy absorption of segmented designs come at the cost of stiffness and strength. Hybrid designs are to solve this issue by combining plain layer(s) and architectured layers. The plain layer(s) are placed at the front to take compressive stresses under puncture, providing strength and stiffness. The architectured layers are placed at the back to take tensile stresses, providing deformability and energy absorption through sliding of the building blocks. The hybrid designs can substantially improve the stiffness and strength of architectured glass designs.

- <u>A design principle for simultaneously improved stiffness, strength and toughness</u>: One of the goals of having well organized material architectures is to have controlled deformation and mechanical behaviors. Through the comparative study on continuous-ply designs, segmented designs and hybrid designs, a design principle can be proposed that geometry and arrangement of building blocks should be designed in a way to reach a critical point where brittle fracture of building blocks can be just suppressed. In addition, various types of material architectures can be combined so that local material architectures are optimized for the local stress state to provide improvements on stiffness, strength and toughness simultaneously.

6.2 Thesis contribution

The following list summarizes the main findings achieved during the present study:

- A fabrication protocol that can generate large volumes of highly controlled three-dimensional material architectures, using high precision ultraviolet laser engraving.
- A transparent, highly deformable and tough bi-layer glass with cross-ply architectures.
- Identification of deformation modes and fracture modes for cross-ply glass under tension and mode-I fracture
- Discovery and explanation of the toughening mechanism of ply rotation mode that lead to the strain hardening and high deformability of cross-ply glass under tension.
- A transparent impact resistant nacre-like glass that duplicates the large-scale tablet sliding in nacre.
- A comparative study of continuous-ply, segmented and hybrid glass designs with various bioinspired architectures.
- The design principle for dense architectured materials with simultaneously improved stiffness, strength and toughness.

6.3 Future works

During of the course of this study, a fabrication protocol was developed that could precisely generate large volumes of well aligned three-dimensional architectures made of hard building blocks and soft interfaces. A tough and deformable bilayer glass with bio-inspired cross-ply architectures, and an impact resistant multilayer glass with nacre-like architectures were developed using the fabrication protocol. The mechanical Deformation and toughening mechanisms of the bio-inpsired architectured glass were studied through analytical models, finite element simulations and mechanical experiments. A design principle of dense architectured materials made of hard building blocks and soft interfaces was proposed to simultaneously improve stiffness, strength and toughness, based on the comparative studies on various bio-inspired glass designs including cross-ply, Bouligand, nacre-like and hybrid architectures. The following guidelines are therefore proposed as a continuation of this work:

- Adjusting the interfacial material: In this study, modifications on the material architectures were mostly done on the geometry and arrangement of hard building blocks but few were done on the interfacial material. For the interfacial material, first, optical properties can be tuned through modifying the chemical composition. The refractive index of the interfacial material can be adjusted to match that of glass to further improve the overall transparency. Mechanical behaviors of the interfacial material can also be changed. For example, introducing shearing thickening or shear thinning to the interfacial material can potentially bring interesting results to overall mechanical performances. The interfacial material as well as the glass building blocks can also be surface functionalized to further improve the adhesion.
- Controlled strengthening through well designed material architectures: In this study, front plain layer(s) were introduced to compensate the stiffness and strength loss in the architectured glass designs compared to monolithic and plain laminated ones. However, the front plain glass layer(s) are still brittle and have uncontrollable mechanical behaviors as a result. Furthermore, though stiffness could be improved substantially by the front plain layer(s), the improvement on strength was relatively limited. For mollusk shells, the inner layer is the brick-and-mortar nacreous structure to absorb energy while the outer layer is the prismatic structure to provide

stiffness and strength. Similarly, it is possible to design architectures in a material to boost overall stiffness and strength in a controlled way. In order to achieve it, the fundamental mechanics need to be investigated on how the interaction between hard building blocks can provide strength, build the constitutive models and explore possible topologies of the building blocks.

- From meso- to micro-/nano- scale: The material architecture is at meso-scale in this study. Structures and materials that are brittle at macro-/meso-scale can be much stronger and more deformable at micro-/nano-scale due to the absence of defects. Therefore, if highly controlled material architectures can be achieved at micro-/nano-scale, it is possible to obtain much stronger and tougher materials than current engineering materials. Fabrication techniques such as colloidal self-assembly, multiphoton lithography and stereolithography can be used to generate highly ordered material micro-/nano-architectures.
- From passive to active: In this study, the structures were all passive. It would be interesting to implement the bio-inspired architectured designs in developing novel active materials and programmable structures that have high mechanical outputs, high toughness, high deformability and high fatigue resistance. The actuation can be achieved by using photo-responsive polymers or shear thickening fluid as the interfacial material. The hard building blocks can guide the overall transformation of the active materials, realizing complex transformation with simple inputs.
- Studies on potential applications: Due to the transparency, high deformability and high toughness, the bio-inspired glass developed in this study are suitable for a wide range of applications. An interesting application would be to use it as the base material for flexible and wearable electronics for its high deformability and high toughness. It can also be used in

flexible photovoltaic systems for its high transparency and high deformability. The findings in this study on the fundamental toughening mechanisms of dense architectured materials can also inspire the fields and applications such as soft robots, bone implants and sustainable building materials.

6.4 Publications

6.4.1 Refereed journals

- Z. Yin and F. Barthelat, Stiff, strong and tough laminated glasses with bio-inspired designs, submitted.
- Z. Yin, F. Hannard and F. Barthelat*, Impact resistant nacre-like transparent materials, ***Science***, vol. 364, **2019**, pp. 1260-1263.
- Z. Yin, A. Dastjerdi and F. Barthelat, Tough and deformable glasses with bioinspired cross-ply architectures, ***Acta Biomaterialia***, vol.75, **2018**, pp.439-450.
- F. Barthelat, Z. Yin and M.J. Buehler, Structure and mechanics of interfaces in biological materials, ***Nature Reviews Materials***, vol.1, **2016**, article#:16007

6.4.2 Conference paper and presentations

- Z. Yin, Florent Hannard and F. Barthelat, Ultra-tough and impact resistant glasses with bioinspired architectures, ***Society of Engineering Science 56th Annual Technical Meeting***, St. Louis, MO, USA, **2019**.
- Z. Yin, Florent Hannard and F. Barthelat, A nacre-like glass that surpasses the impact resistance of tempered glass, ***The minerals, Metals & Materials Society 148th Annual Meeting & Exhibition***, San Antonio, TX, USA, **2019**.

- M. Mirkhalaf, Z. Yin and F. Barthelat, Dense architectured materials in engineering and in nature, ***The minerals, Metals & Materials Society 147th Annual Meeting & Exhibition***, Phoenix, AZ, USA, **2018**.
- Z. Yin and F. Barthelat, Revisiting laminated glass using bio-inspired architectures for improved impact resistance, ***International Mechanical Engineering Congress & Exposition***, Tampa, FL, USA, **2017**.
- Z. Yin and F. Barthelat, Revisiting laminated glass using bio-inspired architectures, ***The minerals, Metals & Materials Society 146th Annual Meeting & Exhibition***, San Diego, CA, USA, **2017**.